1-1-2017

Design Of A Modular Endothelialized Platform For Vascularized Bone Regeneration

Kevin Barrett Miles
Wayne State University,

DESIGN OF A MODULAR ENDOTHELIALIZED PLATFORM FOR VASCULARIZED BONE REGENERATION

by

KEVIN BARRETT MILES

DISSERTATION

Submitted to the Graduate School

of Wayne State University,

Detroit, Michigan

in partial fulfillment of the requirements

for the degree of

DOCTOR OF PHILOSOPHY

2017

MAJOR: CHEMICAL ENGINEERING

Approved By:

_____

Advisor Date

_____

_____

_____

_____

ACKNOWLEDGEMENTS

I deeply appreciate all that Dr. Matthew has done for me and my interest in research. Dr. Matthew's supervision, guidance, mentorship and support has helped steer me through the uncertainties of research and graduate school. Most importantly, Dr. Matthew has taught me how to conduct independent research, and how to keep my curiosity when tackling difficult problems. I would like to express my gratitude to Dr. Mao, Dr. Cao, Dr. Kavdia and Dr. Przyklenk, for their helpful review of my work. I would also like to thank Dr. Charles Chung, who helped train me to perform the Doppler Ultrasound analysis that was so important to my work, and provided helpful analysis during my experiments. I am greatly for Dr. Tristan Maerz for gathering the MicroCT data for my engineered bone. The faculty of the chemical engineering department deserve a special thanks for providing me with moral support during my graduate years.

I would also like to thank the Office for Teaching and Learning (OTL) who provided funding during part of my graduate studies, and who never stopped offering encouragement and moral support. I'd like to acknowledge the funding I received from the Detroit Cardiovascular Training Program (DCTP) for a pre-doctoral fellowship that funded the last year of my studies.

Finally, I am incredibly thankful to my mother, Anne Marie Miles, who initially sparked my interest and curiosity towards science at an early age.

TABLE OF CONTENTS

LIST OF TABLES

LIST OF FIGURES

CHAPTER 1: INTRODUCTION

1.1 General Background of Problem

Sports injuries, natural disasters, and conflicts resulting from the global war on terror have all contributed to the increase in unmet demand for maxillofacial and craniofacial bone repair materials. Surgeons have an arsenal of repair strategies for the uniquely shaped functional bones involved in such injuries, but these are usually inadequate and often invasive, causing pain and prolonging healing time [1]. Typically, autologous bone grafts (autografts), taken from another site on the patient, are seen as the "gold standard" of bone repair; of course this technique is non-ideal, since it requires multiple surgical sites and morbidity at the donor site [2]. The next standard graft material, allogenic bone grafts (allografts), taken from another patient, carry risk of disease transmission [2]. The unmet demand for high quality bone grafts to replace the gold standard autologous bone grafts has fueled substantial research in the area of bone tissue engineering.

Researchers in the field of tissue engineering and regenerative medicine continue to develop promising new strategies aimed at building bone grafts from readily available materials, negating the need for autografts or allografts. In general, the tissue engineering strategy involves fabricating a porous scaffold (usually composed of metal, ceramics, polymers, or some mix of these materials), and seeding them with autologous cells that will (ideally) infiltrate the scaffold via the pores, and secrete a mineralized matrix that will be further developed into bone [3]. Bone marrow mesenchymal stem cells (MSCs) are a standard cell source for bone tissue engineering, since they are readily available via isolation from the iliac crest of the patient with the bone injury [4]. Moreover, researchers and physicians can induce MSCs to differentiate to osteoblasts (a process termed osteogenesis), cells that secrete a mineralizing, bone like extracellular matrix (ECM).

Despite the promises of tissue engineering for bone regeneration, the current results still show significant limitations, specifically with regard to limiting the invasive procedures associated with maxillofacial and craniofacial bone repair. Moreover, researchers and physicians currently have difficulty designing tissue engineering strategies that facilitate the rapid formation of a blood vessel network within tissue engineered bone implants; because a vascular system is required for large-scale bone regeneration, the inability to quickly regenerate a blood vessel network throughout the implant is significantly inhibiting the field of bone regeneration [5, 6]. A deviation from traditional tissue engineering techniques could facilitate the development of a bone regeneration solution that enables the rapid development of a vascular system simultaneously with the regeneration of bone matrix deposited by differentiating MSCs.

1.2 Modular Tissue Engineering

The emerging field of modular tissue engineering focuses on fabricating whole macro-scale tissues from micro-scale constructs. Typically, the micro-scale constructs are modular units containing cells surrounded by a biomimetic microenvironment, or simply cell aggregates or sheets without any foreign material introduced. Fig 1 contrasts the modular approach with the traditional tissue engineering approach [7]. Traditional tissue engineering often employs a "top-down" approach, in that cells are seeded onto a porous scaffold (made of biocompatible and biodegradable material), where they are expected to migrate throughout the pores of the scaffold (from the top, down), secreting matrix, and proliferating to the extent that they replace the volume of the degrading scaffold material. The traditional top-down approach has significant limitations, including diffusion of nutrients and growth factors through the bulk of the scaffold, resulting in engineered tissue limited to 100-200 microns thick [8]. Moreover, cells seeded onto traditional porous scaffolds typically don't migrate to significant depths through the scaffold, resulting in

non-uniform distribution of cells. Similarly, such scaffold seeding techniques cannot facilitate controlled distributions of multiple types of cells, and thus cannot mimic the complexity of desired tissues, such as a network of blood vessels.

The modular approach to tissue engineering builds the larger macro-scale tissue from smaller modular units in a bottom-up strategy. The modular units impart a great deal of freedom in recreating the unique biomimetic features at the micro-scale level, that can recreate the architecture of complex tissues. Multiple strategies exist to fabricate the modular units, including self-assembled aggregation of the cells used [9], micro-fabrication of hydrogels containing cells [10], layer-by-layer stacking of cell sheets [11], or by direct cell printing [12]. After fabrication, the modular units can then be assembled into macro-scale tissues by randomly assembling the units, stacking the layers, or by directed assembly of the modular units.

The modular approach to tissue engineering alleviates many of the limitations of traditional tissue engineering. Fabricating the modular units with a uniform number of cells guarantees uniform cell distribution upon assembly of macro-scale tissue. Constructing macro-scale tissues from modular units that contain different cell types facilitates organization of complex engineered tissues: for example, a modular tissue engineering approach that combines endothelial, smooth muscle, and fibroblast cell sheets to recreate the three cell layers of a blood vessel [11]. Finally, assembling the modular units in a controlled fashion can design the desired porosity into the macro-scale tissue, from the bottom up, facilitating nutrient and waste diffusion into and out of the engineered macro-scale tissue. Sufficiently small modular units can be used to create the basis of a “bio-ink” for a 3D printing strategy to regenerate tissue of varying architecture, or as the basis of an injectable bone regeneration therapy, where the modular units

are injected to the defect site and fuse *in situ*.

1.3 General Approach to the Problem

The series of studies proposed here seeks to design a new bone regeneration platform,

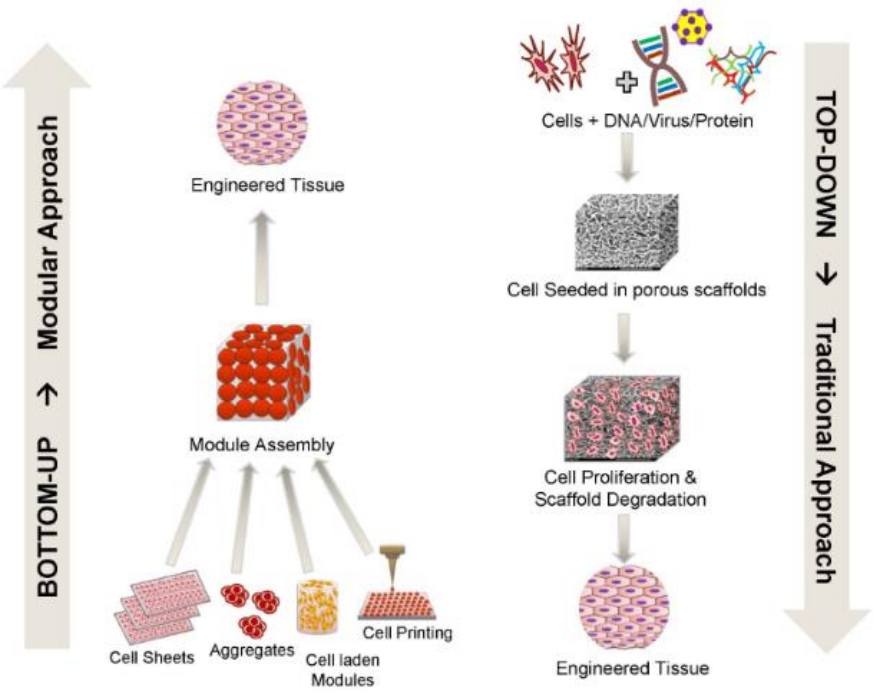

Fig 1.1: Bottom-up (modular) and top-down (traditional) approaches to tissue engineering. In the bottom-up approach, there are multiple methods for creating modular units, which are then assembled into engineered tissues with specific microarchitectural features. In the top-down approach, cells and biomaterial scaffolds are combined and cultured until the cells fill the support structure to create an engineered tissue [7]

involving the construction of larger, porous bone tissue constructs from small modular units, using either a 3D printing strategy or direct injection to a site of bone loss. The modular units will be formed from the encapsulation of MSCs and endothelial cell progenitors (EPs, effectively derived from MSCs differentiated to an endothelial cell lineage) with a bone-like ceramic (hydroxyapatite, HAP) in a polyelectrolyte membrane. The encapsulated MSCs will serve as an osteoprogenitor cell population, capable of differentiating into bone ECM depositing osteoblasts, and the EPs will aid in the rapid establishment of a blood vessel network throughout the larger bone tissue construct.

Because the bone tissue construct would be entirely constructed of cell-laden micromodular units, traditional cell seeding of the construct is unnecessary. Furthermore, the inclusion of EPs throughout the tissue construct, coupled with its porosity, should enable the rapid establishment of a blood vessel network throughout the construct, further aiding the bone regenerative properties of the platform.

CHAPTER 2: RELEVANT BACKGROUND

2.1 Current Gold Standard of Bone Tissue Engineering:

Mastication and ingestion are both critical for survival, as both are the first steps in nutrient absorption from food in healthy and able individuals. Unfortunately, patients suffering from bone defects due to trauma, tumor removal or abnormal skeletal developments concurrently suffer from decrease in masticatory power when the trauma occurs to the maxillofacial bone [13]. Prosthetic jaws and dentures only superficially restore masticatory ability, as mastication in patients fitted with these devices is still reduced to 20% of patients with natural dentition [14]. Thus, bone tissue regeneration (rather than superficial replacement), represents an important challenge for oral-maxillofacial and plastic surgeons tasked with restoring function to the unique bones of the face and jaw. Autologous bone grafts taken from an uninjured area of the patient's skeleton, are frequently used for bone reconstruction, and this material is prized as the "gold standard" of bone repair. Use of the patients own bone is desirable because it lacks immunogenicity, contains a blood vessel network, and directly provides bone forming cells to the injured site; however, the process of removing bone from a patient causes obvious morbidity at the donor site, post-operative pain, increased risk of infection, and hypersensitivity to mechanical stress at the affected area [1, 2, 4]. Surgeons have looked to allogenic bone from human cadavers to avoid the problems associated with autologous grafts. However, the immunogenic potential of allogeneic bone grafts and the risk of virus transfer from donor to recipient represent a serious disadvantage [3]. Furthermore, allogeneic bone has decreased vascularization and a higher resorption rate compared to autologous bone, resulting in a lower rate of bone tissue formation *in vivo* [15]. Surgeons require new bone graft materials to adequately repair and replace bone in patients with serious bone loss.

2.2: Bone hierarchal structure and matrix materials

Like all other tissues, bone is composed of multiple types of biological compounds and cells, with a hierarchical organization spanning several orders of magnitude from the macro-scale (centimeter) to the nano-scale (individual material-material interactions). Specifically, bone ECM is composed of both a non-mineral organic component (collagen type-1 and non-collagenous proteins) and a mineralized inorganic component (carbonated apatite mineralites, predominantly hydroxyapatite, HAP) [16]. In fact, bone ECM consists largely of an architecture of collagen fibers plated with HAP nanocrystals, essentially making the tissue a ceramic/polymer composite: this composite architecture imparts the toughness and compression resistant mechanical properties characteristic of bone. Moreover, bone has anisotropic porosity and mechanical properties. The outer "shell" of bones are made of highly compact mineralized tissue termed "cortical" bone, which has a porosity of 5-10%, a compressive strength of 100-230 MPa and an elastic modulus of 12-20 GPa: by contrast, the center of a piece of bone tissue (termed cancellous bone) will have increased porosity (20-30%), decreased compressive strength of 2-12 MPa, and a decreased elastic modulus of 0.2-0.8 GPa [17]. Cortical bone is composed of osteons, roughly cylindrical structures about 200 μm in diameter surrounding a blood vessel [17]. Unlike a simple bulk ceramic/polymer composite, the changing mineralization and porosity throughout bone imparts complex mechanical properties to the tissue. A multitude of non-collagenous proteins, including osteocalcin [18], osteopontin [19], osteonectin [20], are responsible for calcium sequestration, attachment and migration of bone remodeling cells, and attachment of HAP to collagen, respectively, imparting a wealth of physiological signals throughout the tissue. Bone contains a relatively small amount of glycosaminoglycans (GAGs), of which chondroitin 4-sulfate (C4S) predominates [21]. Research has demonstrated that C4S promotes osteoblast differentiation during bone healing (possible via

the binding of growth factors), and supported bone mineralization via calcium ion sequestration [22]. Bone is organized into a hierarchical structure from the micro-level of ECM composition to the macro-level spatial distribution of the tissue components (porous vs. cortical bone, etc…), and each level contributes to the overall mechanical properties and function of bone.

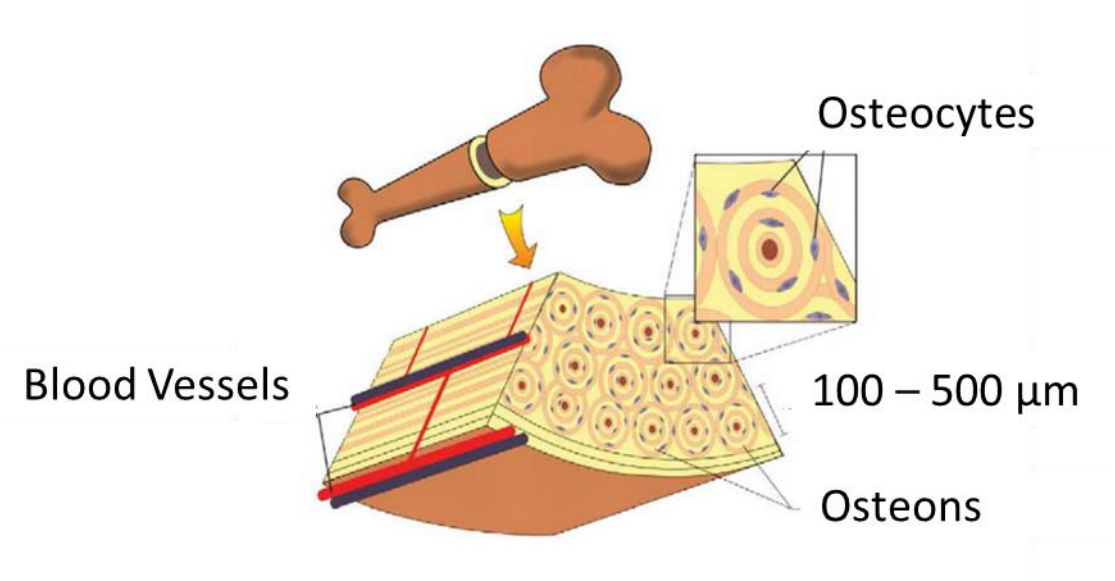

Fig 2.1: Hierarchal organization of bone. Schematic depicting a cutaway cross-section of long bone, showing the osteons encircling the network of blood vessels in the cortical (compact) bone, and weaving through the porous cancellous (spongy) bone towards the center of the long bone shaft. The cutaway section above shows the lacuna of the osteon with embedded osteocytes. Figure from [23]

The hierarchal organization of the materials that comprise bone extends to the cell types that inhabit the bone microenvironment as well. Calcified bone is metabolically active, and osteocytes are found embedded within the calcified bone ECM. Osteocytes are derived from bone-forming cells called osteoblasts, which is the main cell type responsible for depositing a calcified ECM: while osteoblasts mainly deposit the calcified ECM, osteocytes are responsible for secreting various bone specific proteins (BSPs) (osteocalcin, osteopontin, osteonectin, etc…) that facilitate cell attachment, ECM calcification, and remodeling of bone ECM [24]. Osteoblasts migrate to the

bone surface, begin depositing their ECM and, as they surround themselves with their deposited matrix, they effectively burry themselves: the buried osteoblasts then begin to differentiate to mature osteocytes [25]. Both osteoblasts and osteoclasts are derived from mesenchymal stem cells (MSCs), typically originating from the bone marrow cavities of cancellous bone. Bone is in a constant state of remodeling, and thus a bone ECM resorption/metabolizing process compliments the bone ECM forming/depositing process. Specifically, osteoclasts dissolve bone via acidification and proteolysis of the collagen fibers comprising the bone matrix, which facilitates detachment of HAP crystals once linked to collagen [26]. The process of bone resorption removes old structurally unsound bone, injured bone, and controls the shape of bone during development, thus complimenting the process of bone formation. The division of remodeling processes in specific bone cell types represents another level of cellular organization of the tissue.

When moving from the outer cortical regions of bone towards the inner cancellous regions, the cell population of bone changes to have a higher density of MSCs. MSCs reside in the bone marrow in the inner cancellous regions, and are classified by their ability for 1) self-renewal and 2) differentiation to multiple mature cell lineages; as mentioned above, these cells differentiate into osteoblasts [27]. During development in mammals, bones form by the differentiation of MSCs to an osteoblastic precursor cell, and subsequent mobilization to the surface of the bone, where the precursor cell finishes differentiation to an osteoblast [28, 29]. Once the MSCs have differentiated to the osteoblast phenotype, they display several of the osteoblast characteristics, such as calcium deposition and enhanced alkaline phosphatase (ALP) enzyme activity; in fact, the osteoblast characteristics are used by researchers to denote early MSC differentiation (by increase and peak in ALP activity) and late MSC differentiation (deposition of bone specific proteins) [30, 31].

Researchers and clinicians can make use of the inherent osteogenic ability of MSCs in designing therapies to replace damaged tissue, specifically bone.

2.3 Vascularization of bone and bone healing:

Apart from being complex at the matrix and cellular level, bone is also highly vascularized. Studies of blood vessels in long bones (femurs and tibia) indicate that the vessels form an organized network throughout the bone marrow, cortical and periosteal region of bone, with vessels varying in dimension between 10 – 200 μm [32]. Studies of human bone show that the osteons, containing the blood vessels in cortical bone, are distributed homogenously [33]. In fact, studies of human bone show that osteocytes are never more than 100 μm distance from a capillary, and this is possibly a necessity, due to the metabolic requirement of osteoblasts and MSCs [34]. The vessels in bone are lined primarily with endothelial cells (ECs), which constitute the fourth major cell type found in bone. ECs in the microvasculature form tube-like conduits, sealed by adherin junction proteins between opposing endothelial cells, to create a network of capillaries from patches of endothelial cells sealed by cell-cell contact proteins. Specifically, platelet endothelial cell adhesion molecule 1 (PECAM-1) aids in junction formation between ECs, and EC anchorage to the ECM, and PECAM-1 is considered an endothelial marker.

Blood vessel networks require more than ECs to reach a non-permeable state with low EC-cell migration and turnover (i.e., form stable blood vessels). In mature blood vessels, the EC conduit is actually re-inforced and stabilized by cells called pericytes, which wrap around the vessel and generally inhibit vessel permeability (generally, because certain growth factors like VEGF or pathologies can interrupt pericyte stability) [35]. Pericytes maintain blood vessel structural integrity by the contractile protein α-smooth muscle actin (α-SMA), which prevents vascular permeability by contracting around ECs [35]. Some evidence shows that MSCs serve as

a cell source for pericytes [36]. Studies suggest that pericytes send direct or paracrine signals that induce endothelial differentiation and growth arrest, further stabilizing vessel formation [37]. A schematic cross-sectional view of a mature blood vessel, enveloped by pericytes, is shown in fig. 2.3 and gives another example of the scale of organization found in blood vessels. Vascularization plays a significant role in almost all tissue regeneration and healing, and bone is no exception. Large bone defects typically heal via callus production in four overlapping phases, shown in fig. 2.2a [38]. Following damage to the musculoskeletal system and blood vessel network, the coagulation cascade activates and forms a hematoma, enclosing the fracture area [39]. The hematoma formation is associated with the release of several growth factors and cytokines that initiate cell migration to the defect, including stem cells and endothelial cells [39]. Eventually, blood vessels grow into the hematoma, and the hematoma is replaced by an immature vascular network surrounded by fibrocartilage (internal callus) and mineral deposited by intramembranous ossification (external callus), involving the differentiation of a chondrocyte precursor to an osteoblast lineage which initiates calcified matrix deposition [40]. Further osteogenesis of the stem cells and deposition of their calcified ECM transforms the callus from woven bone, which is finally remodeled into secondary lamellar bone. Fig. 2.2b demonstrates overlapping phases in the micro-computed tomography (μCT) images of a rat femur healing from fracture [41]. The recruitment of ECs so early in the bone healing process demonstrates how crucial vascularization is to bone regeneration; thus, the inability to properly regenerate bone quickly in many bone tissue engineering solutions may stem from an inability to recapitulate the blood vessel network required in the earliest part of bone regeneration.

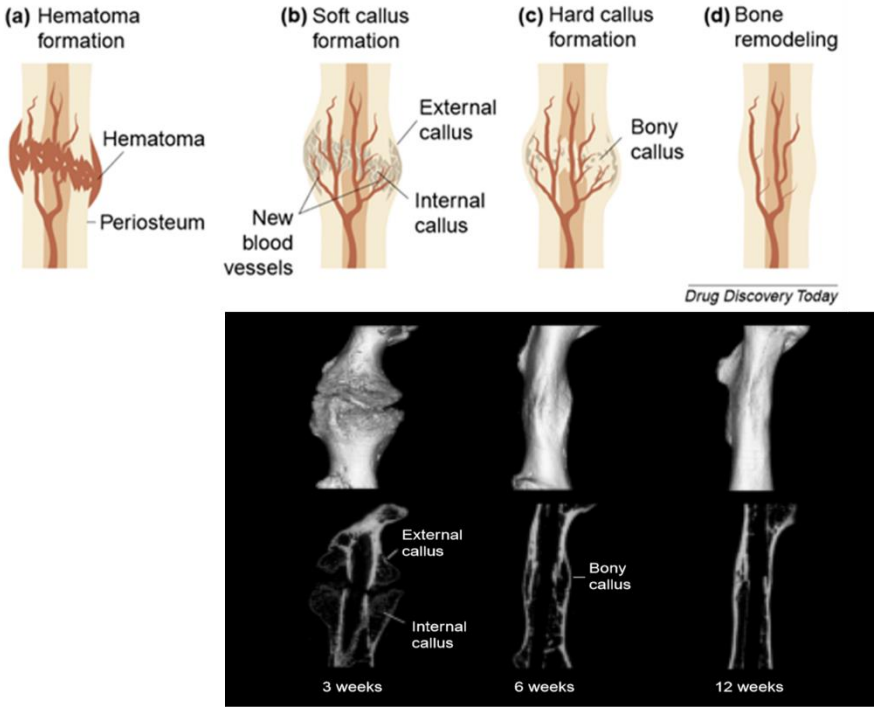

Fig 2.2: Role of vascularization in bone healing: Hematoma formation. Image series (A) shows the stages of fracture repair, including (a) hematoma formation after blood vessel disruption from injury; (b) soft callus formation and the invasion of new blood vessels within the hematoma; (c) hard callus formation as osteoblasts begin secreting a mineralized matrix; (d) bone remodeling, in which the large fracture callus is replaced with physiological bone ECM. Figure from[38]. Image (B) below shows the phases of bone healing in a rat femur at 3, 6 and 12 weeks post fracture. Figure from [39]

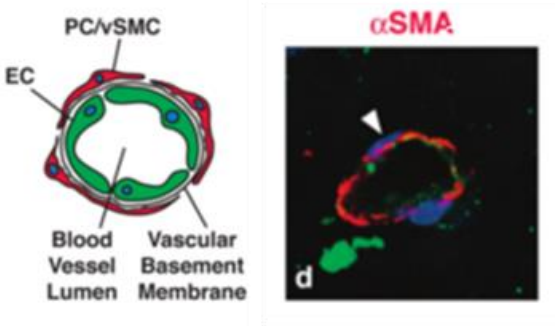

Fig 2.3: Cross-section of a capillary. The schematic to the left shows the layout of a capillary, where an endothelial cell conduit is stabilized by pericytes and vascular smooth muscle cells (PC/vSMC). Fluorescent image to the right shows a histological cross-section of a capillary, with fluorescent probes for lectin (marker for endothelial cells, green), αSMA (red, pericytes) and the nucleus of both cell types (DAPI, blue) [35].

2.4 Traditional tissue engineering bone regeneration materials:

Much of the research until the last few years has focused mainly on combining osteoblast progenitors (OS-progenitors) such as MSCs, with materials that mimic the bone microenvironment, such as various ceramic and hydrogel formulations. HAP, due to its chemical similarity to bone, has been used extensively in tissue engineered scaffold generation: an example study involved the use of a cylindrical collagen-HAP polymer/ceramic composite, seeded with OS-progenitor cells, to regenerate bone in a mouse critically sized calvarial defect [42]. The collagen-HAP scaffold seeded with OS-progenitors did exhibit significant bone regeneration *in vivo*; however, the defect, and thus scaffold, was only 500μm thick, and did not adequately recapitulate the nutrient diffusion limitations that would be experienced in larger bone defects found in human patients. Villa et al commented in their study that the small size of the scaffold (3.5 mm diameter x 0.5 mm height) likely wouldn't be subjected to diffusion limitations, and that a vascularization strategy would be required to regenerate larger bone defects [42]. Still, the study validated the efficacy of HAP as a biomaterial for bone regeneration.

Other groups have demonstrated the utility of biological and non-cytotoxic polymers to regenerate bone. GAGs are an obvious choice, due to their non-cytotoxicity and ability to sequester and attenuate growth factors [43, 44]. Because C4S is the major GAG constituent of bone ECM, many researchers have used this as their main material for bone regeneration, and previous studies have shown that C4S promoted osteoblast differentiation and supported bone mineralization during bone healing [22, 45]. Chitosan is a carbohydrate derived from deacetylated chitin (typically obtained from marine animals) and composed of β-(1→4)-2-acetamido-d-glucose and β-(1→4)-2-amino-d-glucose unit linkages [46]. Chitosan has also been investigated for its utility as a bone tissue engineering scaffold material, due to its ease of scaffolds preparation, relative non-cytotoxicity, and the ability of its positive charge in acidic solution to sequester calcium ions [46]. Chitosan is biodegradable *in vivo* and can be complexed with negatively charged polymers such as GAGs, making it a useful base material to design a bone regeneration system [47].

2.5 Current research towards generating vascularized bone:

With the understanding that establishing a vascular system is critical for bone regeneration, many research groups have attempted to recapitulate the vascular system by seeding traditional TE scaffolds with a combination of osteoprogenitors (usually MSCs) and endothelial progenitors (usually HUVECs). Research elucidated that ECs can have stimulatory effects on MSC osteogenesis when cultured in 3-dimensions. Kang et al cultured HUVECs and MSCs on porous, cylindrical β-TCP scaffolds (5mmx7mm) *in vitro*, found that the HUVECs significantly increased the ALP activity, and the effect was greatest for HUVECs seeded at a ratio of 1:1 HUVECs:MSCs [48]. Furthermore, the HUVECs in the HUVEC:MSC cultured expressed the cell adhesion molecule PECAM-1, which is known to be crucial for vessel formation and maintenance, and the HUVECs formed a branched, networked architecture within the implant. In a similar experiment,

Pedersen *et al* seeded 6mm diameter cylindrical poly(l-lactide)-co-(1,5-dioxepan-2-one)[poly(LLA-co-DXO)] scaffolds with HUVECs and MSCs in a 1:5 ratio HUVEC:MSC, and investigated the osteogenic and angiogenic potential of this system in a NOD mouse subcutaneous skin pouch model [49]. Histological evaluation of the subcutaneous-implant scaffolds demonstrated that α-SMA (a marker for pericytes) was found surrounding functional blood vessels (marked by the presence of red blood cells) of both MSC and HUVEC:MSC co-cultures, with no difference between the groups. Interestingly, ALP gene expression was highest for HUVEC:MSC seeded scaffolds compared to MSC alone, and is likely due to signaling between HUVECs and MSCs. The co-culture of ECs with MSCs clearly enhances MSC osteogenesis, while still permitting EC cell function.

The co-culture of endothelial cells with MSCs has proven to enhance the overall architecture of newly deposited bone ECM by differentiating MSCs. In one study, Yu et al fabricated poly-ε-caprolactone (PCL) HAP composite scaffolds, seeded with both MSCs and EC-progenitors (derived from MSCs differentiated to an endothelial lineage), and investigated the *in vivo* regeneration of vascularized bone in a rat femur model [50]. After 6 weeks, the PCL/EC-progenitor/MSC implant contained a significantly higher capillary density (compared to MSC only control) demonstrated by an increase in concentric positive CD31 and Flt-1 staining. Interestingly, because Yu et al used a sex-mismatched model (male-donor cells were implanted in female rats), the donor cells in the implants could be tracked by staining for the presence of Y-chromosomes; results showed that the new blood vessels were primarily composed of Y-chromosome+ donor cells via Y-chromosome and CD31+ overlap, indicating that the addition of exogenous EC-progenitors enhanced vascularization of the scaffold (see fig. 2.4). The results from the study by Yu et al demonstrate that not only do the EC-progenitors and MSCs enhance vascularization and

osteogenesis within a HAP-based scaffold, but these implanted cells contribute significantly to the formation of the vessel network. The enhanced vascularization from the EC-progenitors seeded in the PCL/HAP scaffolds investigated by Yu et al also significantly enhanced the mechanical properties of the implants: after 6 weeks of implantation, mechanical compression of implants demonstrated that implants containing EC-progenitors had significantly higher ultimate tensile stresses (0.728 ± 0.092 MPa) compared to implants with OS-progenitor MSCs only (0.450± 0.066 MPa). The inclusion of EC-progenitors in other bone regeneration systems should lead to enhanced bone regeneration over OS-progenitors alone.

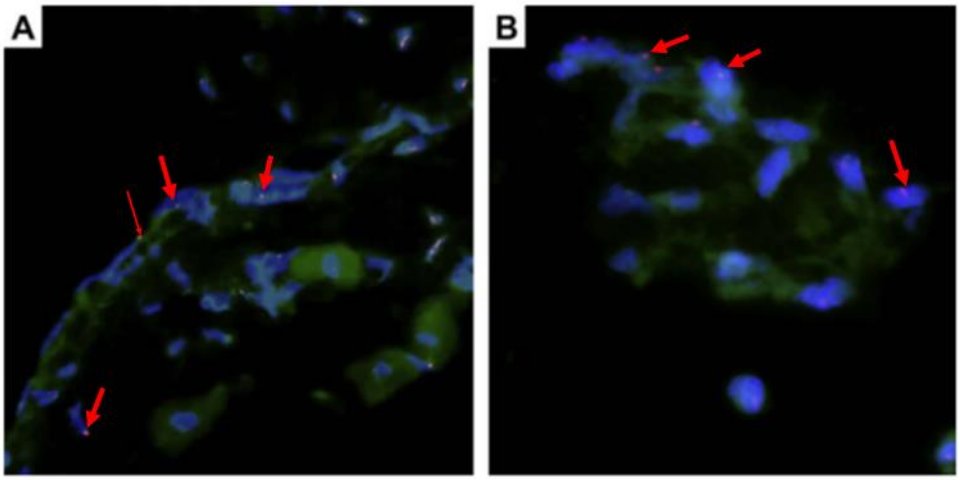

Fig 2.4: Donor cell contribution to vascularization and osteogenesis in a tissue engineered bone graft. Tissue sections from a PCL/HAP implant seeded with EC-progenitors and MSCs and implanted in rat femur defect for 6 weeks. Sections were stained for presence of Y-chromosome (red dots) and CD31 (green) in image (a) to identify EC-progenitors, and osteocalcin (green) in image (b). The nucleus of all cells was stained by DAPI (blue). Images show that the donor cells, containing the Y-chromosome (red arrows aid in identification), contribute significantly to both vascularization and bone specific protein deposition [50].

2.7 Technology gap in the literature:

Tissue engineering research has accomplished several key milestones in the effort to produce functional TE bone grafts that can completely replace the gold-standard and morbidity-

causing auto-graft bone. Currently, the literature has validated the use of ceramic and polymer materials (HAP and various natural polymers), and OS-progenitors and EPs. However, the bone TE literature currently lacks studies evaluating the design of a bone regeneration strategy composed of small modular units, simultaneously laden with OS-progenitors and EPs and compression-resistant ceramics, to regenerate highly vascularized bone: the evaluation of a platform incorporating such a strategy is the goal of this study.

CHAPTER 3: CENTRAL HYPOTHESIS and SPECIFIC AIMS

Our modular bone regeneration platform employs polysaccharide microcapsules containing encapsulated MSCs and HAP microgranules. The polysaccharide microcapsule membrane is composed of a C4S/chitosan polyelectrolyte complex, is relatively thin and porous, and facilitates the diffusion of nutrients and growth factors to support encapsulated cell viability and differentiation. The microcapsules can be fabricated at an average diameter of 400 μm. The microcapsule materials are biodegradable *in vivo*, and the degradation rate depends on materials. These microcapsules will serve as the basis of our modular bone regeneration platform.

The ***central hypothesis*** to be tested is that modular GAG/HAP/Chitosan microcapsule constructs can support osteogenesis of encapsulated MSCs, mineralization to a compression resistant tissue, and rapidly vascularize *in vivo* when coated with endothelial progenitors. This new bone graft design will serve as the basis of a bone regeneration platform that, with subsequent optimization, will regenerate bone in defects from injury or disease (fig 3.1).

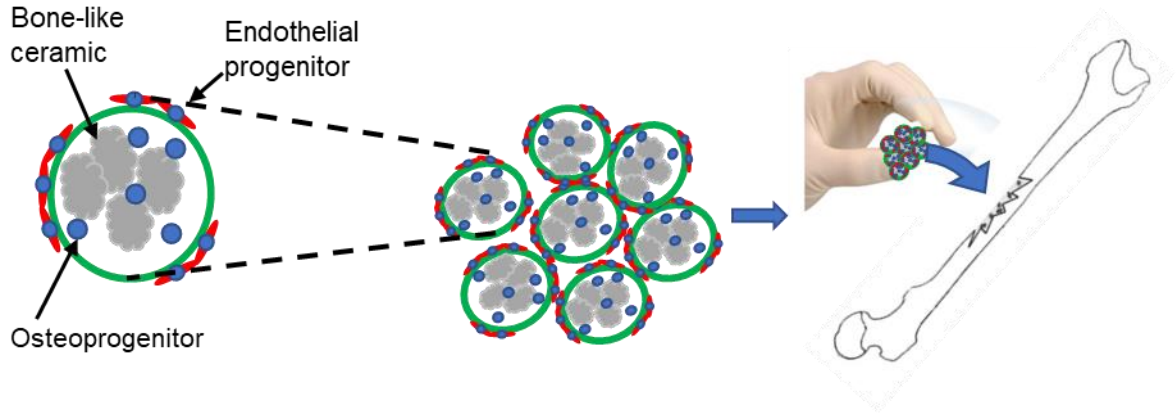

Fig 3.1: Central hypothesis. Microcapsules containing encapsulated osteoprogenitors and HAP ceramic microgranules, with endothelial progenitors attached to the exterior, can be fused into implantable constructs that will quickly regenerate vascularized bone *in vivo*.

The ***specific aims*** of this project are to:

1. Examine the ability of C4S/HAP/Chitosan microcapsules to support osteogenesis of encapsulated MSCs.
2. Characterize how microcapsule mineralization influences mechanical properties of fused microcapsule constructs.
3. Analyze how endothelial progenitors attached to the microcapsule exterior influence the vascularization of fused constructs *in vivo*.

3.1 Overall research design

First, the ability of the microcapsule materials to support proliferation, viability and osteogenesis of encapsulated mesenchymal stem cells (MSCs) was assessed. Secondly, the mechanical properties of fused constructs composed of microcapsules actively mineralized by MSCs were characterized. Additionally, the influence of mineral architecture on mechanical properties was investigated. Finally, the ability of EPs attached externally to microcapsules to enhance the vascularization of fused constructs *in vivo* was evaluated.

3.2 Significance and rationale

Modular tissue engineering principles have great potential to help engineer advanced tissues by facilitating greater control over multicellular organization, unique material composites, and deployment of scaffolds via minimally invasive surgery. The field of modular tissue engineering is relatively new, and will certainly benefit from a new cell/material combination strategy. This study is very significant: many modular tissue engineering studies understandably focus more on mimicking the multicellular organization of native tissues, and not necessarily the

mechanical properties. This study has the capability to not only reproduce tissue with a level of cell organization (endothelial and MSC/osteoprogenitor) similar to bone tissue, but the inclusion of ceramic particles in the microcapsules allow us to produce tissue with enhanced mechanical properties as well.

The modular system described here is versatile, and can accommodate various osteoprogenitor and endothelial progenitor cell types, bone-like mineral, and polymer additives to the microcapsule membrane. Thus, this study holds the promise to produce a new bone graft design that could generate well vascularized bone with some early mechanical stability *in vivo*, in a system amenable to minimally invasive surgical delivery. This new bone regeneration platform could take the place of the current gold standard of bone regeneration (autologous graft harvesting), since this modular design requires only autologous stem cells (harvested in a much less invasive procedure), or allogenic stem cells from a tissue bank. Moreover, the design of a modular construct with organization of multiple cell types could provide a blueprint for other tissue engineers seeking to regenerate complex organs with high degrees of material and cell organization (kidney nephrons, liver lobules, etc…). The microcapsules used for this modular bone regeneration platform could provide tissue engineers with another tool to fabricate advanced tissues.

CHAPTER 4: EVALUATION OF OSTEOGENIC DIFFERENTIATION OF MESENCHYMAL STEM CELLS ENCAPSULATED IN MICROCAPSULES

4.1 Introduction:

GAG/Chitosan/HAP microcapsules must support encapsulated MSC osteogenesis and viability if the microcapsules are to form the basis of any bone regeneration platform. These criteria are a minimum for any bone regeneration strategy that uses stem cells as the primary tissue regeneration component. In this chapter, encapsulated MSCs were induced to osteogenesis while in microcapsule culture, and the extent of osteogenesis was characterized via quantification of osteogenic biomarkers and cell-deposited bone-like matrix components. Additionally, cell viability was assessed over the four weeks of static microcapsule culture. Furthermore, the effects of HAP microgranules on encapsulated MSC osteogenesis were also explored.

4.2 Aim and Rationale:

The main specific aim of this chapter is to examine the ability of the GAG/Chitosan/HAP microcapsules to support encapsulated MSC osteogenesis and viability. The rationale for this aim, is that by examining the osteogenesis of encapsulated MSCs *in vitro*, we can confirm that the microcapsule materials will not inhibit MSC bone regeneration *in vivo*. This aim is significant, because it will allow us to determine if the present microcapsule system is sufficient for the basis of a bone regeneration platform, or if the microcapsule materials/organization requires modification. Moreover, mineralization of the microcapsule system could enhance the mechanical properties of a tissue construct composed of fused microcapsules. Confirming that the microcapsule system supports MSC osteogenesis and mineralization will allows us to analyze fused construct mechanical properties as a function of mineralization, and continue modifying the microcapsule system to promote vascularization.

4.3 Experimental Approach:

Study 1: Viability of MSCs encapsulated in GAG/Chitosan/HAP microcapsules

Encapsulated MSCs were cultured for four weeks in static conditions, and the effects of osteoinduction and HAP microgranules on MSC viability were assessed. Double stranded DNA (dsDNA) was quantified at each week of culture to quantify cell proliferation.

Study 2: Quantification of Osteogenic Biomarkers of Encapsulated MSCs

Common osteogenic biomarkers for MSC osteogenesis were quantified to determine whether microcapsule materials or culture could inhibit osteogenesis. ALP activity (early stage osteogenesis), osteocalcin secretion (early stage osteogenesis) and osteopontin secretion (late stage osteogenesis) were quantified for the four-week culture period. This allowed us to confirm that encapsulated MSCs were differentiating along an osteogenic path.

Study 3: Characterization of Cell-deposited ECM in Microcapsule Interior.

Cell-deposited matrix in the microcapsule interior was observed after four weeks of culture. The amount of collagen and deposited calcium was quantified over the four-week culture period. This study allowed us to confirm that differentiating cells were depositing bone-like mineral in the microcapsule system.

4.4 Materials and Methods:

Unless otherwise noted, all chemical and cell-culture reagents were purchased from Sigma-Aldrich (St. Louis, MO), and were of reagent grade or greater purity. Fetal Bovine Serum (FBS) was purchased from Atlanta Biologicals (Flowery Branch, GA).

4.4.1 Cell culture conditions

MSCs were harvested from the femurs and tibiae of Sprague-Dawley (SD) rats (Envigo, Huntingdon, UK), using an established protocol [51]. Briefly, the femur and tibiae of SD rats were

removed and cleaned of excess soft tissue post-euthanasia, and incubated in a Kreb's-Ringer buffer solution containing antibiotic (gentamicin sulfate, 50 mg/L) and antifungal (2.5 mg/L amphotericin B). After an hour of incubation at 4 ºC, the diaphyses of the bones were removed, and the contents of the bone marrow were flushed out with Low Glucose Dulbecco's Modified Eagle's Medium (L. DMEM) at 37 ºC, filtered through a 70 μm cell strainer, and centrifuged at 200xg for 6 minutes. After removing supernatant, the resulting cell/erythrocyte pellet was resuspended in PBS, and centrifuged again to wash away erythrocytes. After repeating the washing step twice, the MSCs were suspended in standard medium (L. DMEM + 10% FBS) and seeded at a density of 10,000 cells/cm^2 in tissue culture plates. MSCs were maintained in 2D culture for expansion in standard medium at 37 ºC in a humidified 5% CO_2 atmosphere. MSC were cultured until 80% confluency and subsequently subcultured, or used for an encapsulation at passage 4.

4.4.2 Microcapsule Fabrication

C4S/Chitosan/HAP microcapsules were prepared following an established protocol, with slight modifications to encapsulate MSCs and HAP granules [52]. A schematic of the microcapsule formation is shown below (fig. 4.1). MSCs and HAP microgranules were suspended in a C4S solution (4% w/v C4S and 1.5% CMC in Sorbitol-HEPES ((4-(2-hydroxyethyl)-1-piperazineethanesulfonic acid)) buffer, pH 7.0), at a density of 5x10^6 cells/ml C4S solution, and 50% volume microgranules/volume C4S solution. The Sorbitol-HEPES buffer contained the following components: 0.4 g/l KCl, 0.5 g/l NaCl, 3.0 g/l HEPES*Na, and 36 g/l Sorbitol, adjusted to pH 7.4 with 1.0 M NaOH. The resulting C4S solution with suspended MSCs and microgranules was extruded through a 24-gauge catheter as 400 μm droplets, into a rapidly stirring solution of 0.6% (w/v) high molecular weight chitosan and sorbitol. Once the C4S/HAP/MSC suspension hits the chitosan, the C4S complexes with the chitosan, encapsulating the contents of the droplet (HAP

and MSCs). The microcapsules are washed with 0.9% saline 3x, and the positive outer shell of the microcapsules is surface stabilized by washing with a 0.1% (w/v) polygalacturonic (PGA) acid solution. After another saline wash to remove unreacted PGA, the resulting microcapsules (containing the MSCs and HAP microgranules) were equilibrated with cell culture medium, transferred to a dish, and incubated at 37 °C in a humidified 5% CO_2 atmosphere. Two microcapsule conditions (with HAP microgranules and without) and two medium conditions (osteogenic and expansion) were used to elucidate the effects of HAP microgranules and osteogenic or expansion media on MSC osteogenesis and viability. Thus, four microcapsule conditions were generated: 1) encapsulated MSCs cultured in expansion medium (Exp), 2) encapsulated MSCs cultured in osteoinduction medium (Osteo), 3) encapsulated MSCs and HAP microgranules cultured in expansion medium (Exp + HAP), and 4) encapsulated MSCs and HAP microgranules cultured in osteoinduction medium (Osteo + HAP). The medium employed consisted of expansion medium (L. DMEM +10% FBS), and osteoinduction medium, consisting of the expansion medium supplemented with 100 nM dexamethasone, 10 mM β-glycerophosphate, and 50 μM ascorbic acid-2-phosphate [53]. All media were supplemented with 9 μg/ml tetracycline to fluorescently visualize deposited calcium mineral.

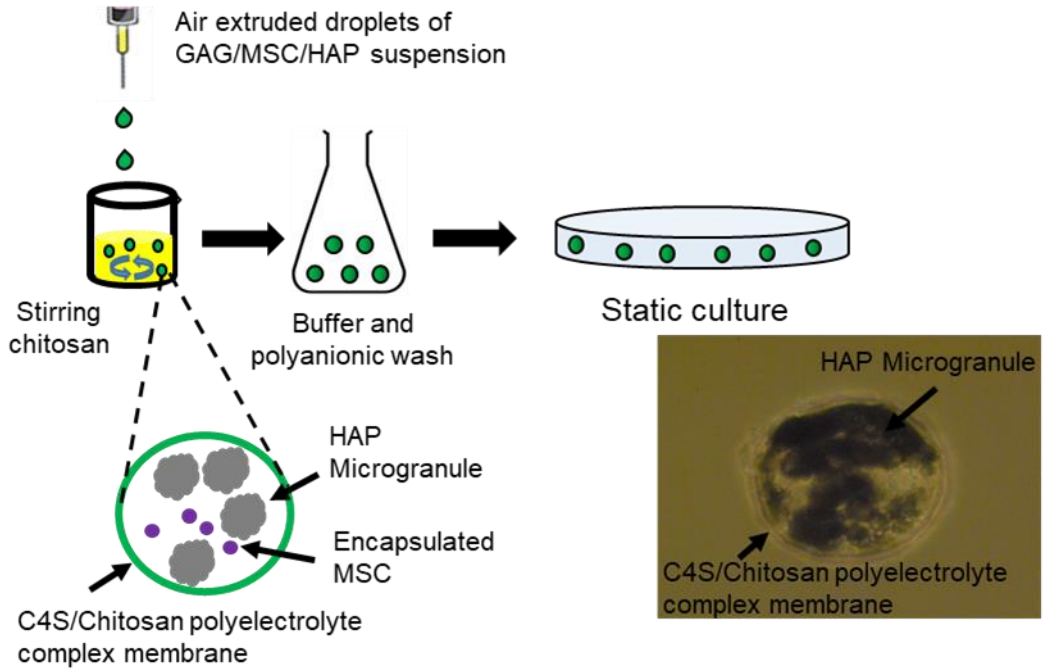

Fig 4.1 Microencapsulation of HAP microgranules and MSCs through complex coacervation. (a) Droplets of MSCs and microgranules suspended in GAG solution are air extruded into rapidly stirring chitosan solution. Interactions between polyanions in the GAG solution and the polycation chitosan form an insoluble polyelectrolyte complex membrane that encapsulates MSCs and microgranules suspended in the droplets. Phase contrast image showing microcapsules membrane and encapsulated HAP microgranules. Microscope objective is focused on microgranules, so membrane appears out of focus.

4.4.3 Assessing Encapsulated MSC Viability

The approach employed involved culturing the four microcapsule conditions detailed above for a series of four weeks, and investigating the viability of encapsulated MSCs using a fluorescent probe. At 1, 2, 3 and 4 weeks of static culture, microcapsules were washed with phosphate buffered saline (PBS), and incubated in L. DMEM supplemented with 4 μM Calcein Red Orange (Calcein RO), at 37 °C in a humidified 5% CO_2 for 30 minutes. After 30 minutes, the microcapsules were washed with PBS twice to remove all extracellular Calcein RO, and the cultures were examined under a fluorescence microscope for live cells containing fluorescent

Calcein RO product. The tetracycline fluorescence of solid calcium deposited by differentiating MSCs was also examined. All steps involving fluorescent probes were performed in the dark.

The dsDNA content of the microcapsules was quantified at each week using the fluorescent, dsDNA binding Hoechst 33258 reagent [54]. After each week, a 0.2 ml volume of settled microcapsules was removed from culture, washed with PBS, and combined with 500 µl of cell lysis buffer (0.05% (v/v) Triton x-100 in 10 mM Tris Buffer, pH 7.0). The microcapsule/buffer suspension was subjected to three freeze-thaw cycles via liquid nitrogen and microcapsules were subsequently crushed with a mortar and pestle to release cell lysate. After cell lysis, 1.5 ml of a Hoechst solution (100 ng/ml Hoechst 33258, 100 mM NaCl, 10 mM Ethylenediaminetetraacetic acid (EDTA) dissolved in 10 mM pH 7.0 Tris buffer) was mixed with 50 µl of the cell/capsule lysate solution, and incubated at room temperature. After 5 minutes of incubation, 200 µl of Hoechst/cell lysate was transferred to a 96 well plate, where the fluorescence was recorded at an excitation of 350 nm, and emission wavelength of 450 nm. Fluorescence data from microcapsule samples was compared to a standard curve generated from calf thymus dsDNA.

4.4.4 Assessing Encapsulated MSC Osteogenesis

To examine the extent of early and late MSC differentiation to an osteogenic lineage, the ALP activity and deposition of bone specific proteins (osteocalcin and osteopontin), respectively, was quantified at timepoints of 1, 2, 3 and 4 weeks: all data was normalized to dsDNA content at each timepoint. At each timepoint, microcapsules were removed from culture and washed with PBS. The washed capsules were equilibrated with cell lysis solution (0.05% (v/v) Triton x-100 in 10 mM Tris Buffer, pH 7.0), and then cracked via shear with a mortar and pestle. A 0.2 ml volume of settled microcapsules is sheared, and 1 ml of cell lysis buffer is added. The cell sheared microcapsules are incubated in the lysis buffer for 15 minutes at room temperature. ALP activity

was quantified using the conversion of p-nitrophenyl phosphate (p-npp) to a colorimetric product by ALP activity. A spectrophotometer was used to quantify the colored product, which was converted to a rate of nmol ALP activity divided by the dsDNA content. Briefly, 300 ul of cell lysis buffer from sheared microcapsules was added to 1 ml of p-npp reagent (Pointe Scientific, Canton, MI) pre-warmed to 37 ºC, and the mixture was incubated at 37 ºC for 30 min. The absorbance of the lysate/p-npp mixture was quantified before (t_0) and after (t_{30}) the 30 min 37 ºC incubation period: 300 ul of lysate/p-npp solution was aliquoted into a 96-well plate, and the absorbance was read at 405 nm. The ALP activity was calculated using equation 1 below, and standardized to the DNA content of the microcapsules. Results were reported as nM ALP/min/ug dsDNA.

Equation 1: Calculation of ALP Activity from Absorbance

$$\frac{\text{nM}}{\text{min}} = \frac{(A_{30} - A_0) \times 1.2 \text{ ml}}{30 \text{ min} \times 18.75 \text{ nM}^{-1}\text{cm}^{-1} \times 0.7 \text{ cm} \times 0.300 \text{ ml}}$$

$$A_0 = \text{Absorbance of cell lystate p} - \text{npp mixture at t} = 0 \text{ min}$$

$$A_{30} = \text{Absorbance of cell lysate p} - \text{npp mixture at t} = 30 \text{ min}$$

Osteocalcin and Osteopontin was quantified via a competitive ELISA similar to published protocols [55]. ELISA plates (96-wells) were coated with either osteocalcin or osteopontin (Abcam, Cambridge, UK) at 20 ng/well overnight at 4 ºC in 50 mM carbonate buffer (pH = 9.6). Coated wells were washed 3x with TBS-T wash buffer (0.05 M Tris-HCl (pH 7.5), 0.15 M NaCl, 0.05% (v/v) Tween 20), and blocked for 24 hours at 4 ºC with 5% (w/v) non-fat dry milk (in TBS-T). Blocked wells were washed 4x with wash buffer. Microcapsule samples were prepared similarly for OC/OP analysis as for ALP activity quantification: 125 µl of cell/capsule lysate (from sheared microcapsules incubated with cell lysis solution) was added to a 125 µl primary antibody (diluted 1:50,000 in blocking solution for both OC and OP), and the mixture was shaken for 24

hours. The primary antibodies for OC and OP were rat anti-osteocalcin developed in mouse (Thermo Fisher Scientific, Waltham, Massachusetts) and rat anti-osteopontin developed in rabbit (Abcam, Cambridge, UK), respectively. After shaking, 250 µl of lysate/antibody solution was added to the blocked wells of the 96-well plate, and incubated at 4 ºC for 24 hours. After 24 hours, plates were washed 3x with wash buffer, and then 250 µl of alkaline phosphatase-conjugated secondary antibody (1:2000 dilution in blocking buffer,) was added to the wells, and incubated for 24 hours at 4 ºC. The secondary antibodies used for OC and OP detection were anti-mouse IgM alkaline phosphatase antibody produced in goat, and anti-rabbit IgG alkaline phosphatase antibody produced in goat, respectively (Sigma Aldrich, St. Louise, MO). After incubation, the wells were washed with wash buffer, and p-npp substrate (SIGMAFAST p-npp tablets, Sigma Aldrich, St. Louis, MO) was applied to the wells. After 5 min, reactions were stopped with 1 M NaOH, and the absorbance was read on a Spectramax 250 spectrophotometer (Molecular Devices, Sunnyvale, CA) at 405 nm. A standard curve of OP and OC was used to determine the OC and OP content of the microcapsule samples, and results were standardized to sample DNA content for reporting as µg OC/µg dsDNA (or µg OP/µg dsDNA).

4.4.5 Characterizing Matrix Production in Microcapsule Interior

The amount of calcified matrix deposited by differentiating MSCs was quantified by the orthocresolpthaliene-complexone (OCPC) indicator method established in the literature [56]. Briefly, the microcapsules fabricated above were removed from culture at 1, 2, 3 and 4 weeks, and incubated in 1 M acetic acid for 24 hours. Every 24 hours, a 50 µl sample of the acetic acid/mineral solution from the dissolving microcapsules was added to 250 µl of the OCPC detector solution, and the absorbance of this solution was read on a spectrophotometer set to 570 nm. Data was compared to calcium chloride standards, and microcapsules were incubated with fresh 1 M acetic

acid until no calcium is detectable (3 days). Collagen content was quantified by measuring the hydroxyproline (HYP) content of the microcapsules, using a published protocol [57]. Briefly, extracts from the microcapsules were oxidized with chloramine T which, upon reaction with P-dimethyl-amino benzaldehyde, produces a colored product whose absorbance can be quantified using a spectrophotometer set to 550 nm. Results were reported as ug calcium/ug dsDNA and ug HYP/ug dsDNA.

4.4.6 Evaluating Matrix Interior Topography via SEM

The interiors of the microcapsules for all four conditions were assessed via Scanning Electron Microscopy (SEM) after four weeks of culture, to characterize the cell-deposited ECM and microarchitecture within the microcapsules. After four weeks of culture, microcapsules were rinsed with PBS and fixed in 2.5% (v/v) glutaraldehyde in 0.1 M cacodylate buffer (pH 7.4) for 24 hrs at 4 °C. The fixed microcapsules were then washed twice with PBS to remove glutaraldehyde, equilibrated with DI water for three changes, flash frozen with liquid nitrogen, and lyophilized for 48 hours. After lyophilization, the microcapsules were fractured with a razor blade to expose their cross-sections, and examined with SEM coupled with EDX spectrometry (JEOL 7600 FESEM, JEOL USA, Inc., Peabody, Massachusetts) for ECM microarchitecture, and the relative distribution of calcium and phosphorus in the samples.

4.4.7 Analysis of Growth Rate of Encapsulated MSCs via alamarBlue®

The cell metabolism assessment reagent alamarBlue® (Invitrogen, Carlsbad, CA) was used to assess cell metabolism and quantify cell proliferation, to determine whether mineral deposition within microcapsules could limit cell proliferation by blocking nutrient diffusion. To accomplish this, microcapsules for all conditions were immobilized to the bottom of 24 well plates, and cultured on a rotary shaker. To immobilize the microcapsules, chitosan films were cast in the wells

of the 24-well plate. A 1% (w/v) suspension of chitosan in DI H_2O was sterilized by autoclaving, and chitosan was subsequently dissolved with 0.2% acetic acid (added aseptically). Undissolved particles were centrifuged out, and 200 µl of 1% chitosan solution were added each well of the 24-wel plate, and air-dried (to allow acetic acid evaporation) under sterile conditions for 24 hours. Microcapsules were prepared as previously described, and 0.1 ml of settled microcapsules were added (in PBS at 37 ºC) to the films. The microcapsules attached to the films almost instantly, and the PBS was aspirated, replaced with standard medium (L.DMEM + 10% FBS), and cultured on a rotary shaker at 66 rpm with a 1 inch rotation diameter for 24 hours in standard culture conditions (37 ºC and 5% CO_2 hydrated atmosphere). After 24 hours, the culture medium was replaced with either standard medium (Exp or Exp+HAP microcapsules) or osteogenic medium (Osteo or Osteo+HAP) for 3 weeks. The metabolism of the encapsulated cells was quantified with alamarBlue® 48 hours after the culture medium switch (week 0), and on 1, 2 and 3 weeks afterward. A 10% (v/v) solution of alamarBlue/L.DMEM (without phenol red) was applied to the immobilized cultures for 4 hours: after 4 hours, the resulting medium containing reduced alamarBlue® was removed, 200 µl samples were aliquoted to wells of a 96-well plate, and the fluorescence intensity was measured on a fluorimeter (Perkin Elmer, Waltham, MA) at an excitation of 550 nm and emission of 590 nm. The percent reduction of alamarBlue® was computed using equation 2 below:

Equation 2:

$$\%\ \text{Reduction} = \frac{FI_{sample} - FI_{unreduced}}{FI_{reduced} - FI_{unreduced}} \times 100\%$$

%Reduction alamarBlue®

FI_{sample} = Fluorescence intensity of alamarBlue/medium from microcapsules

$FI_{unreduced}$ = Fluorescence intensity unreduced alamarBlue/medium

$FI_{reduced}$ = Fluorescence intensity of 100% reduced alamarBlue

The specific growth rate of the encapsulated cells was calculated using the percent reduction of alamarBlue® by equation 3, below:

Equation 3:

Specific Growth Rate of Encapsulated Cells

$$\mu = \frac{\ln(\frac{R}{R_o})}{(t - t_o)}$$

μ = Specific growth rate (day^{-1})

R = Percent reduction alamarBlue at time t

R_o = Percent reduction alamarBlue at time t_o

t_o = Time 1 week previous to time t (days)

Results are reported as percent reduction of alamarBlue® and specific growth rate (Day^{-1}) vs. weeks of culture.

4.4.8 Statistical Analysis

Statistical analysis was carried out using GraphPad Prism software. All statistical comparisons were made by performing a two-way analysis of variance (ANOVA), followed by Bonferroni's multiple comparison tests to evaluate significance between two data sets at a time and correct for false positives of significance. P values less than 0.05 were considered statistically significant. All data is reported as the mean $\pm$ standard deviation.

4.5 Results:

4.5.1 Encapsulated Cell Viability and Mineral Deposition

MSCs were successfully encapsulated in C4S/chitosan complex microcapsules. MSCs encapsulated in C4S/chitosan complex and cultured in standard media (Exp) formed aggregates early at week 1 of culture (fig. 4.2a) that persisted through 4 weeks of culture (fig. 4.2b-d). MSCs in Exp microcapsules typically formed one aggregate per capsule. Exp capsules maintained MSC viability over all four weeks of culture, demonstrated by the presence of Calcein RO fluorescence

localized to the cells, and not present over the entire field of view (fig. 4.2e-h). Encapsulated MSCs in Exp capsules deposited very little calcified mineral, as evident by the absence of green tetracycline fluorescence from weeks 1-3 of culture (fig. 4.2e-g); however, tetracycline fluorescence was evident by week 4, indicating possible active MSC mineralization of capsule membrane by week 4, since tetracycline is incorporated into newly-mineralized ECM (fig. 4.2h) [58]. Moreover, the sections of the Exp microcapsule membrane appeared rough and thicker in places by week 4 of culture, relative to prior weeks 1-3, indicating possible matrix deposition by encapsulated MSCs (fig. 4.2d). The membranes of Exp microcapsules between weeks 1-3 had appeared smooth.

MSCs encapsulated in C4S/chitosan microcapsules and cultured in osteogenic induction media (Osteo) formed aggregates in the first week of culture (fig. 4.2i), but aggregates appeared smaller than in Exp microcapsules, and capsules appeared to have multiple aggregates. Initially, the Osteo microcapsule membrane was relatively homogenous and translucent. As osteoinduction of the encapsulated MSCs continued, the microcapsule membrane exhibited a rougher appearance and became increasingly opaque, due to mineral deposited by MSCs undergoing osteogenesis (fig. 4.2j-l). By week 2 of culture, Osteo microcapsules exhibited significant green tetracycline fluorescence that increased to week 4, indicating that MSCs had deposited significant calcified mineral in the microcapsules (fig. 4.2n-p). The tetracycline fluorescence in Osteo microcapsules was localized around the capsule membrane and the MSC aggregates (yellow fluorescence was due to green and red overlap). After four weeks of osteoinduction, the microcapsule membrane as well as part of the capsule interior was intensely fluorescent with tetracycline and opaque, indicating significant MSC-deposited calcified mineral (fig. 4.2l, p).

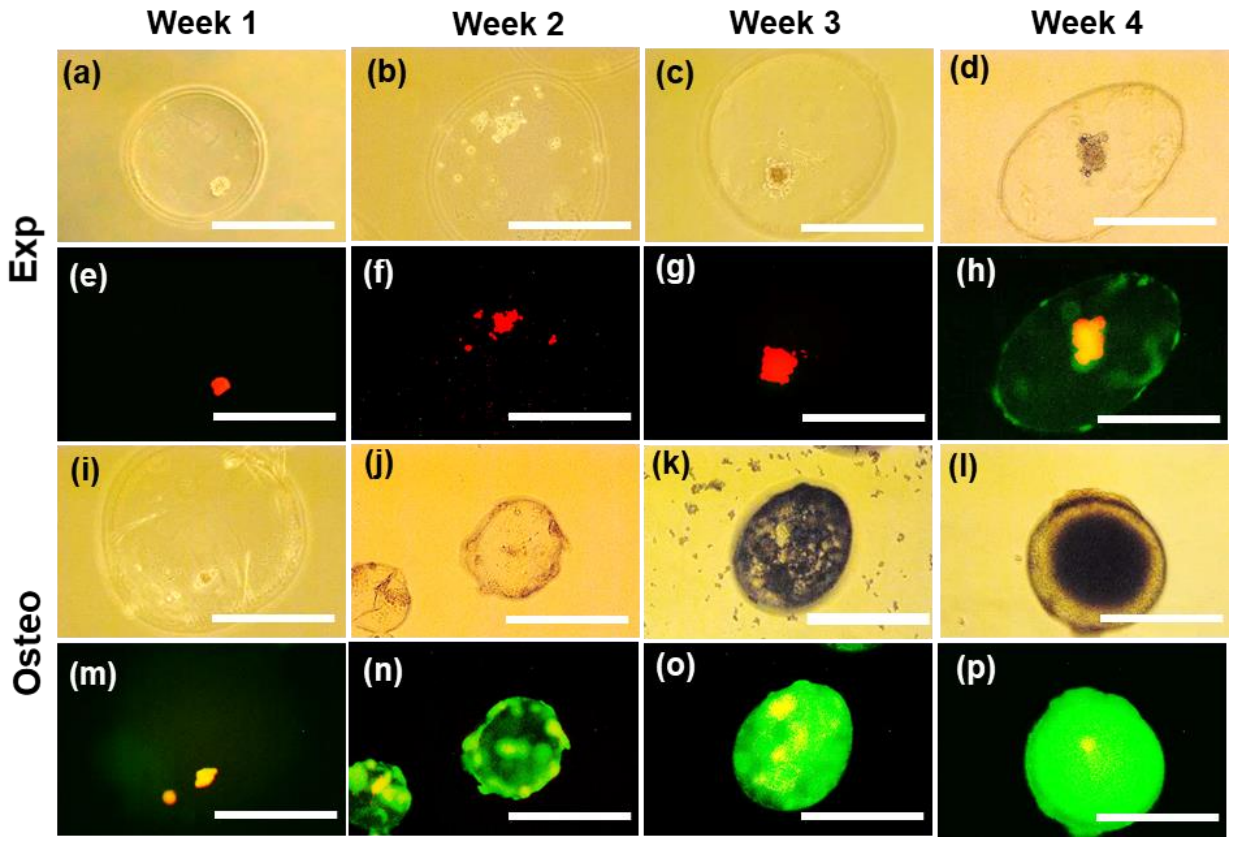

Fig 4.2: Fluorescent images of capsules without HAP microgranules. (a-d) Phase contrast images of Exp capsules in static cultures for weeks 1 – 4, (e-h) corresponding Calcein Red Orange (RO) and tetracycline fluorescent images to (a-d). (i-l) Phase contrast images of Osteo capsules in static culture for weeks 1-4, and (m-p) corresponding Calcein RO and tetracycline fluorescence. Significant calcium deposition was evident after 2 weeks of osteogenesis, and localized around cells (yellow) and the capsule wall (green). (scale bars = 250 um)

Suspension of HAP microgranules in the GAG solution resulted in the coencapsulation of HAP microgranules and MSCs. Gravity caused the HAP microgranules to settle towards one end of the microcapsules. The addition of the completely opaque HAP microgranules made it difficult to discern MSC position from the phase contrast microscope images alone, so observation of cell position relied entirely on the Calcein RO fluorescence (fig. 4.3a-d, i-l). Calcein RO fluorescence

around the microcapsule membrane demonstrates that including HAP microgranules and culture in standard media initially disperses the cells to the membrane of the microcpasules in the Exp+HAP condition at week 1 of culture (fig. 4.3e). The coencpasulation of HAP microgranules maintained MSC viability over the four-week culture period, as demonstrated by fluorescence of Calcein RO (fig. 4.3e-h). By week 2 of culture, the encapsulated MSCs had attached to the HAP microgranules and formed an MSC/HAP microgranule composite aggregate inside the microcapsules in the Exp+HAP condition that persisted through 4 weeks of culture (fig. 4.3f-h). Very light tetracycline fluorescence was present after two weeks of culture in the Exp+HAP condition, indicating active mineralization by encapsulated MSCs (fig. 4.3f). Acellular microcapsules containing HAP microgranules did not exhibit tetracycline fluorescence (data not shown).

HAP microgranules initially dispersed the MSCs in the Osteo+HAP condition, but by week two, the MSCs had attached to HAP microgranules to form the MSC/HAP microgranule aggregate (fig. 4.3m-p). MSCs in the Osteo+HAP microcapsules deposited mineral early during week one of culture, as exhibited by tetracycline fluorescence (fig. 4.3m). MSCs continued to mineralize Oste+HAP microcapsules through the four-week culture period: the tetracycline fluorescence (and thus mineral deposition) was initially localized to the HAP microgranules, but later extended to the microcapsule interior and possibly the microcapsule membrane (to a lesser extent).

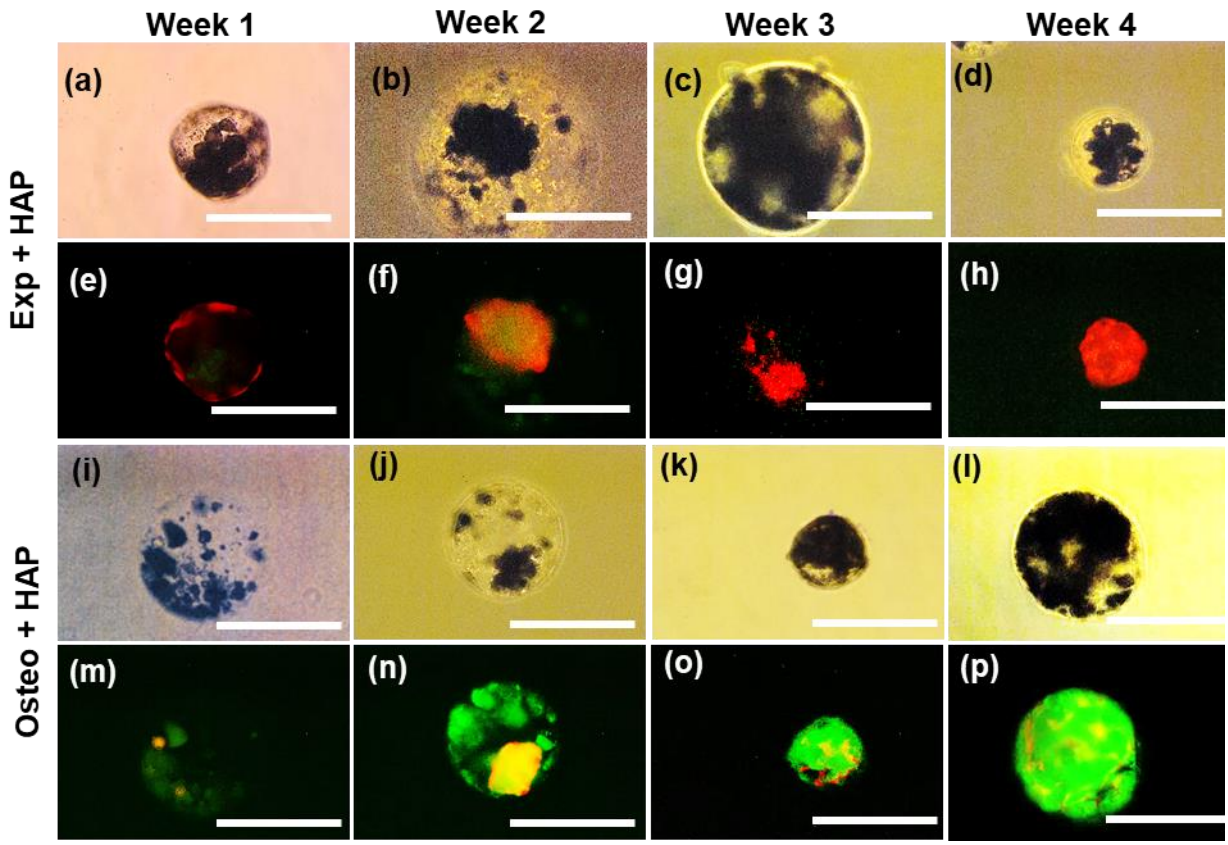

Fig 4.3: Fluorescent images of capsules with HAP microgranules. (a-d) Phase contrast images of Exp + HAP capsules in static cultures for weeks 1 – 4, (e-h) corresponding Calcein Red Orange (RO) and tetracycline fluorescent images to (a-d). (i-l) Phase contrast images of Osteo + HAP capsules in static culture for weeks 1-4, and (m-p) corresponding Calcein RO and tetracycline fluorescence. (Scale bar = 250um)

4.5.2 Encapsulated Cell Proliferation

MSC proliferation in the microcapsule conditions was measured by comparing dsDNA content in microcapsules at each week of culture. dsDNA content, and thus MSC proliferation, showed a general upward trend for all microcapsule conditions through four weeks of culture (fig. 4.4). Microcapsules without HAP microgranules (Exp and Osteo) exhibited the fastest MSC proliferation initially, between weeks one and two, while MSC proliferation in microcapsules with HAP microgranules (Exp+HAP and Osteo+HAP) remained low. After week two, MSC proliferation in Exp and Osteo microcapsules plateaued, and remained unchanged between weeks

2 and 4 of culture. In contrast, MSC proliferation in Exp+HAP and Osteo+HAP microcpasules increased between weeks 2 and 3 of culture, while remaining unchanged between weeks 3 and 4. The lack of proliferation after week 2 in Exp cultures is likely due to the MSCs unable to fully spread and adhere to the microcapsule interior wall (the cells attach as aggregates), limiting cell proliferation by reducing focal adhesions. The cells in the Osteo microcapsules may be experiencing low levels of nutrients due to mineralization of the microcapsule wall, that could limit their proliferation. Because the HAP microgranules initially disperse the MSCs in the capsule after encapsulation, the effects of cell-cell contact and growth inhibition are observed later after 3 weeks of culture.

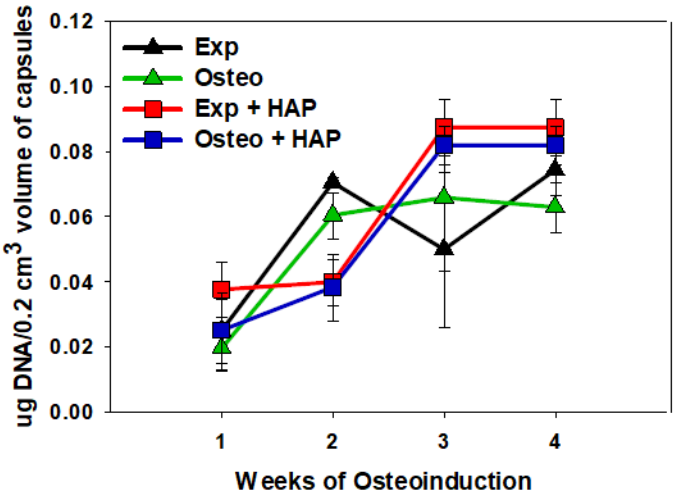

Fig 4.4: Encapsulated MSC viability and proliferation in static culture. The total dsDNA of 0.2 cm^3 samples of capsules from each condition was quantified over all weeks of culture.

4.5.3 Biochemical Markers of MSC Osteogenesis

Cell secreted ALP was quantified and normalized to dsDNA for all conditions over the four-week culture period (fig. 4.5a). ALP significantly increased between weeks 1-3 for all osteoinduced microcapsule conditions. The ALP activity for both osteoinduced conditions (Osteo, Osteo+HAP) was significantly higher than the non-induced (Exp, Exp+HAP) at week 2, and higher than Exp at weeks 3 and 4 ($P < 0.05$). The osteoinduced cultures hit a peak of ALP activity after three weeks of osteoinduction before falling off by week 4. Interestingly, at week 3, MSCs in Exp+HAP microcapsules had statistically similar ALP activity to the osteoinduced conditions ($P < 0.05$).

Encapsulated MSCs deposited bone specific proteins in the microcapsules in response to osteoinduction during microcapsule culture. Osteoinduced conditions (Osteo and Osteo+HAP) contained significantly higher levels of secreted OP over weeks 3 and 4, compared to Exp and Exp+HAP during the same time ($P < 0.05$, fig. 4.5b). Additionally, the osteoinduced conditions exhibited an increasing microcapsule OP content between 1 and 4 weeks of culture. Microcapsule OC content also increased in response to osteoinduction of encapsulated MSCs. MSCs cultured in Osteo and Osteo+HAP microcapsules deposited significantly more OC than Exp microcapsules between weeks 2-4 of culture ($P < 0.05$, fig. 4.5c). OC content of Osteo microcapsules was significantly higher than Exp and Exp+HAP at week 2; however, by week 3, MSCs in Exp+HAP had deposited a statistically similar amount of OC as Osteo ($P < 0.05$). Osteo, Osteo+HAP and Exp+HAP microcapsules had significantly higher OC content than Exp microcapsules after 3 and 4 weeks of osteoinduction ($P < 0.05$). OC content in the Exp microcapsules increased between weeks 2 and 3, but the amount was significantly lower compared to all other conditions ($P < 0.05$). Osteoinduction of encapsulated MSCs was enough to stimulate expression of osteogenic markers

ALP, OC and OP: additionally, HAP microgranules stimulated an upregulation of OC and ALP, but not OP. The ability for HAP to stimulate osteogenesis in MSCs has been documented to a limited extent, and previous studies have demonstrated co-culturing HAP and MSCs increased ALP and BSP expressions, in the absence of other osteoinduction factors [59]. The osteoinduction of MSCs cultured with HAP are likely due to calcium and phosphate ions released by HAP near MSCs, that stimulate the upregulation of BMP-2 gene expression, leading to the expression of osteogenic markers like ALP and BSPs [60].

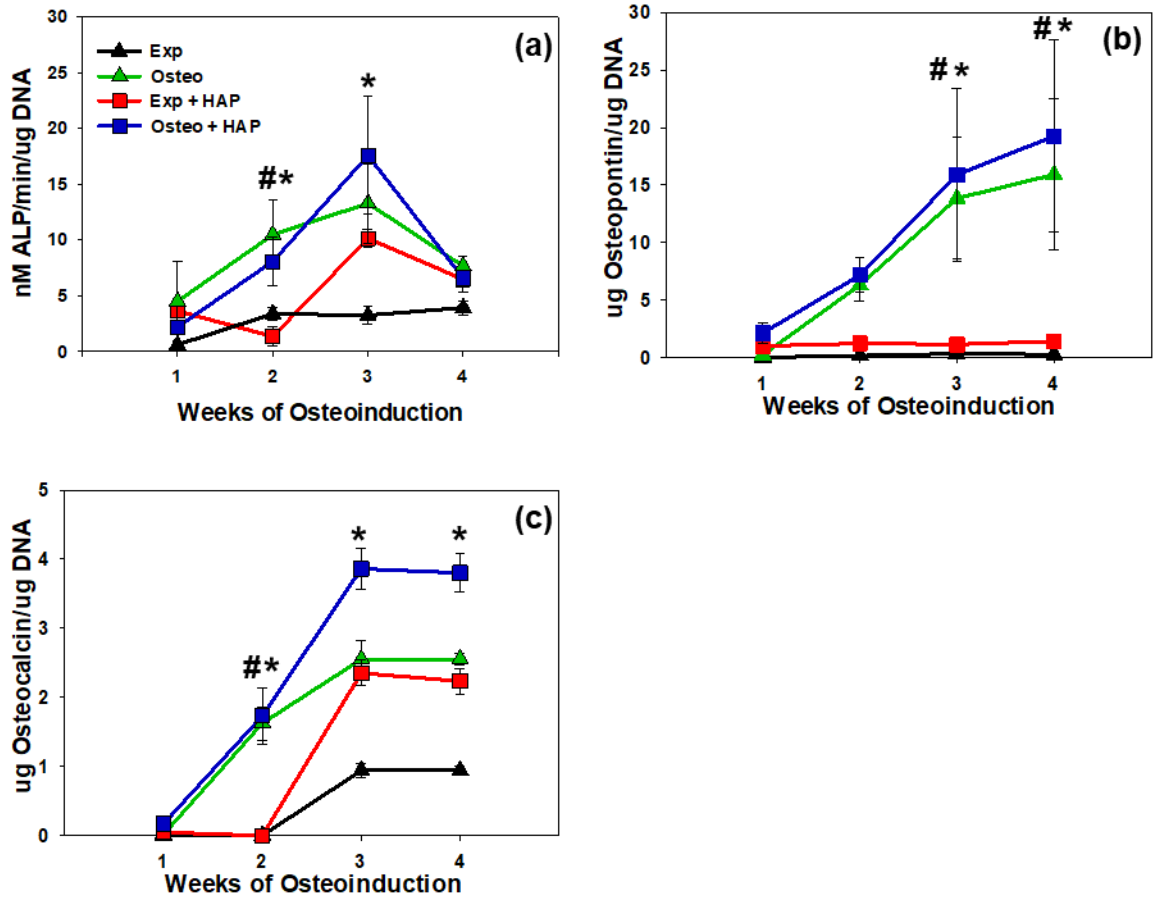

Fig 4.5: Biochemical markers of MSC Osteogenesis. (a) Alkaline phosphatase (ALP) activity of MSCs in static culture. (b) Osteopontin (OP) deposition by MSCs in static culture. (c) Osteocalcin (OC) deposition by MSCs in static culture. *= P< 0.05 (N=4) relative to Exp. #=P < 0.05 (N=4) relative to Exp and Exp+HAP

The increase in OC expression but not OP expression in Exp+HAP microcapsules was an interesting finding for this series of experiments. Results from literature demonstrate that, in the absence of other osteoinductive factors, inorganic phosphate at a 10 mM concentration in static medium promotes OP expression via signaling through the extracellular signal-regulated kinase (ERK1/2) pathway [61]. Similarly, increases in the cytosolic levels of calcium in pre-osteoblasts lead to osteogenesis via the p38 MAPK pathway [62]. As previously discussed, the culture of MSCs on calcium phosphate surfaces promotes MSC osteogenesis, due to augmented cell attachment/focal adhesions and the dissolution of the material into calcium and phosphate ions [59, 63]. Specifically, culture on calcium-phosphate ceramics upregulated OC expression in the absence of chemical osteoinduction factors, likely due to the release of calcium ions from the ceramics [60]. It is possible that the HAP co-encapsulated with the MSCs in the Exp+HAP microcapsules released enough calcium ions to promote OC expression, but not enough phosphate (< 10 mM) to promote OP expression.

4.5.4 Osteogenic Matrix Deposition by Encapsulated MSCs

The osteogenic ECM components calcium and collagen, secreted by encapsulated MSCs, were quantified for all microcapsule conditions and standardized to microcapsule dsDNA during the four-week culture period. The collagen content was measured indirectly by quantifying the microcapsule hydroxyproline content. The calcium content of acellular microcapsules containing HAP microgranules was subtracted from Exp+HAP and Osteo+HAP microcapsules, so that all calcium data reported was deposited by encapsulated MSCs. MSCs in Osteo and Osteo+HAP microcapsules deposited significantly more calcium in the microcapsule system after 3 and 4 weeks, compared to the microcapsules cultured in standard media ($P < 0.05$, fig. 4.6a). Osteo microcapsules contained significantly more cell-deposited calcium than Exp+HAP microcapsules

at week 2. The calcium/dsDNA content of the osteoinduced microcapsules exhibited a significant upward trend that continued for the four-week culture period. The Exp+HAP microcapsules exhibited a modest deposition of calcium in the microcapsule system between weeks 1 and 3, but this was significantly lower than the osteoinduced cultures at week 3 ($P < 0.05$). The calcium/dsDNA content of the Exp microcapsules remained unchanged during the four-week culture period. The hydroxyproline content of the osteoinduced microcapsules increased over the four-week culture period, and was significantly higher than the Exp and Exp+HAP microcapsules between weeks 2-4 ($P < 0.05$, fig. 4.6b). Biochemical analysis suggests that the osteoinduced MSCs are depositing a calcium/collagen composite, which could be the precursor to a mineralized matrix found in new bone. Cells can use the microcapsule materials (C4S/chitosan membrane and HAP microgranules) as a template to begin bone regeneration by first depositing a collagen-calcium matrix, that could be further remodeled into bone *in vivo*.

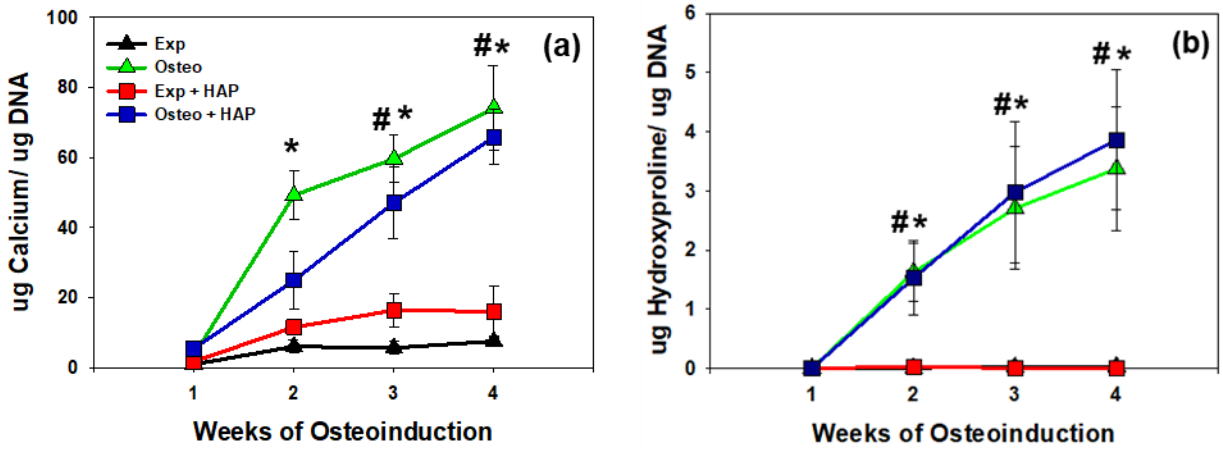

Fig 4.6: Osteogenic matrix deposition by encapsulated MSCs. (a) Mass of cell-deposited solid calcium content of capsules normalized to dsDNA. Total calcium mass of acellular HAP capsules was subtracted from Exp + HAP and Osteo + HAP values for all time points. (b) Mass of hydroxyproline content of capsules normalized to dsDNA. Hydroxyproline is a unique component of collagen. *= $P < 0.05$ (N=4) Osteo relative to Exp and Exp+HAP. #=$P < 0.05$ (N=4) Osteo + HAP relative to Exp and Exp+HAP

4.5.5 SEM/EDS Analysis of Microcapsule Interior

To better visualize the contents of the microcapsule interior after four weeks of culture, microcapsules were fixed, lyophilized, and cut in half to expose the contents for SEM/EDS analysis. Both low magnification (fig. 4.7a-d) SEM images of cut microcapsules in full view, and higher magnification (fig. 4.7e-h) SEM images of the microcapsule interiors were acquired. Exp microcapsules had a smooth membrane that appeared to fold/collapse in on itself after cutting, exposing the interior (fig. 4.7a). SEM revealed cell aggregates attached to the microcapsule wall in the interior of the Exp microcapsules, surrounded by strands of ECM-like fibrils, possibly collagen deposited by cells in culture (fig. 4.7e). Osteo microcapsules had a rigid membrane that partially kept its shape after cutting (the membrane did not fold over), and the membrane had a rough appearance due to mineral deposition (fig. 4.7b). The Osteo microcapsule interior was full of loosely organized mineral crystals that covered the microcapsule membrane, and filled most of the microcapsule space (fig. 4.7f). MSCs were attached to the mineral. Results show that differentiation of encapsulated MSCs promotes active mineralization that can drastically augment the microcapsule interior, and fill it with an osteoid-like mineral matrix.

Microcapsules fabricated with HAP microgranules had a substantially different interior composition than the Exp and Osteo conditions. Exp+HAP membranes appeared relatively smooth, with some mineral-like nodules present on the interior of the microcapsule membrane (fig. 4.7c). The microcapsule membranes folded slightly after cutting, likely due to the weight of the HAP microgranules. Additionally, some of the internal HAP microgranules spilled out onto the carbon tape after cutting, indicating a lack of ECM deposition by encapsulated MSCs that could have bound the HAP microgranules together. The interior of Exp+HAP microcapsules showed encapsulated MSCs had attached to HAP microgranules, and not only aggregated by

attaching to other cells, like the Exp condition (fig. 4.7g). Similarly, Osteo+HAP microcapsules appeared relatively smooth on the outside; however, the interior was crowded with encapsulated MSCs, HAP microgranules and ECM, so it was difficult to observe the interior of the microcapsule membrane (fig. 4.7d). Unlike the Exp+HAP microcapsules, the interior matter (HAP microgranules and cells) mostly stayed inside the Osteo+HAP microcapsule interior after cutting. Encapsulated MSCs were attached and spread around and between HAP microgranules in the Osteo+HAP condition (fig. 4.7h). Additionally, the Osteo+HAP microcapsules had visibly more material in the interior of the microcapsules, compared to the Exp+HAP condition.

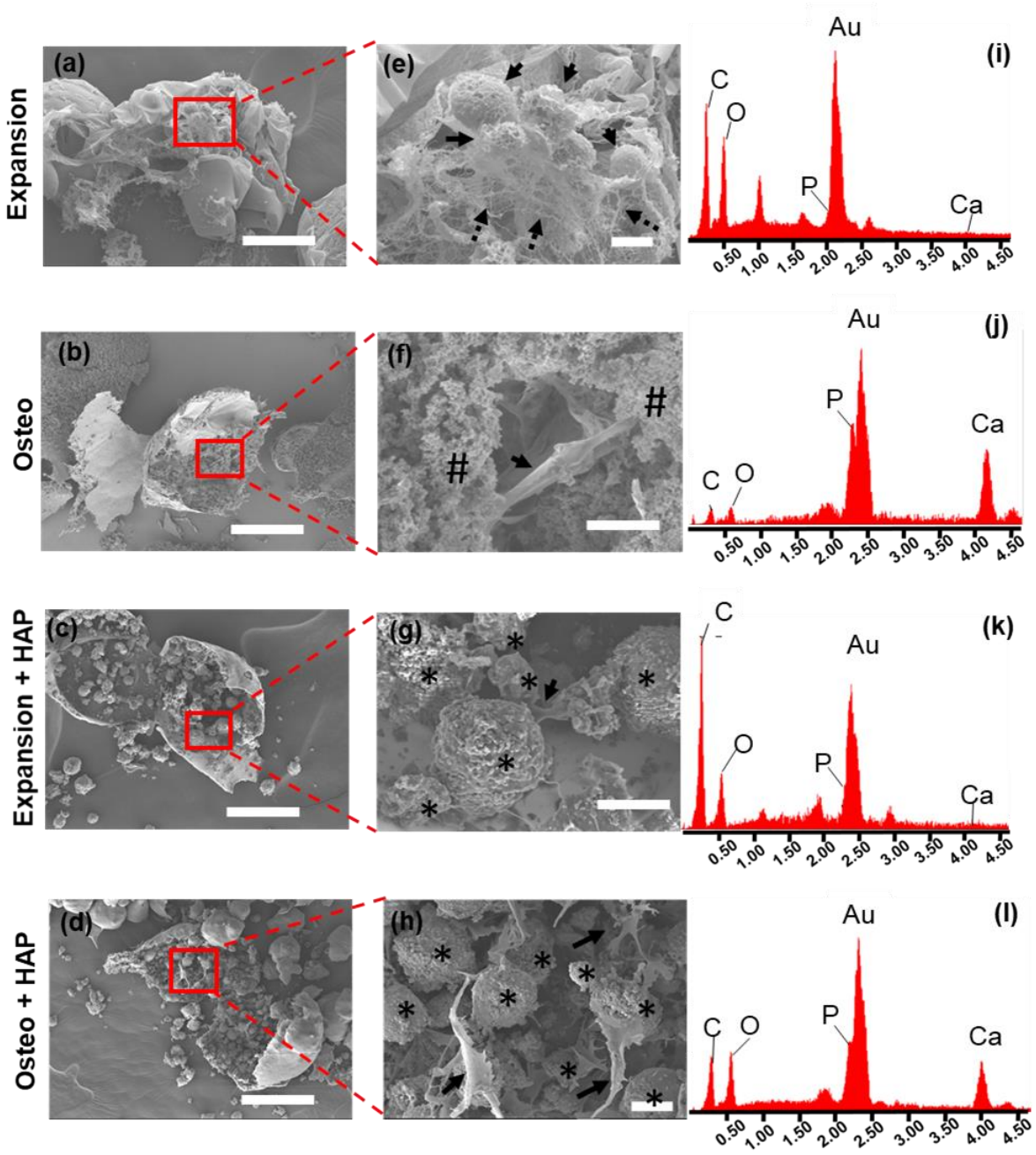

Fig 4.7: SEM images of internal capsule extracellular matrix (ECM). (a-d) SEM images of the inner cores of split capsules after 4 weeks of static culture in standard (Exp and Exp + HAP) and osteogenic (Osteo and Osteo + HAP) media (scale bar = 100 um). (e-h) Corresponding magnification of (a-d) (scale bar = 10 um). Black arrows denote cells and cell aggregates, dashed arrows denote fibrillar ECM, * denote HAP microgranules, and # denote

cell deposited crystalline mineral. (i-l) EDS spectra corresponding to SEM images (e-h), showing relative amounts of Calcium (Ca), Phosphorus (P), Carbon (C) and Oxygen (O).

Elemental analysis of the microcapsule interior revealed significant differences between the microcapsule conditions that depended mainly on whether the MSCs were induced to osteogenesis. EDS spectra for Exp microcapsules showed a low content of Calcium and Phosphorus, relative to the reference elements Carbon and Oxygen (fig. 4.7i). A similar EDS spectra was observed for Exp+HAP (fig. 4.7k). Despite the presence of HAP microgranules, the Exp+HAP capsules had a similar spectrum to the Exp microcapsules. Osteoinductive culture of encapsulated MSCs produced EDS spectra suggesting encapsulated MSCs actively mineralized the microcapsule interior with a calcium-phosphorus apatite. The EDS spectrum for Osteo microcapsules showed significantly higher levels of Calcium and Phosphorus, compared to reference elements (fig. 4.7j). A similar EDS spectra was observed for the Osteo+HAP microcapsules (fig. 4.7l). Table 4.1 shows the calcium/phosphorus ratios calculated from the EDS spectra for each microcapsule condition. Microcapsule formulations containing HAP microgranules had much higher Ca/P ratios than the conditions without microgranules, and these values (2.16 ± 0.21 for Exp+HAP and 2.41 ± 0.86 for Osteo+HAP) were like Ca/P ratios present in cortical bone *in vivo* [64, 65]. Most of the calcium and phosphorus present in the Exp+HAP sample likely came from HAP microgranules already included in the formulation, however it is impossible to separate HAP-associated calcium and phosphorus from cell-deposited elements in EDS spectra with the current apparatus. Osteo microcapsules without initial HAP microgranules also showed Ca/P ratios (1.69 ± 0.22) approaching *in vivo* bone. Data shows that encapsulated and osteoinduced MSCs can deposit a mineralized ECM with Calcium and Phosphorus content like HAP.

Microcapsule Condition	Bulk Ca/P ratio from EDX Spectra
Exp	0.31 ± 0.33
Exp+HAP	2.16 ± 0.21
Osteo	1.69 ± 0.22
Osteo+HAP	2.41 ± 0.86

Table 4.1 Ca/P ratios from EDS analysis of microcapsule interior

A closer SEM analysis of the microcapsule membrane and HAP microgranules in the microcapsule conditions revealed that actively mineralizing osteoinduced MSCs deposited substantial mineral on the membranes and microgranules. Acellular microcapsule membranes exhibit the rough surface of a porous hydrogel, without other materials (fig. 4.8a, g). The Exp microcapsule membranes appear significantly less porous and more smooth compared to acellular microcapsules, likely due to protein deposition on the membrane and in the pores during four weeks of culture (fig. 8b, h). In contrast, the membranes of the Osteo microcapsules are covered in mineral crystals of two phases: plate-like crystals roughly 1 um across and organized in a flowerlike configuration, with spherulite crystals found between the plates (fig. 4.8 c, i). The mineral crystals in the Osteo condition have the same plate and spherulite appearance as HAP observed in bone, particularly at the mineralization front [66-68]. Moreover, the mineral crystals on the Osteo membrane resemble those formed on other biomaterial systems containing C4S [69, 70]. Additionally, chitosan has demonstrated ability to nucleate HAP when combined with polyanionic additives (polyacrylic acid, for example) [71]. The C4S/chitosan polyelectrolyte capsule membrane serves as a favorable material that supports mineralization by osteoinduced MSCs.

The osteoinduced MSCs demonstrate a similar ability to modify the surfaces of HAP microgranules included in microcapsules. Neat HAP microgranules (not modified by

encapsulation or exposed to cell culture) display smooth facets between the grains of sintered HAP particles (fig. 4.8d, j). The HAP microgranules in the Exp+HAP microcapsules exhibit slightly rough (compared to neat HAP microgranules) facets of the microgranules due to protein deposition over four weeks of culture, but the surface of these microgranules still appears relatively unmodified. The actively mineralizing MSCs in the Osteo+HAP microcapsules significantly mineralized the surfaces of the HAP microgranules, and rough spherulite mineral crystals, about 1-2 μm in diameter, are shown protruding off the microgranule surface (fig. 4.8f). Higher magnification SEM images show the spherulites in the Osteo+HAP condition are composed of even smaller fused spherulites, 10-30 nm in diameter (fig. 4.8l). The spherulites growing off the HAP microgranules share similar size and shape characteristics with calcospherulites found in bone [72, 73]. Interestingly, only the spherulite mineral phase was observed in the Osteo+HAP microcapsules, while both the plate and spherulite phases were observed in the Osteo microcapsules. Crystal Nucleation Theory (CNT) suggests (with vindication through experiments) that the topography of a substrate determines the shape of the crystals nucleated on the substrate, by augmenting the free energy barrier the system must overcome for nucleation to proceed [74]. Surfaces containing pits, pores or cavities with acute angles and high curvature will decrease the surface energy cost of nucleation (decreasing surface energy relative to volume of crystal nuclei) compared with flat and relatively featureless surfaces [75]. Nucleation on a low curvature surface (such as the smooth surfaces of the HAP microgranules) will produce spherical crystals as the crystal nuclei seek to decrease their surface energy to volume ratio, to decrease the free energy barrier to nucleation [74]. In the Osteo+HAP microcapsules, the osteoinduced MSCs are mineralizing next to the HAP microgranites, causing the bulk of the mineral nucleation to occur on the HAP microgranule surface in this microcapsule condition. The flat surface of the HAP

microgranules makes the spherulite crystal the most energetically favorable phase for HAP to nucleate in this system; in contrast, the porous and rough membrane of the microcapsules provides several nucleation points that decrease the energy barrier to nucleation, making different (plate-like) crystal phase nucleation possible.

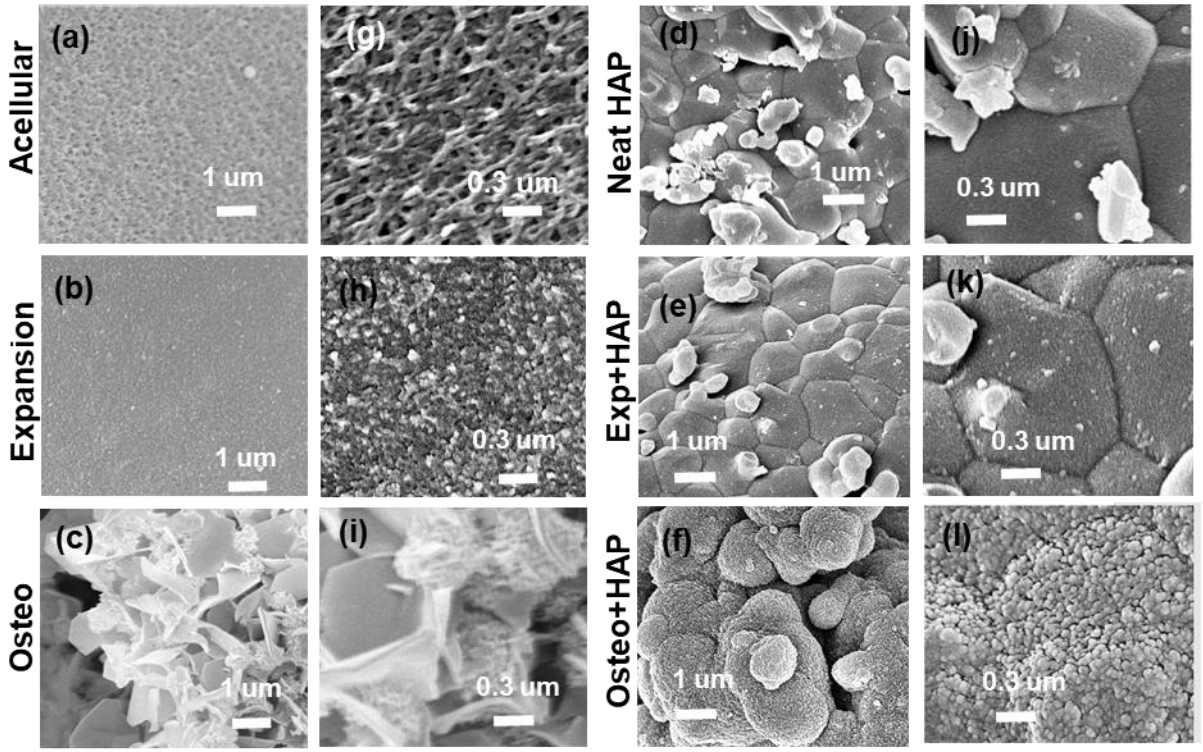

Fig 4.8 SEM of Microcapsule Membrane Mineralization. (a-c) SEM images of the interior surfaces of microcapsule membranes for Acellular, Expansion and Osteo microcapsule conditions. (d-f) SEM images of the surface of neat HAP microgranules, Exp+HAP microgranules, and Osteo+HAP microgranules. (g-l) Higher magnification images of a-f.

Another unique feature of the Osteo microcapsule condition was that MSCs migrated out of the microcapsule interior, and attached and spread on the mineralized exterior of the microcapsules. SEM analysis demonstrated that some Osteo microcapsules had MSCs growing on the mineralized exterior, with their lamellipodia spread out in what appear to be focal attachments

(fig. 4.9a-b). MSC migration and attachment on the exterior of other microcapsule conditions was not observed. The attachment of the MSCs to mineralized membrane was likely aided by ECM proteins that adsorbed on the mineralized microcapsule exterior [76, 77]. Moreover, the generation of a hypoxic environment in the Osteo microcapsule interior could have induced encapsulated MSCs to migrate to the microcapsules exterior since mineralization of the microcapsule membrane may have inhibited nutrient diffusion to the microcapsule interior [78]. Because the mineralization of the Osteo+HAP microcapsules was likely localized to the HAP microgranules, the Osteo+HAP microcapsule membrane maintained sufficient porosity so that normoxic conditions were maintained.

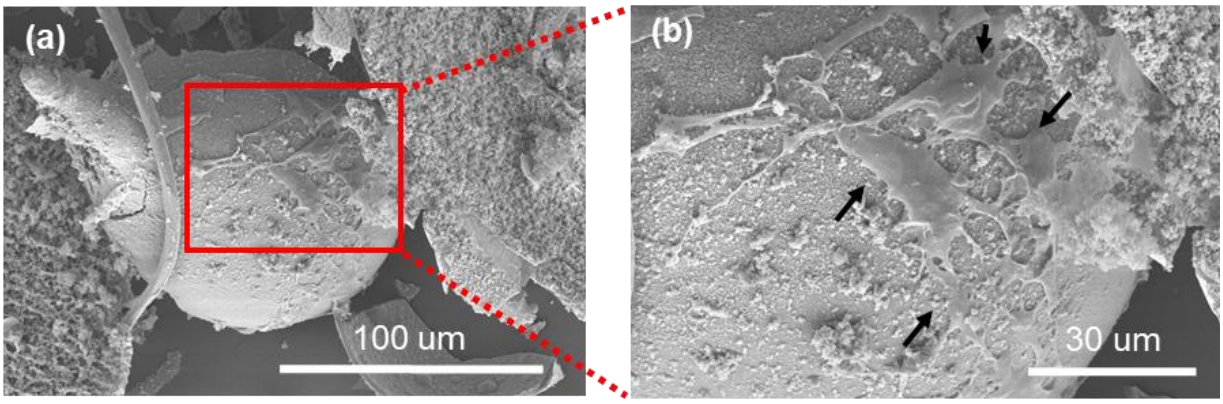

Fig 4.9 SEM of Cell Attachment on Osteo Microcapsules. (a) SEM image of cells attached and spreading on outer wall of Osteo microcapsules. (b) Higher magnification image of (a). Arrows denote attached cells.

4.5.6 Analysis of Growth Rate of Encapsulated MSCs

The SEM results show in some conditions, particularly the Osteo microcapsules, the capsule interior and capsule membrane may mineralize to such an extent that the mineral restricts nutrient flow to the encapsulated cells and restrict their proliferation. The results of alamarBlue® reduction (fig. 4.10a) show for Exp, Exp+HAP, and Osteo+HAP microcapsules, the percent

reduction of alamarBlue® generally increased over weeks 1-4 of culture, indicating more metabolic activity and (likely) a higher cell number in the microcapsule cultures after 3 weeks in culture. Interestingly, it appears that the percent reduction of alamarBlue® plateaus or slightly decreases after the second week of culture, indicating either no cell growth, a decrease in cell metabolism, or possible cell death. Calculation of the specific growth rate (fig. 4.10b) demonstrates that cells encapsulated in Exp had a similar growth rate over all 3 weeks of culture. Cells encapsulated in Exp+HAP and Osteo+HAP microcapsules appeared to show a decrease in specific growth rate during the 3 weeks of rotary culture, but the differences were not significant between each week. Interestingly, cells in the Osteo microcapsules had a significantly lower growth rate between weeks 2-3 than weeks 1-2 of culture (-0.010 ± 0.036 day^{-1} vs. 0.13 ± 0.036 day^{-1}, respectively), again indicating decrease in cell metabolism or possible cell death. Moreover, the Osteo growth rate between weeks 2-3 was significantly lower than the Exp microcapsules. The decrease in growth rate in Osteo microcapsules occurs at a similar time point with the microcapsule membrane mineralization observed from tetracycline fluorescence, and mineralization observed in SEM analysis of microcapsules. Analysis of the encapsulated cell growth rate suggests that microcapsule membrane mineralization may inhibit cell proliferation in Osteo microcapsules. The Osteo+HAP microcapsules did not show such pronounced decrease in cell growth rate, possibly due to lack of mineralization of microcapsule membrane (and preferential mineralization of HAP microgranules, discussed previously).

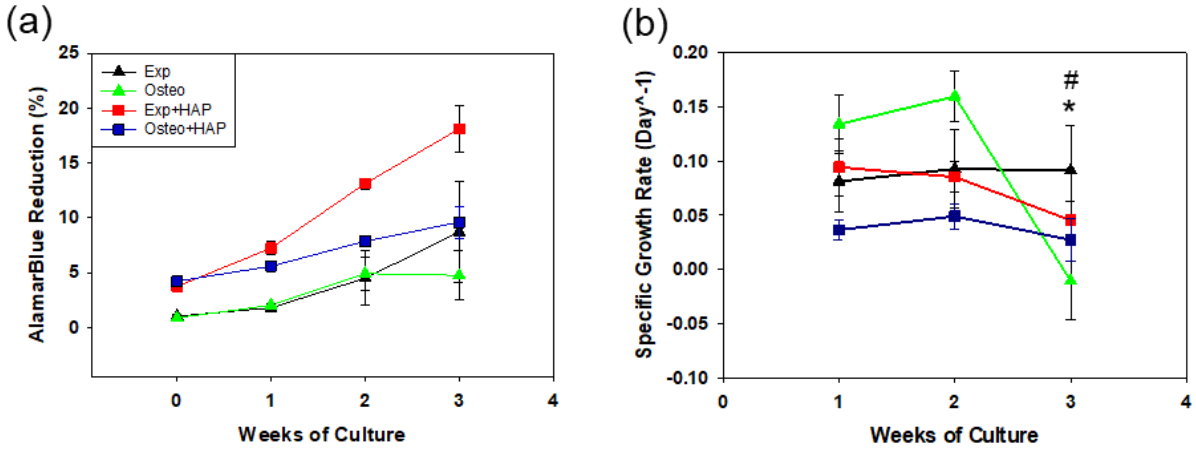

Fig 4.10 Growth rate of encapsulated MSCs exposed to medium flow. (a) Percent reduction of alamarBlue® over 3 weeks of rotary culture. (b) Specific growth rate computed from alamarBlue® reduction. * ($P < 0.05$) Osteo significantly different from previous time point. # ($P < 0.05$) Osteo significantly different from Exp at same time point.

4.6 Summary and Discussion:

For this first step in the characterization of the modular platform, we demonstrated that the microcapsule materials 1) maintain MSC viability and limited proliferation in static culture, 2) facilitate MSC osteogenesis, and 3) facilitate deposition of an osteoid/mineralized matrix within the microcapsule interior. The GAG/Chitosan/HAP microcapsules support encapsulated MSC viability over at least four weeks of static culture, and that viability is maintained during osteogenic induction of and subsequent mineralization by MSCs. The microcapsules facilitate osteogenesis of encapsulated MSCs as evident by the temporal secretion of early (ALP) and late (OC and OP) biomarkers for MSC differentiation to osteoblasts. Additionally, the osteogenesis promotes deposition of a calcium and collagen rich bone-like ECM, as well as mineral deposition within the microcapsule interior. Differentiating MSCs deposited mineral on the microcapsule membrane and encapsulated HAP microgranules. Interestingly, the morphology of the cell-deposited mineral depended on the substrate of mineral nucleation, which can be explained by CNT. Furthermore,

the C4S/chitosan microcapsule membrane proved a suitable substrate for mineral growth by actively mineralizing MSCs.

The four-week culture period used to generate *in vitro* tissue engineered bone microcapsules introduces significant lead time that would not be practical for clinical applications. However, this *in vitro* characterization of encapsulated MSC osteogenesis and bone-like ECM deposition validates the use of the microcapsules with the current GAG/Chitosan/HAP formulation as the basis for a bone regeneration platform. The base microcapsule materials, C4S and chitosan, have demonstrated Osteoinductive capability *in vitro* and *in vivo*, and chitosan has exhibited the potential to nucleate HAP when combined with a suitable polyanion [71]. Our *in vitro* results suggest that the combination of HAP and C4S can promote MSC osteogenesis to a limited degree, a feature also noted in the literature. These phenomena strongly suggest that the GAG/Chitosan/HAP microcapsules would regenerate bone *in vivo* if implanted with a suitable pre-osteoblast cell type. Moreover, the combined pro-angiogenic effects of C4S and chitosan [79-81] could promote the rapid vascularization of a GAG/Chitosan/HAP microcapsule construct after *in vivo* transplant in a bone defect.

CHAPTER 5: ANALYSIS OF MINERAL ARCHITECTURE ON FUSED CONSTRUCT MECHANICAL PROPERTIES

5.1 Introduction

A bone regeneration platform must replace the natural skeletal support and resistance to compression properties of natural bone. Ideally, the regeneration platform would have mechanical properties similar to native bone immediately upon implantation; however, this is more difficult with a modular system that uses cells to facilitate implant integration, as this often requires some initial soft-tissue component to be implanted with the hard tissue. In this chapter, fused constructs were fabricated from microcapsules, and the mechanical properties of the fused constructs were evaluated with respect to microcapsule mineralization from 4 weeks static culture, and for the effects of HAP microgranules. Additionally, the overall mineral density of fused constructs, as well as the density of the deposited mineral phase, were quantified and used to elucidate the effects of mineralization on fused construct mechanical properties. Results from this chapter will allow us to evaluate the mechanical properties a fused construct would have immediately upon implantation, and to estimate how a fused microcapsule construct would perform after mineralization *in vivo*.

5.2 Aim and Rationale:

The main specific aim of this chapter is to characterize how active mineralization of the microcapsules and HAP microgranules by the encapsulated MSCs influences the mechanical properties of fused microcapsule constructs. Additionally, the overall mineral density of the fused constructs, as well as the density of the mineral itself, will be characterized, and their relation to the mechanical properties of the fused constructs will be discussed. The rationale for this aim, is that examining the mineralization of the microcapsules in response to both MSCs and HAP microgranules in the capsule formulation will allow us to hypothesize how the mechanical

properties of our material will perform upon mineralization *in vivo*. Additionally, characterizing the mechanical properties in response to mineral organization and architecture will facilitate development and design considerations to optimize the materials included in the microcapsule formulation, and whether actively mineralizing cells are necessary for mechanical property enhancement. This aim is significant, because it will allow us to determine if our bone regeneration platform can approach the mechanical properties of native bone, and hypothesize whether improvements in microcapsule mineralization will affect mechanical properties of the fused constructs. Characterizing the response of fused construct mechanical properties to microcapsule mineralization will allow us to proceed with modifications of the microcapsule system that can enhance vascularization, and possibly bone regeneration, *in vivo*.

5.3 Experimental Approach:

Study 1: Evaluation of Mineralized Fused Construct Mechanical Properties.

Fused constructs were fabricated from microcapsules cultured for four weeks in static conditions, and the effects of active mineralization and/or HAP microgranules on fused construct elastic moduli and compressive yield point were evaluated.

Study 2: Quantification and Analysis of Fused Construct Mineral Density and Bone Volume.

The overall mineral density and organization of mineral in fused constructs was evaluated via MicroCT imaging, and the influence of HAP microgranule and osteogenic culture on mineral density and organization were evaluated. Results were used to better understand how microcapsule mineral content affects fused construct mechanical properties.

Study 3: Examine the Organization and Architecture of Mineral on Microcapsule Membranes.

Mineralization on the microcapsule membrane was analyzed via SEM and EDS, and results were used to better understand how the location of mineral within the microcapsule (on the membrane vs. in the bulk interior) affects the mechanical properties of the fused constructs.

5.4 Materials and Methods:

5.4.1 Fused Construct Assembly

Microcapsules from all conditions were cultured for four weeks (same conditions as 4.4.2), and subsequently assembled into fused modular constructs via a polyelectrolyte deposition between packed capsules (summarized in fig. 5.1). After four weeks, microcapsules were removed from culture, rinsed with 37 ºC PBS, and reloaded with a dilute polyanion solution (0.4% C4S/0.15% mCMC). After reloading, the microcapsules were transferred to a cylindrical mold with a mesh base (70 μm pore size). After draining excess polyanion solution, the mold was perfused with dilute chitosan (0.06% w/v) solution at a rate of 1 ml/min. The chitosan solution was drained, and the fused construct was further perfused with dilute polyanion and subsequently with 0.9% saline to remove unreacted polymers. The fused constructs were carefully removed from the mold, and placed in 0.9% saline at room temperature to await compressive mechanical testing.

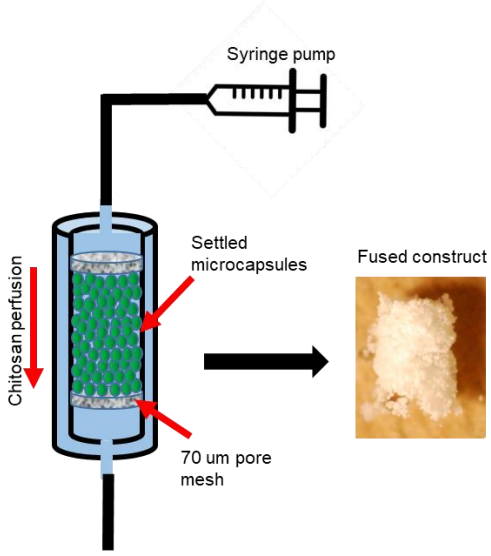

Fig 5. 1 : **Assembly of microcapsules into a fused construct**. This fusion method yielded self-supporting fused constructs, even when the microcapsules contained heavy (relative to the polyelectrolyte complex) HAP microgranules.

5.4.2 Mechanical Testing of Fused Constructs

Compression of fused constructs between parallel plates was performed on an MTS bionix 100 mechanical testing apparatus (MTS Systems Corporation, Eden Prairie, MN), with a constant strain rate of 0.1mm/min until failure in a 0.9% saline bath, as per literature and ASTM standards [82, 83]. Data was used to construct representative stress-strain plots, average yield compressive stresses, and elastic moduli for fused microcapsule constructs after 4 weeks of static osteoinductive or standard culture. The yield point will be defined as the point of transition from the elastic deformation (linear stress-strain behavior) to plastic deformation (non-linear behavior), and determined by reporting the stress value at a 0.2% strain offset. The elastic modulus will be calculated from the slope of the elastic portion of the stress-strain curve.

5.4.3 MicroCT Analysis of Fused Mineralized Constructs

After four weeks of static culture, microcapsules from all four conditions will be fused via the methods discussed previously, fixed in 10% neutral buffered formalin (NBF), and imaged via micro computed tomography (μCT). Acellular microcapsules containing HAP microgranules (referred to as Acellular HAP) will be fused and imaged as well, as a "blank" to differentiate between cell-deposited mineral, and HAP mineral already present in HAP microcapsules. Fused constructs were imaged in solution (sterile PBS/30% (w/v) sucrose as cryoprotectant) using μCT (μCT40, Scanco Medical, Brüttisellen, Switzerland) at 45 kVp, 177 μA (8W), 250 ms integration time, with a resultant isotropic voxel size of 8 μm. Image sets were calibrated to a series of known hydroxyapatite (HA) concentrations and processed with a Gaussian noise-reduction filter ($\sigma = 1.2$, support = 2). Each construct was manually outlined and a threshold of 75 mg HA/ccm was utilized for segmentation. The construct volume (TV), the bone/mineralized tissue volume (BV), bone volume fraction (BV/TV), apparent bone mineral density (BMD), and inherent bone tissue mineral density (TMD) were calculated using on-board Scanco software. BMD refers to the combined density of the hard and soft (mineral and hydrogel/ECM/cell body) components of the fused microcapsule constructs, and TMD refers to the density of the hard tissue components only. The BV/TV from Fused Acellular HAP microcapsules will be subtracted from the Exp+HAP and Osteo+HAP, to report data on cell-deposited mineral that contributes to BV/TV results.

5.4.4 SEM Analysis of Mineralized Membrane Cross-Section

The interior of the microcapsules was assessed via SEM in a protocol similar to section 4.4.6. After four weeks of culture, microcapsules were rinsed with PBS and fixed in 2.5% (v/v) glutaraldehyde/0.1 M cacodylate buffer (pH = 7.4) for 24 hrs at 4 C. The fixed microcapsules were then washed twice with PBS to remove glutaraldehyde, equilibrated with DI water for three

changes, frozen with liquid nitrogen, and lyophilized for 48 hours. After lyophilizing, the microcapsules were cut with a razor blade under a microscope to expose their cross-sections, and examined with SEM coupled with EDX spectrometry (JEOL 7600 FESEM, JEOL USA, Inc., Peabody, Massachusetts). For this study, special attention was given to high magnification analysis of the microcapsule membrane, as the bulk of the microcapsule interior was analyzed in section 4.5.5.

5.4.5 Statistical Analysis

Statistical analysis was carried out using GraphPad Prism software. All statistical comparisons were made by performing a one-way analysis of variance (ANOVA), followed by Bonferroni's multiple comparison tests to evaluate significance between two data sets at a time and correct for false positives of significance. P values less than 0.05 or 0.10 (for microCT analyses) were considered statistically significant. All data is reported as the mean $\pm$ standard deviation.

5.5 Results:

5.5.1 Compressive Mechanical Properties of Fused Microcapsule Constructs

Acellular microcapsules were fused into porous cylindrical constructs via the process depicted in fig 5.1, without exposure to culture medium, and their hydrated stress-strain mechanical properties were tested under uniaxial compression. Representative stress-strain curves for the acellular microcapsules are shown in fig. 5.2a (Empty and HAP microcapsules), and fig. 5.2b (Empty microcapsules only). The Empty microcapsules contained no load bearing element other than the polyelectrolyte microcapsule membrane, and the HAP microcapsules contained HAP microgranules as a reinforcement against compression. Thus, it is not surprising that the HAP microcapsules exhibited a noticeably higher average yield stress compared to empty microcapsules

(446.2 $\pm$ 27.4 kPa and 5.9 $\pm$ 1.1 kPa, respectively, fig. 5.2c). Results show that fused constructs containing HAP microgranules, without any additional mineral content, can provide some resistance against compression. Unfortunately, the yield stress of the HAP microcapsules falls short of native bone (131-205 MPa) [84]; moreover, the significant resistance to compression occurs after the constructs have been compressed roughly 50% of their height. The initial lack of resistance to compression during the test is likely due to water quickly evacuating the fused construct into the surrounding water bath, since all compression tests were unconfined (as per ASTM standards). Additionally, the microcapsules contained significant void space, even when HAP microgranules were included: recall from Chapter 4 that the maximum HAP microgranule content in the GAG solution that could be extruded to create microcapsules was 50% (v/v). The mechanical properties of the fused microcapsule constructs may be enhanced significantly if either more mineral was deposited in the void space in the microcapsule interior, or if the mineral was organized in such a way that it reinforced the microcapsule membrane to keep it from collapsing during the initial stages of compression. The rest of this study will focus on mechanical properties of fused constructs composed of microcapsules with an interior mineralized by osteogenic MSCs, as a model of how the microcapsules could perform when mineralized *in vivo*.

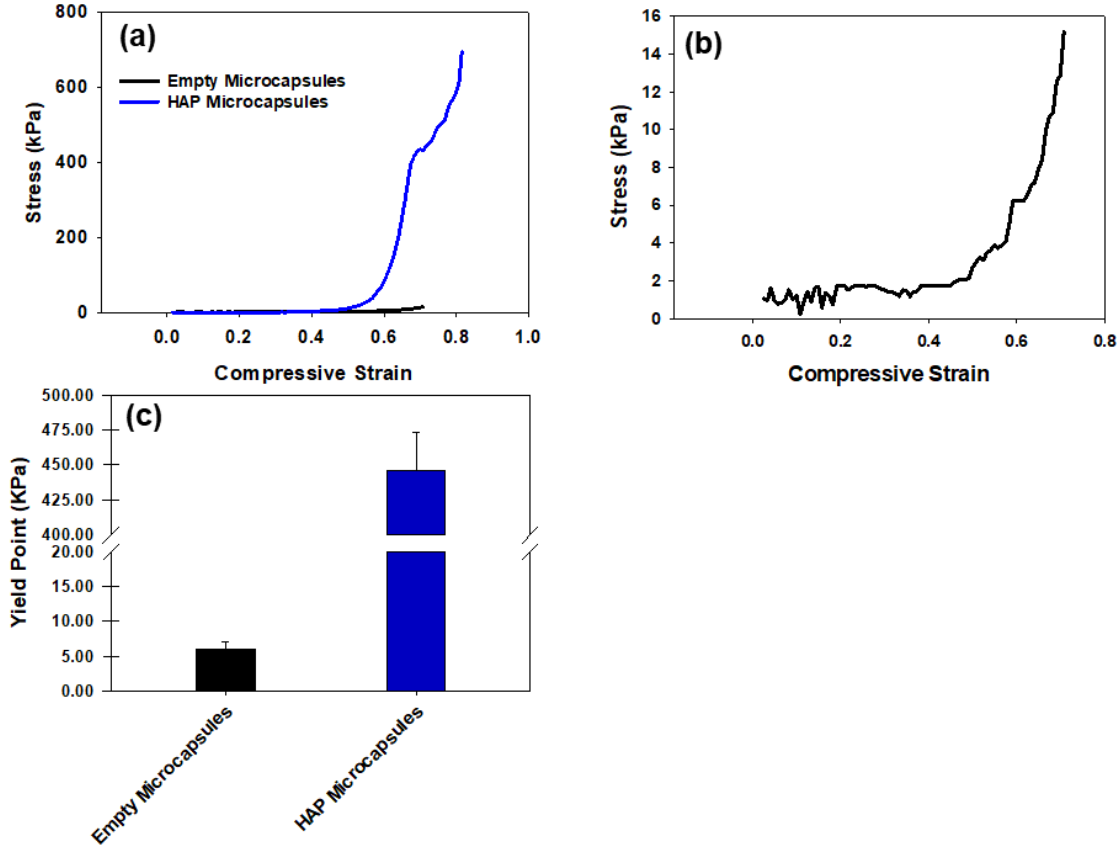

Fig 5.2: Compressive mechanical properties of acellular fused constructs. (a) Representative stress-strain curves for Empty and HAP microcapsule constructs, and (b) representative curve of Empty microcapsule constructs only. (c) Average yield point for both Empty and HAP microcapsule constructs.

To evaluate the effects of mineralization on fused construct mechanical properties, microcapsules containing MSCs were cultured for four weeks in osteogenic or standard media, and their hydrated stress-strain mechanical properties were tested under uniaxial compression. Representative stress-strain graphs of fused constructs demonstrate how active mineralization produced much more mechanically robust fused constructs (Fig. 5.3a). Both Osteo and Osteo+HAP fused constructs were capable of withstanding higher compressive stress at lower strains than both Exp+HAP (fig. 5.3b) and Exp (fig. 5.3c). The average yield point of actively mineralized microcapsules was significantly higher than either of the non-mineralized

microcapsule conditions ($P < 0.05$, fig. 5.4a). Moreover, the Osteo fused constructs had a significantly higher yield point (6.4 $\pm$ 2.8 MPa) than Exp+HAP fused constructs (0.5 $\pm$ 0.3 MPa), despite the inclusion of HAP microgranules in the Exp+HAP constructs ($P < 0.05$). There was no statistical difference in the average yield point between the Osteo and Osteo+HAP (6.4 $\pm$ 2.8 MPa and 10.4 $\pm$ 4.4 MPa, respectively) fused constructs ($P < 0.05$). The Exp+HAP fused constructs had a significantly higher average yield point than the Exp constructs (0.5 $\pm$ 0.3 MPa and 0.006 $\pm$ 0.001 MPa, respectively, $P < 0.05$). Furthermore, osteoinduction of the microcapsules significantly enhanced the elastic modulus of the fused constructs. The elastic modulus of the Osteo (43.9 $\pm$ 36.0 MPa) and Osteo+HAP (42.9 $\pm$ 34.6 MPa) fused constructs was significantly higher than constructs formed from the Exp (0.022 $\pm$ 0.011 MPa) and Exp+HAP (2.9 $\pm$ 0.4 MPa) microcapsules ($P < 0.05$, fig. 5.4b). Like the average yield point, there was no statistical difference in the elastic modulus between the Osteo and Osteo+HAP constructs. The Exp+HAP fused constructs also had a significantly higher elastic modulus than the Exp constructs ($P < 0.05$). Mechanical property results demonstrate that including HAP microgranules in the microcapsules can significantly enhance fused construct mechanical properties; however, microcapsule mineralization by osteoinduced, encapsulated MSCs drastically improved the mechanical properties of fused constructs, even without the aid of HAP microgranules.

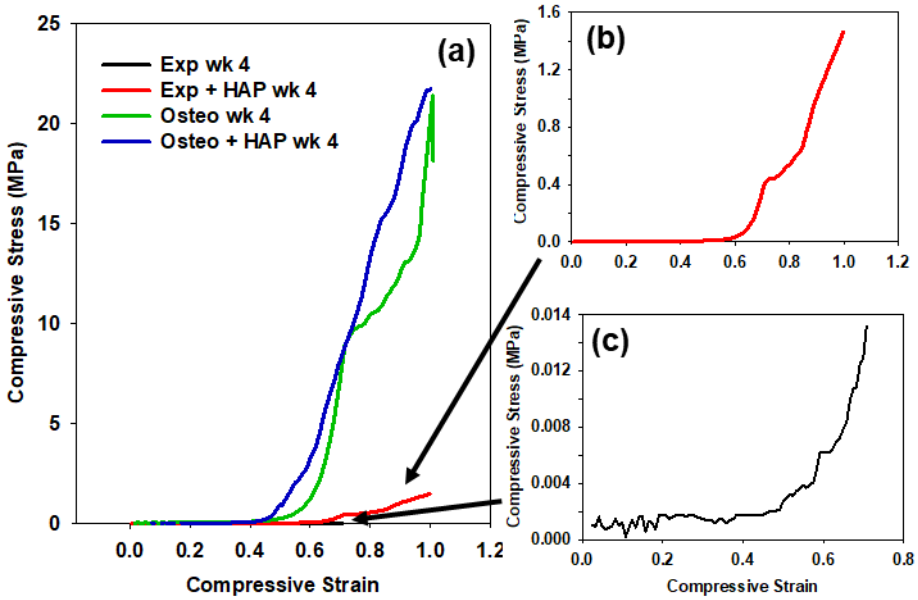

Fig 5.3: **Representative compressive mechanical properties of fused microcapsule constructs**. (a) All representative compressive stress vs. strain curves for each condition. (b) Magnified compressive stress curve for Exp + HAP wk 4 constructs. (c) Magnified compressive stress curve for Exp wk 4.

The mechanical property improvements in Osteo microcapsules likely stem from mineralization of the microcapsule membrane itself, rather than just mineral deposition around cell aggregates in the microcapsule interior. The actively mineralizing MSCs in the Osteo microcapsules may modify the polyelectrolyte membranes into a calcified-polyelectrolyte composite, transforming the microcapsules from soft polyelectrolyte hydrogel microcapsules, into microcapsules with a tougher calcified shell. The subsequent sections of this chapter will explore the organization and density of mineral in fused constructs composed of mineralized capsules.

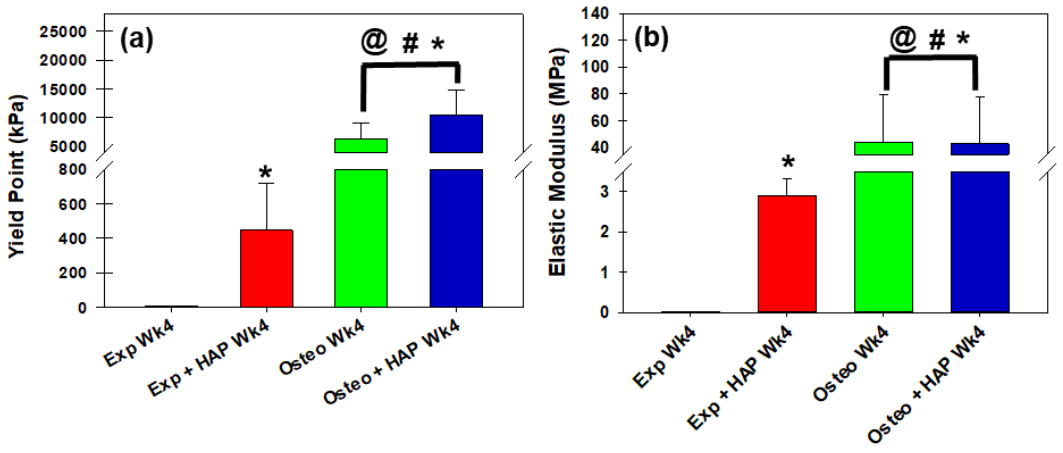

Fig 5.4: Average mechanical properties of fused microcapsule constructs. (a) Average yield point for fused constructs composed of microcapsules from 4 weeks of static culture in either osteoinduced (Osteo, Osteo+HAP) or standard (Exp, Exp+HAP) medium. (b) Elastic modulus of fused capsule constructs under compression. @ = No statistical difference between conditions. * = $P < 0.05$ (N=4) relative to Exp+HAP.

5.5.2 MicroCT Analysis of Fused Microcapsule Construct Mineral Density

MicroCT analysis of fused microcapsule constructs at a threshold of 75 mg HAP/cm^3 or greater density, revealed mineral content in the Exp+HAP, Osteo, and Osteo+HAP fused constructs assembled from microcapsules cultured for four weeks. The 75 mg HAP/cm^3 was chosen as a limit to distinguish sparse/immature mineral from surrounding hydrogel/tissue [85, 86]. No radiopaque mineral data was detected for the Exp microcapsules. The MicroCT images demonstrate (fig 5.5) that all microcapsules containing either HAP microgranules or cell-deposited mineral contained some mineral above the 75 mg/cm^3 density threshold for immature bone. Moreover, the microcapsules containing HAP microgranules in the formulation (Exp+HAP and Osteo+HAP) exhibited more overall mineralization than the microcapsules relying only on active mineralization by encapsulated MSCs (Osteo). Additionally, the Oste+HAP and Exp+HAP fused constructs appear to have more homogenously-distributed mineral throughout (fig. 5.5 e- f, h-i),

compared to the Osteo constructs (fig 5.4b-c). The microCT reconstructions demonstrate that the inclusion of HAP microgranules in the microcapsule formulation produces fused constructs with more homogenous mineral content. During microcapsule fabrication, a well-mixed GAG/HAP/MSC slurry will ensure that the droplets (and resulting microcapsules) extruded into chitosan will have relatively similar amounts of HAP microgranules. Because the HAP microgranules are much more dense than mineral deposited by osteoinduced MSCs *in vitro* (at least over the 4-week time period discussed here), the presence of HAP microgranules contributes the most to overall fused construct mineral content, exhibited by the more homogenous mineralization apparent in the Osteo+HAP fused construct (fig. 5.4d-f) compared to the Osteo fused construct (fig. 5.4a-c). It's interesting that the Osteo fused constructs had significantly higher compressive mechanical properties compared to the Exp+HAP constructs, despite the obvious lower overall mineral density. The increased mechanical properties may be a function of mineral organization, and not merely mineral content, in the fused microcapsule system discussed here.

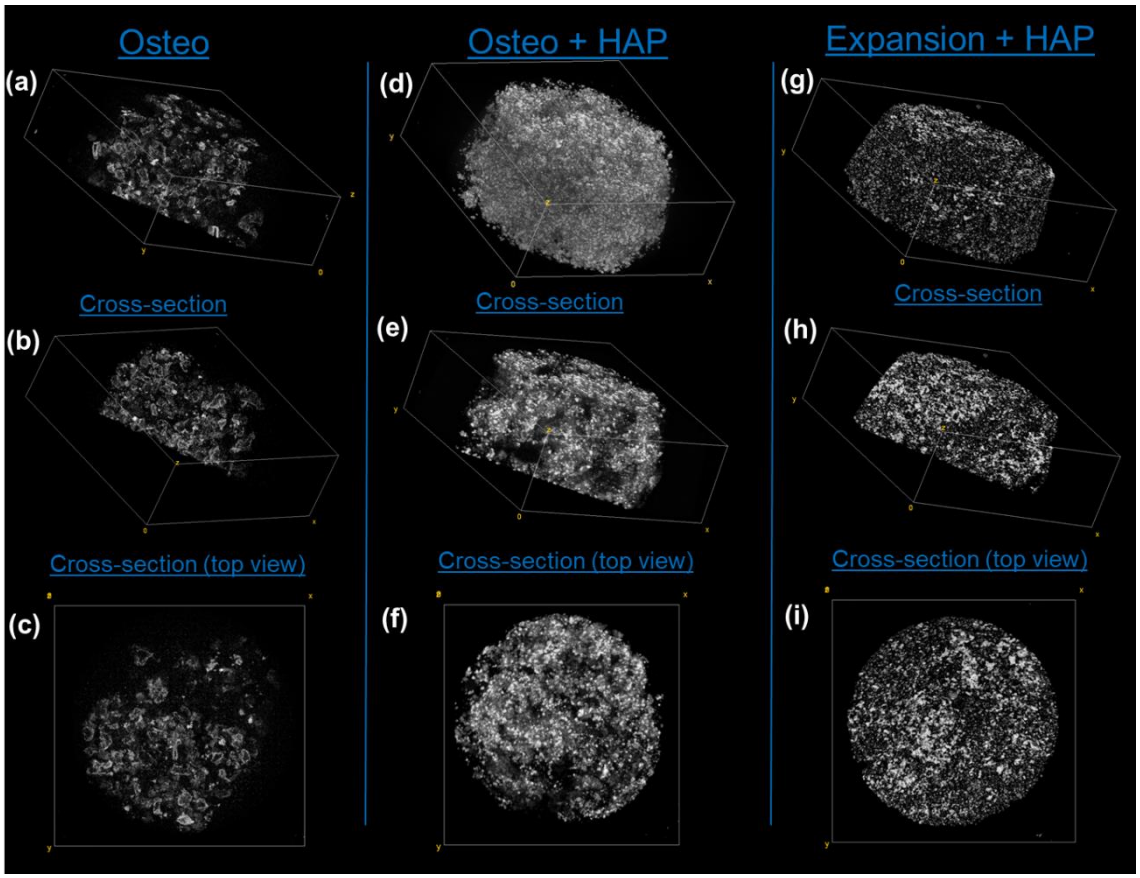

Fig 5.5: **Micro CT reconstruction of fused constructs at 75 mg HAP/cm^3 threshold**. (a-c) Osteo fused constructs, (d-f) Osteo+HAP fused constructs, and (g-i) Exp+HAP fused constructs. Mineral appears as gray (less dense) to white (most dense mineral) in reconstructed images.

A higher magnification look at the fused constructs elucidates differences in mineral organization in the microcapsule systems with and without HAP microgranules. Cutaways of 3D reconstructions of Osteo fused constructs demonstrate that actively mineralizing MSCs deposited radiopaque mineral that mostly nucleated around the C4S/chitosan membrane (fig. 5.6a-b). The cutaway shows the roughly spherical mineralized membranes of the Osteo microcapsules packed together in the fused construct (fig. 5.6b). Smaller points of mineralization, possibly not directly nucleated on the microcapsule membrane, are also present. The HAP microgranules included in

the Osteo+HAP condition were the dominant tomographic feature, shown as bright aggregates in the 3D cutaway (fig. 5.6c). Less intense tomographic material was present around the HAP microgranules, indicating cell-mediated mineralization around the HAP microgranules and microcapsule interior (fig. 5.6d). Unlike the Osteo microcapsules, it appears cell-deposited mineral nucleated around the already present HAP microgrnaules in the Osteo+HAP formulation. Fused Exp+HAP microcapsule constructs exhibited well-defined points of tomographic material from the HAP microgranules originally included in the Exp+HAP formulation (fig. 5.6e-f). The absence of any tomographic material between these bright, well-defined points suggests that any cell-mediated mineralization of these microcapsules was significantly less dense (below the 75 mg HAP/cm^3 threshold) than the actively mineralized Osteo and Osteo+HAP conditions. The closer look at the organization of mineral in the microcapsules indicates differences in organization, depending on the presence of HAP microgranules during microcapsule fabrication. This difference in mineral organization likely affects the overall mechanical properties of fused microcapsule constructs, as the strategic location of mineral to the microcapsule membrane, for example, can better reinforce the microcapsule membranes against compression, compared to loose mineral.

MicroCT analysis showed that active mineralization by osteoinduction of encapsulated MSCs contributes to the overall hard tissue volume above the 75 mg/cm^3 threshold after the four-week culture period (fig. 5.7). The Osteo+HAP fused constructs exhibited the highest overall BV/TV (0.52 $\pm$ 0.012) of the cultured microcapsule conditions, and this was significantly higher than the Exp+HAP (0.24 $\pm$ 0.15) ($P < 0.1$) and Osteo (0.067 $\pm$ 0.028) ($P < 0.05$) fused constructs. There was no statistical difference between the overall BV/TV of Acellular HAP and Osteo+HAP constructs. As previously discussed, the HAP microgranules make the most significant contribution to the overall BV/TV of the fused microcapsule constructs, if they are included during

microcapsule fabrication. When the cell-deposited BV/TV was assessed (BV/TV of Acellular HAP was subtracted from Exp+HAP and Osteo+HAP, fig. 5.7b), microCT analysis shows that actively mineralizing MSCs in both Osteo and Osteo+HAP constructs deposited similar levels of mineral above the 75 mg HAP/cm^3 detection threshold (0.067 $\pm$ 0.028 and 0.091 $\pm$ 0.012, respectively). Interestingly, the Exp+HAP had significantly less bone volume density than the acellular fused microcapsules constructs, as shown by the negative BV/TV value for the Exp+HAP after subtracting the fused construct blanks (-0.19 $\pm$ 0.15).

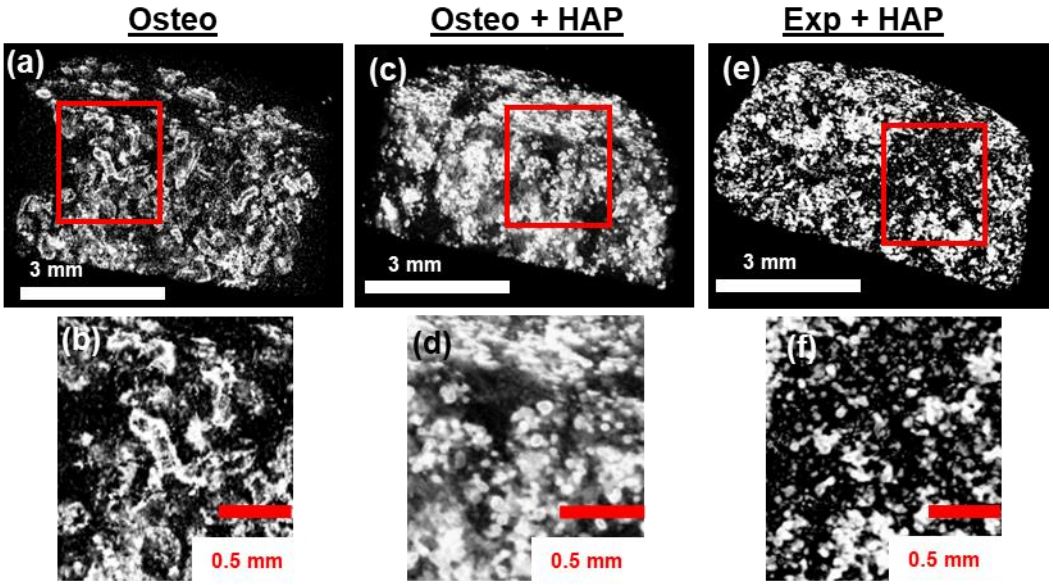

Fig 5.6: Higher magnification of microCT reconstruction of mineralized fused constructs. Images show cross sections of (a) Osteo, (c) Osteo+HAP, and (e) Exp+HAP fused constructs, along with higher magnification images of the inset in (b), (d) and (f), respectively.

MicroCT analysis was also used to investigate the density of the hard tissue/mineral components of the fused microcapsule constructs, or the Tissue Mineral Density (TMD). All fused microcapsule constructs had similar TMD (233.1 – 330.9 mg/cm^3), and there were no statistical differences among the conditions (fig. 5.7c). The constructs containing HAP microgranules would demonstrate high TMD values, due to the dense HAP microgranules included in these

formulations; however, the high density of the cell-deposited mineral in the Osteo fused constructs (233.1 $\pm$ 94 mg HAP/cm^3) was an interesting find. The osteoinduced MSCs deposit and remodel mineral into a similarly dense material as the HAP microgranules (307.5 $\pm$ 30 mg HAP/cm^3 for Acellular fused constructs). The TMD values for Osteo+HAP and Exp+HAP were similar (291.7 $\pm$ 16.3 and 330.9 $\pm$ 32.6 mg HAP/cm^3, respectively). Cortical bone has a significantly higher TMD of 1200 $\pm$ 53 mg HAP/cm^3 [87]. Of course, the BMD (mineral density of entire construct, including non-mineral components, fig. 5.7d) of all fused microcapsule constructs mirrors the overall BV/TV trend (fig. 5.7a), with the fused constructs containing HAP microgranules exhibiting higher BMD than the Osteo fused construct. The Osteo+HAP fused constructs had the highest BMD at 125.1 $\pm$ 13.7 mg HAP/cm3, but this is substantially lower than the average human BMD for cortical bone of 271 – 439 mg HAP/cm^3 [88]. Again, because the HAP microgranules contribute significantly towards the mineral density of the entire tissue volume, it is expected that the Acellular HAP, Exp+HAP and Osteo+HAP would have higher BMD than the Osteo fused constructs. These results indicate that an optimal microcapsule design for bone regeneration should include synthetic (or allogenic) bone mineral that closely matches the TMD of human bone, and as much mineral should be included in each microcapsule to increase the BMD to levels similar to human bone. Additionally, the results indicate that the osteoinduced MSCs deposit a mineral that is at least as dense as the synthetic HAP microgranules, and this mineral contributes to the compression resistance observed in Osteo fused constructs.

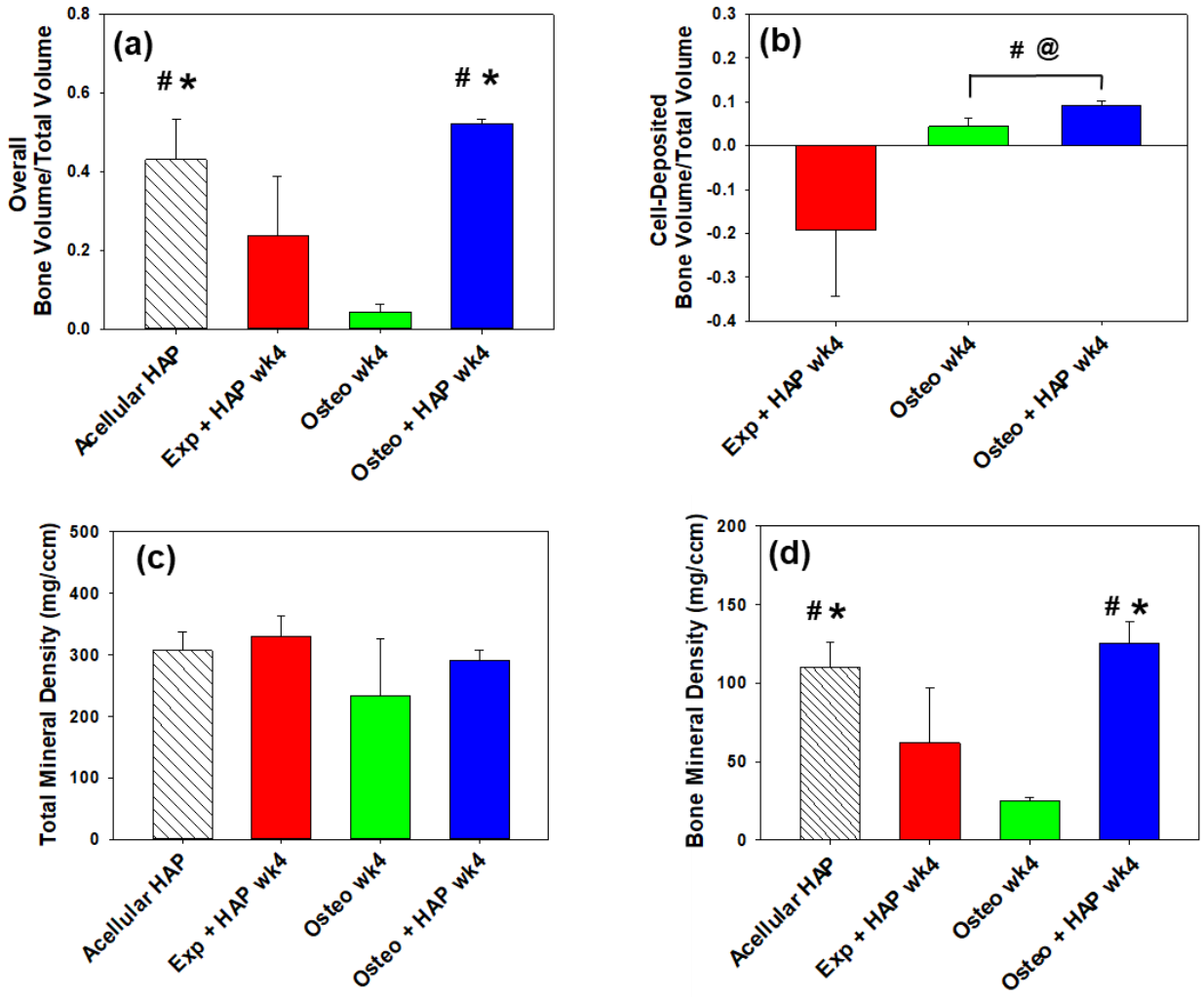

Fig 5.7: Mineral density of fused constructs. (a) Overall Bone Volume/Total Volume of fused constructs. (b) Cell deposited Bone Volume/Total Volume of fused constructs, determined by subtracting the BV/TV for Acellular HAP constructs from overall BV/TV for Exp + HAP and Osteo+HAP constructs. (c) Total Mineral Density (TMD) of fused constructs, and (d) Bone Mineral Density (BMD) of fused constructs. (N = 3) # $P < 0.1$ relative to Exp+HAP, * $P < 0.05$ relative to Osteo. @ $P < 0.1$ no statistical difference between conditions.

The significantly lower BV/TV of Exp+HAP fused constructs after 4 weeks of culture compared to freshly made acellular microcapsules with HAP microgranules is unexpected, and is likely due to the following factors. To form Exp+HAP microcapsules, the GAG/HAP slurry is mixed with a cell precipitate prior to encapsulation, while the GAG/HAP slurry is encapsulated

without additions to fabricate Acellular HAP microcapsules: the addition of cells (a soft tissue component) to the Exp+HAP microgranules dilutes the amount of HAP microgranules that can be included per microcapsule during encapsulation. Essentially, the Exp+HAP fused constructs will be composed of less minerally-dense microcapsules, because these microcapsules contain MSCs and HAP microgranules. Moreover, the MSC pellet would have contained some residual culture medium from the cell suspension after centrifugation, which would have affected the concentration of polyanion in the C4S/HAP/MSC suspension. The change in polyanion concentration would have affected the formation of the polyelectrolyte microcapsule membrane, and could have changed the swelling/stretching dynamics in the Exp+HAP microcapsules, compared to acellular microcapsules. Additionally, static culture of the Exp+HAP may have partially eroded the HAP microgranules, so that some of the HAP microgranule tomographic volume was under the 75 mg HAP/cm^3 threshold after four weeks of culture. The lysozymes in the culture medium (from the FBS) may have partially degraded the microcapsule membrane (lysozyme degrades the chitosan portion), causing the membrane to partially stretch after 4 weeks in culture and increasing cultured microcapsule volume compared to fresh microcapsules [89]. It is also possible that the microcpasules in the Exp+HAP fused constructs were less densely packed than freshly prepared microcapsules, leading to higher total volumes of construct: the microcapsules were settled by gravity in the capsule fusion apparatus, and the Osteo+HAP microcapsules would certainly be heavier, due to the added mineral from differentiating MSCs. The following parameters listed above introduce significant variations when comparing microCT data for cell-containing fused constructs with Acellular microcapsules to elucidate cell-deposited mineral contributions to BV/TV of fused constructs. Regardless, the microCT data shows that cells deposit a dense mineral

with a TMD value close to the HAP microgranules included in the microcapsule formulation, and that HAP microgranules have the greatest effect on overall TMD and BMD of fused constructs.

5.5.3 Mineral Architecture of Osteo Microcapsule Membrane

After the mechanical property analysis of the fused constructs suggests that the cell-mediated mineralization controls the overall compressive mechanical properties of fused microcapsule constructs, and the microCT reconstruction images show that highly dense mineral appears to be localized to the microcapsule membrane, we further characterized the mineral architecture of the Osteo microcapsule membranes via SEM. A cross-section SEM image of the Osteo microcapsules shows how the rigid, mineralized microcapsules retained their shape after cutting for SEM (fig. 5.8a). Additionally, a closer magnification on the inner surface of the microcapsule interior shows the rough, plate-like mineral crystals covering the interior (fig. 5.8b). When attention is turned to the cross-section area showing the microcapsule membrane, we see the relatively thin microcapsule membrane supporting a thick layer of mineral crystals, jutting from the membrane into the microcapsule interior (fig. 5.8c). This mineral layer had an average thickness of 4.8 $\pm$ 0.9 μm (n=3), and appeared to cover most of the interior surface of the Osteo microcapsules. Moreover, EDS analysis of the mineral on the Osteo microcapsule interior demonstrated the cell-deposited mineral had a Ca/P ratio similar to rat cortical bone [64]. In contrast, the surfaces of the Exp microcapsules were relatively featureless (fig. 5.8d), save for the porous C4S/chitosan membrane (fig. 5.8e). Additionally, the Exp microcapsule membranes couldn't support their own weight after the microcapsules were cut in half, and the membrane folded in on the microcapsules. Results indicate that the cell-deposited mineral in the Osteo microcapsules localizes primarily on the microcapsule membrane, and is of a similar quality (Ca/P ratio) to native rat cortical bone: it's likely this mineral organization and architecture that gives the

Osteo fused constructs a resistance to compression and elastic modulus similar to the Osteo+HAP fused constructs.

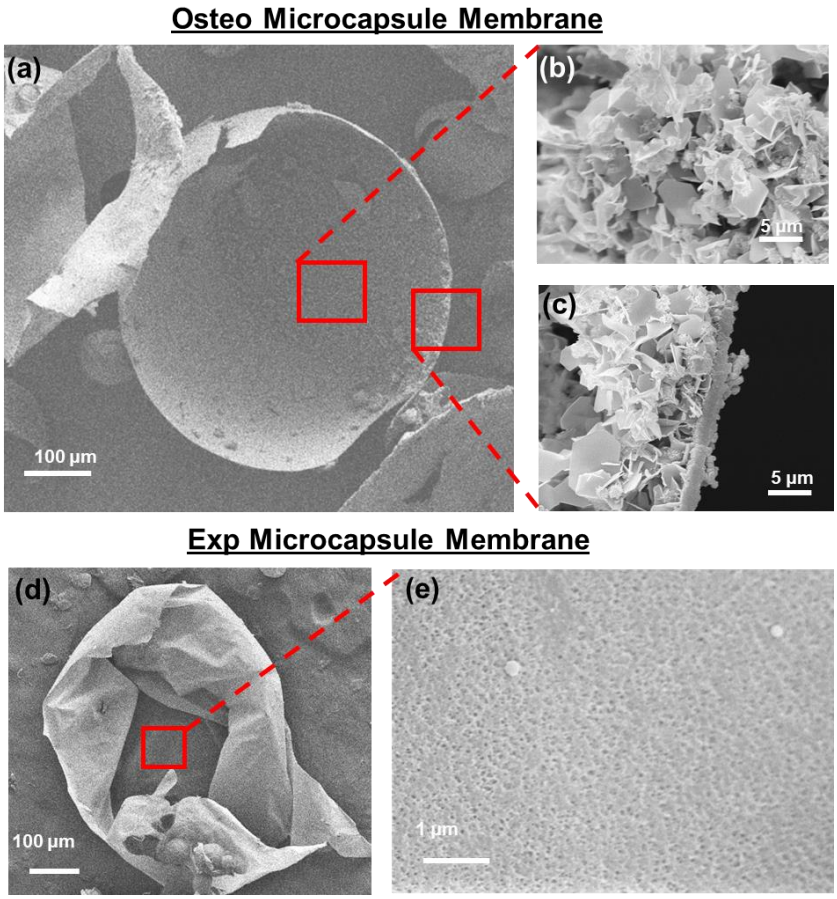

Fig. 5.8: Analysis of mineralization of microcapsule interior via SEM. (a) Macroscopic SEM view of mineralized interior of Osteo microcapsule. (b) Calcium phosphate mineral crystals nucleated and growing off of the interior of the Osteo microcapsule membrane. (c) Cross-section of microcapsule membrane edge showing thick mineral layer in interior. (d) Macroscopic SEM view of non-mineralized Exp microcapsules. (e) High magnification view of Exp interior membrane.

Microcapsule Condition	Bulk Ca/P ratio from EDS Spectra
Exp	0.31 ± 0.33
Osteo	1.69 ± 0.22
Rat Cortical Bone	1.96 ± 0.11

Table 5.1: EDS Analysis of Microcapsule Membranes compared to Rat Cortical Bone. Data for Rat Cortical bone obtained from [64].

After four weeks of osteoinduction culture, the encapsulated MSCs transform the Osteo microcapsules into calcified, compression-resistant spheres, with a relatively thick mineral shell. When these Osteo microcapsules are fused together to create a construct, the mineralized microcapsule membrane imparts significant resistance to compression for the entire construct, regardless of the lack of HAP microgranules in the interior. The organization of the mineral to the membrane of the Osteo microcapsules contrasts with the Osteo+HAP microcapsule condition: the SEM analysis in section 4.5.5 suggests that osteoinduced MSCs deposit mineral around and in-between HAP microgranules. Regardless, it is difficult to obtain a clear view of the microcapsule membrane in the Osteo+HAP SEM images, because the HAP microgranules and ECM obscure the interior of the membrane. The visible parts of the Osteo+HAP interior microcapsule membrane are relatively featureless compared to the Osteo membrane after 4 weeks of culture.

The mineralization of the C4S/chitosan microcapsule membrane could occur by several mechanisms. Encapsulated MSCs form aggregates that attach to the microcapsule wall early (see Chapter 4), and appear to remain attached for the duration of the microcapsule culture and osteoinduction. Research demonstrates that osteoblasts secrete vesicles containing amorphous calcium phosphate, that are released to the extracellular space [90]. Fig 5.9 shows several

mechanisms of vesicle-based mineralization. In one mechanism, intracellular vesicles accumulate calcium phosphate from mitochondria, and are exported to the extracellular space: alternatively, vesicles bud off from the osteoblast membrane, and accumulate calcium and phosphate ions (aided by vesicle-associated enzymes, like ALP) as they travel through the extracellular space [91]. Regardless of how the vesicles are loaded with calcium phosphate, the vesicles will travel through the extracellular space and nucleate HAP mineral upon contact with a suitable substrate. As previously discussed, C4S and chitosan are capable of mineralization by nucleating calcium and phosphate [69, 70, 92]. Additionally, osteoinduced MSCs deposit collagen, which promotes calcium phosphate nucleation and mineralization *in vivo* [93, 94]. While MSCs are osteoinduced during microcapsule culture, they release mineralizing vesicles in 360º, and enough of these vesicles contact the C4S/chitosan membrane and deposited collagen matrix that the microcapsule membrane becomes relatively homogenously mineralized over the 4 week culture period. Results demonstrate that the materials in the microcapsule design facilitate robust mineralization via encapsulated MSCs through a vesicle-based mechanism, and this mineralization could likely be duplicated *in vivo* by vesicle-secreting osteoblasts near a bone injury site, or by osteoinduced MSCs implanted within the microcapsules.

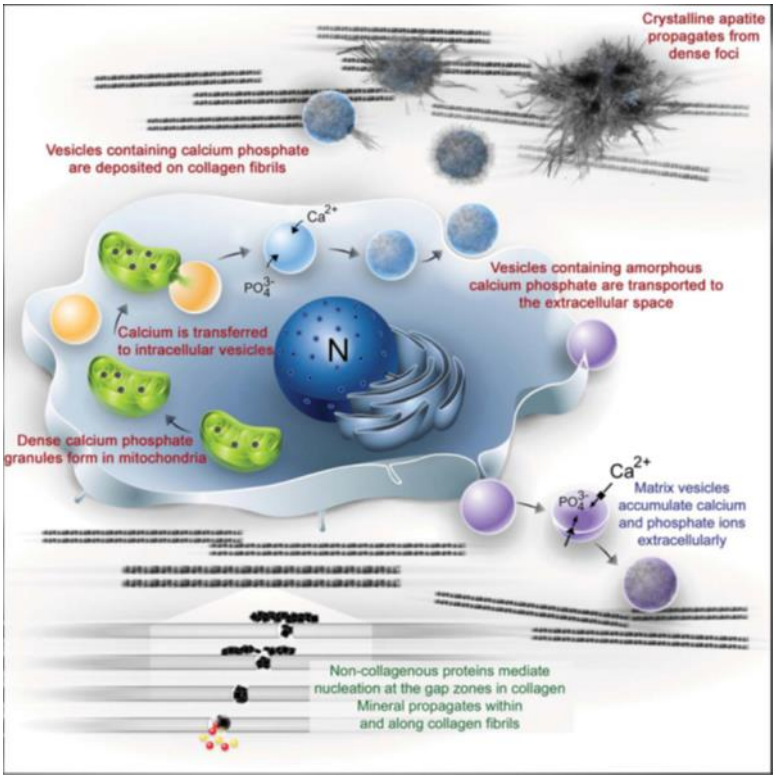

Fig. 5.9 Mechanisms of osteoblast ECM mineralization by vesicles. Diagram shows osteoblasts secreting vesicles containing calcium phosphate, which nucleate to form mineralized HAP on the ECM in developing bone. Image taken from [90]

5.6 Summary and Discussion:

Analysis of the compressive mechanical properties of the fused microcapsule constructs show that active mineralization by osteoinduced MSCs significantly enhances the compressive yield stress and elastic moduli of the fused constructs. This is somewhat intuitive; however, it was interesting to find that mineralization of the microcapsule membrane in microcapsules without HAP produced mechanical property improvements similar to microcapsules fabricated with HAP microgranules. Regardless, the addition of HAP microgranules to the microcapsule fabrication is beneficial for several reasons, including 1) superior mechanical properties prior to additional mineralization (compared to empty microcapsules), 2) ease of handling, as the HAP microgranules cause the microcapsules to settle out of suspension in a solution, and 3) providing a substrate for

encapsulated MSCs to attach to, which could confer benefits to proliferation and osteogenesis [95-97]. Future iterations of the basic microcapsule design discussed here should include some sort of dense mineral microgranule/interior to enhance encapsulated cell osteogenesis and impart initial resistance to compression to the microcapsules.

Human bone itself is an anisotropic tissue, and the mechanical behavior (average values of compressive stress and elastic moduli) varies with the direction of the applied load during measurement. Additionally, the difference in mineral density and porosity in the trabecular and cortical regions influence the mechanical properties of the tissue. Table 5.2 provides a summary of the average mechanical properties of human bone, compared to the fused constructs described in this study and some other *in vitro* scaffold systems from the literature. Cortical bone has a compressive stress and elastic moduli that ranges from 131-205 MPa and 6,000 – 20,000 MPa, respectively, while trabecular bone has compressive stress and elastic moduli ranges of 5-10 MPa and 50-100 MPa. Unfortunately, the modular construct with the closest mechanical properties, Osteo+HAP, falls very short of human cortical bone compressive stress (10.4±4.4 MPa vs. 131 MPa) and elastic moduli (42.9±30.5 MPa vs. 6,000 MPa). The Osteo+HAP fused constructs are somewhat comparable to the mechanical properties of trabecular bone (5 MPa compressive stress and 50 MPa elastic modulus). It's likely that after implantation, the mechanical properties of the fused construct design proposed here would drastically improve above the values from the *in vitro* mineralization, due to exposure to the growth factor milieu encountered *in vivo*.

Tissue Type	Compressive Stress	Elastic Modulus
Human Cortical Bone	131 - 205 MPa [84]	6,000-20,000 MPa [84]
Human Trabecular Bone	5-10 MPa [98]	50 - 100 Mpa [99]
Modular Osteo + HAP (4wk in vitro mineralization)	*10.4 ± 4.4 MPa*	*42.9 ± 30.5 MPa*
Calcium-Phosphate Alginate Hydrogel	4 ± 0.8 MPa [100]	1200 ± 200 MPa [100]
Polycaprolactone – HAP Composite	2.2 ± 0.2 MPa [101]	21.4 ± 1.4 MPa [101]
Poly(D,L-lactic acid-co-glycolic acid) – HAP composite (6 wk *in vitro* mineralization)	N/A	18.9 ± 8.1 MPa [102]

Table 5.2 Comparison of Modular Osteo+HAP fused construct mechanical properties to human bone and bone biomaterials cultured in vitro.

When compared to other bone regeneration systems analyzed *in vitro*¸ the mineralized fused microcapsule constructs certainly have competitive mechanical properties. Table 5.2 includes the yield stress and elastic moduli from several published studies for comparison: the Calcium Phosphate Alginate Hydrogel system is of particular note, since their system combines human umbilical cord mesenchymal stem cells (hUCMSCs) encapsulated in alginate microcapsules, embedded in a calcium phosphate bone cement [100]. Compared to this alginate/cement modular system, the Osteo+HAP constructs have a higher yield stress (4 MPa vs. 10.4 MPa, respectively), while their elastic modulus was significantly larger (1,200 MPa vs. 42.9 MPa), indicating a stiff but brittle system, likely due to the calcium phosphate cement. It should be noted that the only porosity in the alginate/cement system would occur when the alginate beads degrade, whereas the modular system presented here has inherent porosity between the fused microcapsules immediately after fusion, which would likely enhance cell infiltration once implanted in a bone defect. Several other modular bone tissue engineered systems reported in the literature do not include data on *in vitro* mechanical properties for their system, and therefore it is difficult to comment on how the modular system presented here improves upon these systems [103, 104].

Interestingly, the microCT analysis revealed that all fused construct formulations that included HAP microgranules in their formulation had significantly more mineral per volume than the Osteo microcapsules, yet the Osteo and Osteo+HAP microcapsules had similar elastic moduli and yield stress. The localization of the mineral to the microcapsule membrane, reinforcing the membrane against compression, demonstrates that the mineral architecture primarily affects the

fused construct mechanical properties. Reports from the literature concur that overall mineral density alone does not determine bone mechanical properties, and properties including porosity, degree of trabecular interconnectivity, and the plate or rod configuration of mineral also affect the overall mechanical properties of bone [105-108]. The study presented here adds to the literature from a biomaterials perspective, and demonstrates with a novel system that it's not merely the amount of mineral, but where it's located within the system, that matters. The ability to influence mechanical properties of the microcapsule system by localizing mineral to the membrane could give inspiration for further iterations of the microcapsule design, such as microcapsules containing HAP microgranules and an exterior calcified shell for added reinforcement.

As discussed in Chapter 4, the four week culture period adds significant lead time for clinical applications, if the mineralized microcapsules were to be implanted. The mechanical property analysis discussed in this chapter demonstrates that mineralization by osteoinduced MSCs significantly reinforces the microcapsule fused constructs against compression: this result should be replicable *in vivo*, either through the addition of osteogenic growth factors to the microcapsule system (BMP-2, etc…), or from the interaction with growth factors secreted physiologically at the implant site [109]. Moreover, it is likely that tissue ingrowth through the fused construct, combined with subsequent mineralization *in vivo*, will significantly enhance the mechanical properties of fused construct implants, facilitating bone regeneration. The next series of experiments will focus on examining the host response, tissue regeneration and vascularization in fused constructs fabricated form microcapsules containing vascularization-enhancing accessory cells in a subcutaneous model of ectopic bone formation.

CHAPTER 6: ANALYSIS OF FUSED CONSTRUCT VASCULARIZATION and TISSUE REGENERATION *IN VIVO*

6.1 Introduction

Bone is a highly-vascularized tissue, and implants generated from GAG/Chitosan/HAP microcapsules should ideally vascularize rapidly after implantation to provide nutrients to cells implanted with the microcapsules, and the facilitate tissue growth into the implant. The ability to attach and culture accessory cells on the exterior of the microcapsules offers a unique strategy to control the organization of multiple cell types in an implant. Attaching endothelial-like cells to microcapsules prior to fusion into a construct will pre-vascularize the construct, and place blood vessel forming cells in the fused construct pore space. The organization of endothelial-like cells to the intercapsule pore space of the fused construct can help promote rapid vascularization of the construct *in vivo*. This chapter details the process of differentiating MSCs to endothelial progenitors (EPs) containing some endothelial character and function, and examining how the attachment of EPs to the exterior of microcapsules containing encapsulated osteoprogenitors (OPs) influences vascularization of fused constructs *in vivo*. The *in vivo* analysis will be conducted in a rat subcutaneous model, and vascularization will be analyzed via Doppler Ultrasound (US). Moreover, the tissue infiltration and matrix composition within the implants will be evaluated over the course of the life of the implants *in vivo*. The influence of EPs over vascularization, tissue ingrowth and matrix deposition will be compared to MSCs attached to the microcapsule exterior, and to microcapsules without accessory cells.

6.2 Aim and Rationale:

The specific aim for this chapter is to characterize the *in vivo* response to fused constructs composed of GAG/Chitosan/HAP microcapsules and vascularization-enhancing accessory cells. Attention will be paid to blood flow and blood vessel construction through implanted constructs.

The rationale for this aim, is that attaching vascularization-enhancing accessory cells (Endothelial Progenitors) to the microcapsule exterior will enhance vascularization and new-bone regeneration *in vivo.* This aim is significant, because it will provide preliminary data on how our modular bone graft design with accessory cells performs *in vivo* with respect to immune response, tissue regeneration, and vascularization. Confirming that the addition of appropriate accessory cells enhances the vascularization of the fused constructs *in vivo* will facilitate later optimization of the bone graft system, by optimizing cell type and ratio of vascular cells to fused construct volume.

6.3 Experimental Approach:

Study 1: Confirm Accessory Cells can Attach to GAG/Chitosan/HAP Microcapsules

EP cells were generated from MSCs using established protocols, and examined for the expression of endothelial markers and tube formation in basement membrane. EP cells were seeded on to GAG/Chitosan/HAP microcapsules and examined for attachment via cell fluorescence and SEM. This study allows us to confirm that MSCs can be differentiated to EPs that express endothelial markers, and that GAG/Chitosan/HAP Microcapsules support accessory cell attachment.

Study 2: Examine Blood Flow Through Fused Constructs *in vivo* via Doppler Ultrasound (US)

Disk constructs formed from fused microcapsules with attached accessory cells were implanted subcutaneously in the backs of rats, and imaged at 1, 2, and 4 weeks post-surgery via Doppler US to observe blood flow through the constructs. The microcapsules contained encapsulated osteoprogenitors (OP) to promote bone formation in the constructs *in vivo*. The ability of EPs to enhance construct vascularization will be compared to an MSC control, microcapsules without accessory cells, and completely acellular microcapsules. This study allows us to characterize blood flow through the implanted constructs in real time, and investigate whether EPs enhance fused construct vascularization.

Study 3: Evaluate Tissue Regeneration in Fused Constructs *in vivo* via Histology.

After each Doppler US imaging session, implanted constructs will be harvested and assessed for tissue regeneration via histology. Attention will be paid to the type and organization of matrix, immune cell response, and blood vessel formation within the implants over the 4-week *in vivo* period. This study allows us to confirm that the fused microcapsule system can support *in vivo* tissue regeneration without a detrimental immune response, and that the addition of accessory cells enhances tissue regeneration.

6.4 Materials and Methods:

All materials and reagents used were purchased from Sigma-Aldrich (St. Louis, MO) unless otherwise noted, and were of analytical, cell culture grade or higher. Sprague Dawley rats were purchased from Envigo (Huntington, UK).

6.4.1 Cell culture conditions

MSCs were differentiated to OPs for 3 weeks prior to encapsulation in C4S/chitosan microcapsules, to promote ECM deposition and possible mineralization *in vivo* within the microcapsules. All cells were cultured in a humid atmosphere with 5% CO_2 at 37 ºC. MSCs were induced to osteogenesis using the same method and osteoinduction medium as section 4.4.2: MSCs were cultured for 3 weeks in L.DMEM supplemented with 10% FBS, 100 nM dexamethasone, 10 mM β-glycerophosphate, and 50 μM ascorbic acid-2-phosphate. Representative cultures were stained with Alizarin Red S after 3 weeks of differentiation, and inspected for the presence of red-stained mineral nodules to confirm differentiation to OPs. Briefly, 3 weeks after differentiation, cultures were washed with PBS, fixed in 10% neutral buffered formalin (NBF) overnight, and washed again with DI water (3x, 5 min each). Cultures were then incubated in Alizarin Red S working solution (2% (w/v) pH 4.2, adjusted with ammonia) until red lakes began to form on the

cell monolayer (after 10 minutes), after which the Alizarin Red S solution was aspirated, and residual staining removed by a brief wash with DI water. Cultures were viewed under brightfield microscopy for orange/red-stained mineral nodules. Microcapsules were formed via the same protocol as section 4.4.2., and OPs were encapsulated at a density of 5 million cells/ml C4S/HAP suspension. Microcapsules with OPs were immediately processed for collagen coating after encapsulation, described in 6.4.3 below.

6.4.2 Differentiation of MSCs to EPs

MSCs were differentiated to an endothelial lineage (EPs) via an established protocol [110, 111]. MSCs at passage 1 were seeded at $5x10^3$ cells/cm^2 and maintained for 10 days in endothelial differentiation medium, consisting of 100 ng/ml VEGF, 50 ng/ml EGF, 1 µg/ml hydrocortisone, and 5% FBS in L.DMEM. Differentiation to EPs was validated via assessment of tube formation in basal membrane (Matrigel ®, Dow Corning, Midland, MI), and immunofluorescent staining of the common endothelial markers von Willibrands Factor (vWF) and Platelet Endothelial Cell Adhesion Molecule 1 (PECAM-1). For the Matrigel assay, 50 µl of Matrigel was gelled in each well of a 96 well plate. EPs were trypsinized after 10 days of endothelial differentiation, and plated at a density of $5x10^3$ cells/cm^2 onto the surface of the Matrigel. The ability of the EPs to form tube-like networks on Matrigel was assessed between t=0 (when the cells were plated) and t=12 hrs. If MSCs were properly differentiated to EPs, these EPs should form tube-like networks in the absence of angiogenic growth factors like VEGF [110, 111]; so, EPs were seeded onto the Matrigel in standard medium (L.DMEM+5% FBS) without VEGF supplement. MSCs seeded in standard medium served as a negative control, and MSCs seeded in medium supplemented with 50 ng/ml VEGF served as a positive control.

For PECAM-1 and vWF staining, cells grown on plastic were washed with PBS, and permeabilized with 0.25% (v/v) Triton X-100 at room temperature for 40 minutes. Permeabilized cells were washed 3x with PBS (5 min each), and blocked with 1% (w/v) bovine serum albumin (BSA) in PBS for 1.5 hrs. Cells were then washed 3x with PBS (5 min each) and incubated with primary antibody. Primary antibodies for vWF staining and PECAM-1 were Anti-von Willebrand Factor IgG antibody produced in rabbit (Sigma-Aldrich, St. Louis, MO), and Anti-PECAM-1 IgG1 antibody produced in mouse (EMD Millipore, Darmstadt, Germany), respectively, and each was diluted 1:50 in 1% BSA/PBS. Cells were incubated with primary antibodies at 4 ºC overnight. After overnight incubation, primary antibody solutions were removed and cells were washed 3x with PBS (5 min each), and the secondary antibodies were applied to cells and incubated at room temperature on a shaker for 2 hours. Fluorescein Isothyocyanate (FITC) conjugated secondary antibodies for vWF and PECAM-1 were Anti-rabbit IgG-FITC and Anti-Mouse IgG-FITC, respectively, and were diluted 1:50 in 1% BSA/PBS. All work with secondary antibodies was performed in the dark, to prevent FITC photobleaching. Cultures without incubation in primary antibodies were incubated in secondary antibodies as a negative control. After 2 hours incubation, cells were washed 3x with PBS (5 min each), and DAPI solution (1 µg/ml PBS) was applied to stain nuclei for 5 minutes. DAPI was removed, and cells were washed 3x with PBS, and imaged for vWF and PECAM-1 expression. vWF and PECAM-1 expression of EPs was compared to a negative control of undifferentiated MSCs.

6.4.3 Coating Microcapsules in Collagen and EPs

To facilitate accessory cell attachment to the microcapsule exterior, microcapsules were coated with an adsorbed layer of collagen Type 1 prior to external cell attachment using an established protocol [7]. All reagents used were sterile and used at 4 ºC unless otherwise noted.

Microcapsules were washed with dilute chitosan solution (0.06% (w/v) chitosan in 0.04% (v/v) acetic acid) for 2 min, washed briefly with 0.9% (w/v) saline, and washed with dilute collagen solution (0.2 mg collagen Type 1/ml in 1 mM acetic acid) for 2 min. Collagen solution was removed, and coated capsules were washed briefly with 0.9% saline, and equilibrated with L.DMEM for 30 minutes. During coated capsule incubation, accessory cells (MSCs and EPs) were trypsinized, centrifuged, and seeded at a density of $5x10^5$ cells per ml of settled microcapsules in 37 ºC medium. The cell suspension was incubated with the microcapsules at 37 ºC for 60 minutes, with gentle resuspension every 10 minutes, to facilitate attachment of accessory cells to coated microcapsules. After incubation, seeded capsules were transferred to culture dishes for 48 hours in standard media at 37 ºC prior to capsule fusion.

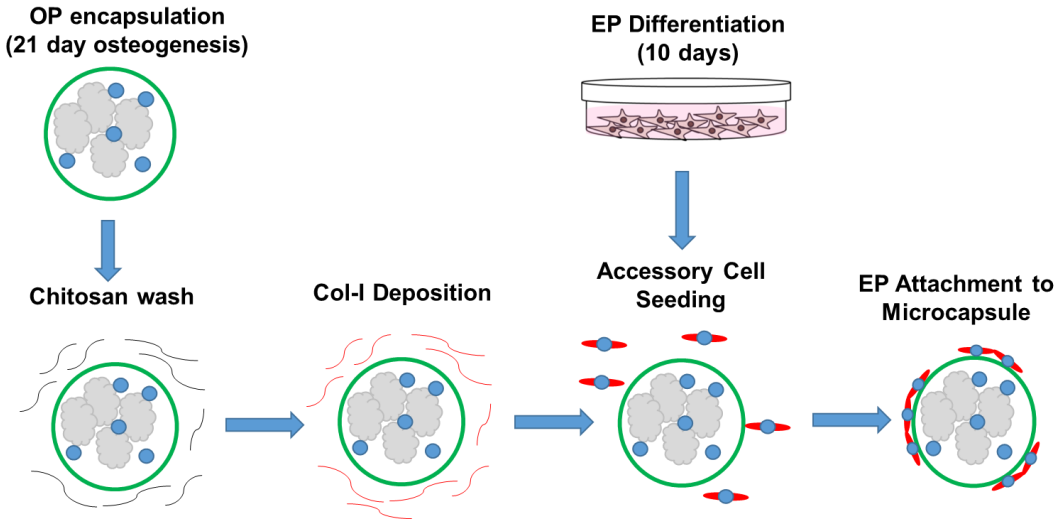

Fig 6.1: Attachment of MSCs to collagen coated microcapsules. After OP encapsulation, microcapsules were washed in chitosan, coated in collagen Type 1 (Col-I), and accessory cells were allowed to attach to adsorbed Col-I fibers on microcapsule exterior.

6.4.4 Subcutaneous Implant of Fused Microcapsule Constructs

After 48 hours of static culture, the collagen and cell coated microcapsules were fused into disc constructs (6 x 5 mm, diameter x height) using a similar method as Chapter 5, section 5.4.1,

for *in vivo* evaluation of vascularization (summed in fig 6.3). Briefly, cultured microcapsules were rinsed with PBS, reloaded in dilute polyanion solution, and transferred to a mold with a porous base. After draining excess polyanion solution, the mold was perfused with dilute chitosan. After draining the chitosan solution, the fused constructs were perfused with dilute polyanion and subsequently washed with 0.9% saline. The disc constructs were carefully removed from the mold, and placed in Hanks Balanced Salt Solution (HBSS) and stored at 4 ºC to await subcutaneous implantation. All solutions were sterile, and used at 4 ºC to protect cell metabolism.

Doppler US analysis of blood flow and analysis of tissue regeneration in the fused constructs was evaluated by implanting the fused constructs into Sprague Dawley (SD) rats (summed in fig 6.2). In this study, female rats (Charles River Laboratories, Wilmington, MA) aged 6-8 weeks, between 175-200 grams were used for all *in vivo* studies. All fused constructs contained microcapsules with HAP microgranules, Aceullar fused constructs were implanted without cells, OP fused constructs contained encapsulated OPs in the microcapsules, OP+MSC fused constructs contained OP microcapsules with MSCs attached to the microcapsule exterior, and OP+EP fused constructs contained EPs attached to the microcapsule exterior. A total of nine rats were used for this study, each receiving one fused construct from each condition (four implants per rat), and the implants were placed subcutaneously between the dorsal muscle and skin. Groups of four or five rats were initially housed together following surgery. Prior to surgery, Buprenorphine SR Lab was administered as an analgesic at a dose of 0.4 mg/kg. Rats were anesthetized with 1-3% isoflurane, and maintained on this for the duration of the surgery. Briefly, a 4 cm x 4 cm patch of dorsal skin was shaved, sterilized, and four 1 cm long incisions with 1.5 cm of undermining (for subcutaneous pocket formation) were made in the sterilized dorsal area: care was taken so that incisions were at least 1 cm away from each other to insure separation of all implants. Each rat received 2

subcutaneous pockets on the left and right dorsal side of each rat, above the external oblique muscle. After placing the fused constructs in the incisions, the incisions were closed with 3-0 monofilament nylon sutures. Care was taken so that the implants did not lie directly under the sutures. Blood flow through the implants was analyzed *in vivo* via Doppler US at 1, 2 and 4 weeks post-surgery. Implants were excised at 1, 2 and 4 weeks for gross macroscopic analysis and histology.

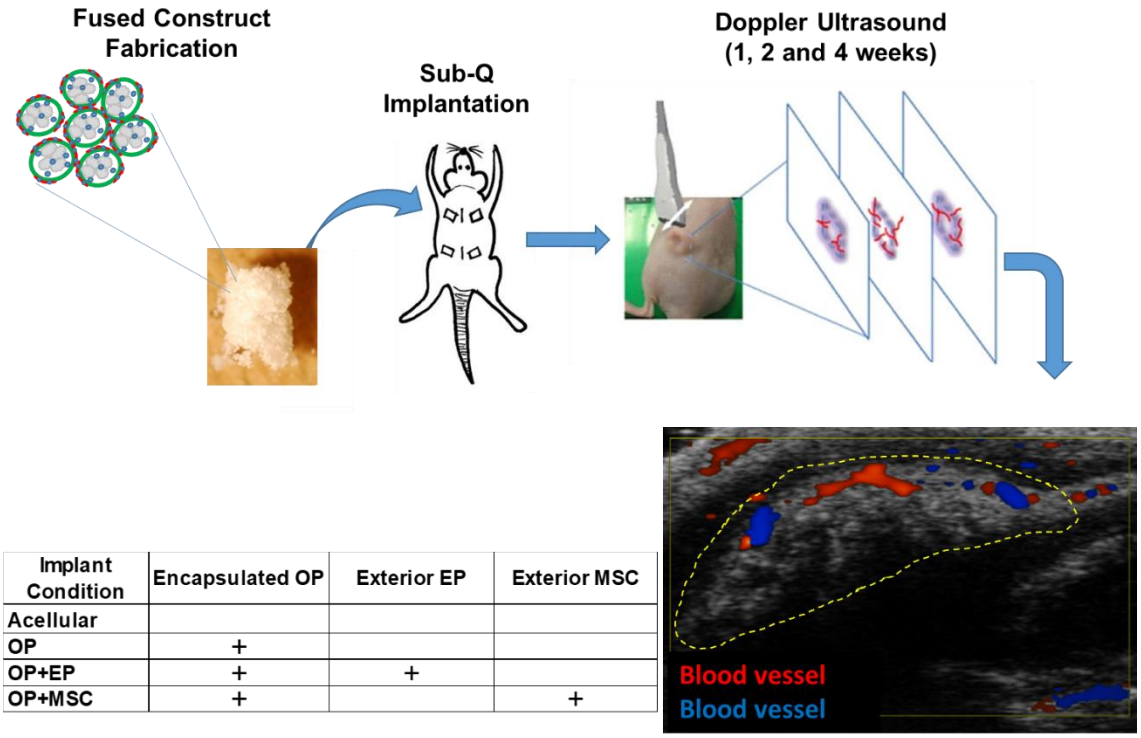

Implant Condition	Encapsulated OP	Exterior EP	Exterior MSC
Acellular			
OP	+		
OP+EP	+	+	
OP+MSC	+		+

Fig. 6.2: Implanting fused constructs in rat subcutaneous pockets. Fused constructs that were Acellular, or contained OP, OP+EP or OP+MSC were implanted and imaged via Doppler Ultrasound (US) after 1, 2 and 4 weeks post-surgery. Doppler US produces gray scale images of implant (outlined in yellow dashes), with overlaid blood flow in red and blue (color depends on direction of flow).

6.4.5 Doppler Ultrasound Analysis of Blood Flow through Fused Constructs

At 1, 2 and 4 weeks post-surgery, blood flow through implanted fused constructs was analyzed via Doppler US in accordance with established protocols, and at least 3 rats were

analyzed per timepoint [112, 113]. Rats were anesthetized with 1-3% isoflurane, and the hair on the skin above implanted constructs was removed via depilatory cream (Nair ®). Briefly, a thick layer of depilatory cream was applied to the hair, let sit for 1 minute, and removed with gauze and DI water. After hair was removed, the affected skin was washed thoroughly with DI water and cleaned gently with baby wipes (Charmin ®) to thoroughly remove residual cream. Rats were placed on a precision xyz-stage, and ophthalmic ointment was applied to the eyes of the rats. Ultrasound hydrogel was applied to the skin around the implants, and a focused US transducer probe (32 MHz frequency) connected to a Vevo 2100 US system (Siemens, Munich) was applied to acquire photoacoustic (PA) images of the implant (B-mode) and blood flow through the implants (photoacoustic/Doppler mode, 35 dB gain). The PA images were overlaid on the B-mode images to identify the location of blood vessels relative to implant material. The transducer probe was fitted to a holder and lowered to contact US hydrogel on the implants, and the precision stage was used to move the probe along the surface of the skin above the implant. Images of B-mode implant overlaid with PA blood flow were captured every 0.5 mm along the surface of the implant (moving from head to tail). US data was used to calculate an average vascular area fraction (VAF) for each implant by counting the number of colored pixels in an implant region of interest (ROI), and dividing this by the number of pixels in the implant ROI, using ImageJ software (NIH, Bethesda).

6.4.6 Histological Analysis of Implants: Hematoxylin and Eosin, and Masson's Trichrome

After 1, 2 and 4 weeks, at least 2 rats were euthanized via CO_2 inhalation, and implants were harvested for cell density and tissue ECM deposition via histology. Implants were removed and immediately fixed and stored in neutral buffered formalin (NBF, 10%). After extensive washes with first PBS and then DI water, the specimens were decalcified in a solution of 12% (v/v) HCl,

0.07% (w/v) EDTA, 0.014% (w/v) sodium tartrate, and 0.8% (w/v) sodium and potassium tartrate for 24 hours [114]. After 24 hours, the decalcified tissue was immediately removed and washed in running room-temperature tap water for 30 minutes, then equilibrated with 3x changes of DI water (30 minutes each). Washed tissue was dehydrated through a graded ethanol series (70% overnight, 90% (2x) for 2 hrs, 95% (2x) 2 hrs, 100% (2x) for 2 hrs), cleared in xylene under vacuum (3x changes, 30 minutes each), and incubated with paraffin (2x 1 hr each). The implants were finally incubated in a third change of paraffin overnight. Paraffin embedded implants were sectioned parallel to the muscle/skin sides of the implant, to obtain 7 μm thick horizontal sections beginning at 1 mm into the implant from the muscle side, to examine tissue and ECM towards the center of the implant. Sections were deparaffinized in xylene (2x, 5 min each), rehydrated through a graded ethanol series (100% to 40%), and incubated in DI water (3x, 5 min each).

For routine hematoxylin and eosin (H&E) staining, nuclei on sections were stained with Weigert's iron hematoxylin (10 minutes), washed in warm running tap water (5 minutes), blued in 0.2% ammonia water (10 minutes), washed in warm running tap water (5 minutes), and equilibrated with DI water (2x changes, 5 min each). Sections were then rinsed in 70% (v/v) ethanol, and counterstained in Eosin Y working solution (2 minutes). Sections were then dehydrated through an ethanol gradient (85%, 95%, 100%, 2x changes of each for 2 minutes each), equilibrated with xylene (2x changes, 3 minutes each), and finally cover slipped in xylene-based medium (Permount ®). To determine blood vessel density of each implant (including capillaries with $D < 30$ μm), blood vessels were counted in H&E stained sections. For this study, blood vessels were defined as luminal structures containing erythrocytes. Data will be reported as vessels/mm^2

For Masson's Trichrome staining, rehydrated sections were incubated in mordant (Bouin's solution) for 24 hours prior to staining, and staining was conducted using reagents from a kit

(Sigma-Aldrich, St. Louis, MO). Sections were washed in running tap water (10 min), equilibrated with DI water (2x changes, 5 min each), and stained in Mayer's hematoxylin (8 min). Stained sections were blued in Scott's tap water (10 min), washed in running tap water (5 min) and washed in DI water (2x 5 min each). Sections were then stained in Biebrich Scarlet-Acid Fuschin (5 min), rinsed in DI water (5 min), stained in working phosphotungstic/phosphomolybdic acid solution (5 min), and placed in aniline blue solution (5 min). After staining, sections were differentiated in 1% (v/v) acetic acid, and dehydrated through an ethanol gradient, equilibrated with xylene and cover slipped in a similar protocol to H&E staining. Stained sections were observed for cell infiltration and tissue/ECM deposition in the microcapsules and between microcapsules (intercapsule space), at the edges and centers of the implants. Implant edges were defined as the regions 1 mm from the periphery of the implant-tissue interface towards the center, and the center of the implant was defined as a 2 mm diameter region equidistant from the implant edges.

6.4.7 Histological Analysis of Undecalcified Implants: Alizarin Red Staining.

After harvesting implants, some implants were left undecalcified, and embedded in methyl-methacrylate (MMA) blocks for hard tissue sectioning, to analyze mineral deposition between weeks 1 and 4. Because the sectioning process is expensive (sectioning was conducted at Rush Medical School, Chicago, IL), only Acellular, OP+EP and OP+MSC implants from week 1 and 4 were analyzed. After fixation, implants were washed, dehydrated in 70%, 90%, 95%, and finally 100% ethanol (2 days each), cleared in xylene (1 day), and incubated in a series of MMA solutions, each for 48 hours at 4 ºC: 1) a 17:3 solution of MMA:diphthalate (DP), 2) a 17:3 solution of MMA:DP with 1% (w/v) benzoyl peroxide, 3) a two changes of a 17:3 MMA:DP solution with 2.5% (w/v) benzoyl peroxide. Air bubbles were removed from the implants in 2.5% benzoyl peroxide 17:3 MMA:DP solution by placing under vacuum for 24 hours, and releasing the vacuum

every 30 minutes. The MMA was cured around the implants by heating the vessels in a water bath at 42 ºC overnight. The resulting MMA blocks were sectioned at Rush Medical Center (Chicago, IL) to create 8 μm sections.

After sectioning, MMA embedded sections were deplasticized in acetone (3 changes, 10 min each), and rehydrated in an increasing ethanol gradient (95%, 80%, 70%, 50%, 40%, 25%, 2 changes for 2 min each). Sections were finally hydrated in 3x changes of DI H_2O (5 min each). Alizarin Red S working solution (2% (w/v) Alizarin Red S in DI H_2O, pH 4.2 adjusted with ammonium hydroxide) was applied to the slides, and slides were observed under a microscope for red staining of mineral deposits (~ 5 min). After staining, excess Alizarin solution was removed, slides were blotted, and dehydrated in acetone for 20 dips. Slides were subsequently dehydrated in 50:50 acetone:xylene solution (20 dips), dehydrated in 3x changes of xylene (3 min each), and finally mounted with a coverslip. Mineralization on sections was visualized via bright field microscopy.

6.4.8 Statistical Analysis

Statistical analysis was carried out using GraphPad Prism software. All statistical comparisons were made by performing a two-way analysis of variance (ANOVA), followed by Bonferroni's multiple comparison tests to evaluate significance between two data sets at a time. P values less than 0.05 were considered statistically significant. All data is reported as the mean $\pm$ standard deviation.

6.5 Results:

6.5.1 Endothelial Progenitors Display Endothelial Markers

Induction of MSCs in endothelial induction medium produced Endothelial Progenitors (EPs) that displayed *in vitro* angiogenic activity and membrane markers characteristic of

endothelial cells. The *in vitro* angiogenic activity was assessed via capillary-like network formation on Matrigel. EPs seeded in Matrigel in the absence of VEGF quickly formed a capillary network after 12 hours in culture (fig. 6.3a), while un-induced MSCs retained aggregate/spherical morphology with some lamellipodic spreading on the Matrigel. Undifferentiated MSCs did construct capillary networks when seeded on Matrigel in the presence of VEGF (50 ng/ml, fig. 6.3a). The ability to form capillaries on a semi-solid medium is a hallmark of endothelial cells [110, 115]. Additionally, EPs presented cell-membrane markers vWF and PECAM-1 (Fig 6.3b), while these membrane markers were absent from un-induced MSCs. PECAM-1 and vWF are both characteristic membrane markers of endothelial cells: vWF allows endothelial cells to mediate the progression of thrombus formation by binding to platelets, and PECAM-1 facilitates cell-cell adhesion in endothelial cells that promotes tube formation [116, 117]. The results of tube formation and vWF/PECAM-1 expression presented here agree well with reports from the literature of MSC differentiation to an endothelial-like lineage [110, 111, 118]. Additionally, these results are similar to those obtained for EPs that promoted vascularization and bone regeneration when implanted *in vivo* in published studies [119]. This brief study confirms that MSCs harvested for this study can be differentiated to an endothelial-like lineage (EPs), and the next series of studies will analyze how the addition of these EPs can enhance the vascularization of fused microcapsule constructs *in vivo*.

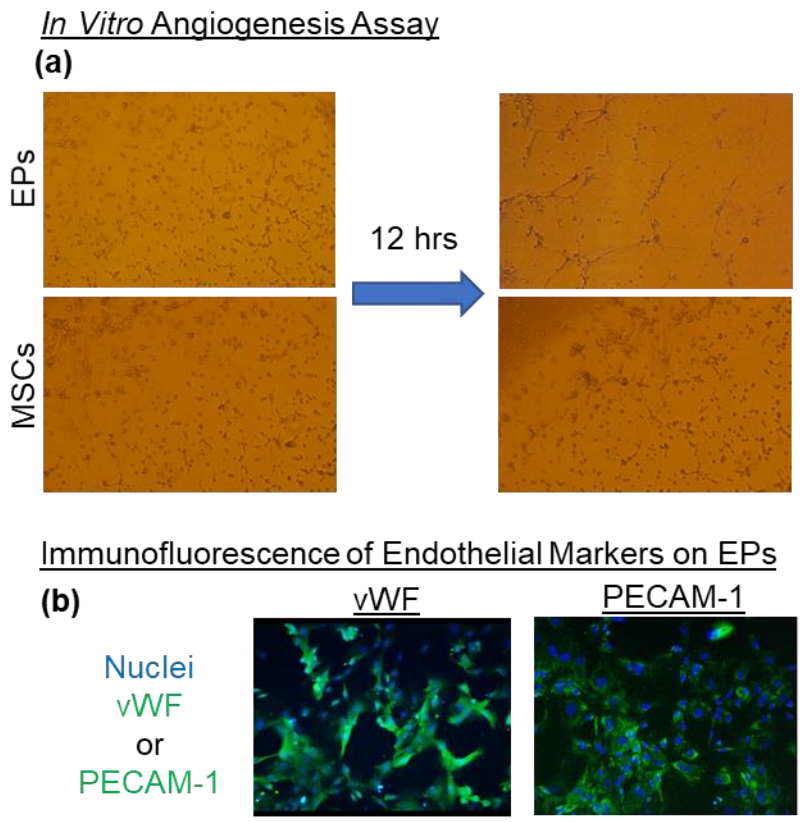

Fig. 6.3 Confirmation of MSC differentiation to Endothelial Progenitor (EPs). (a) EPs formed a tube-like network across the surface of Matrigel after 12 hours in culture, without the aid of exogenous VEGF supplemented in medium. EPs were compared to MSCs as a negative control. (b) EPs expressed common endothelial markers von Willebrand's Factor (vWF) and Platelet Endothelial Cell Adhesion Molecule 1 (PECAM-1).

6.5.2 EPs Attachment to Collagen Coated Microcapsules

Differentiation of MSCs to OPs during three weeks of culture prior to encapsulation was confirmed via Alizarin red staining of representative cultures that showed reddish/orange mineral deposits across the cell monolayer (fig 6.4). After OP encapsulation, coating of microcapsules with collagen and attachment of EPs or MSCs, microcapsules were cultured for 48 hours prior to fused construct fabrication and implantation. Labelling of representative OPs, MSCs and EPs with fluorescent cell tracking probes (Cell Tracker Red for OP, Cell Tracker Green for MSCs and EPs) to show how accessory cells attach to the microcapsule exterior (fig 6.5). Accessory cells attach

as aggregates (or attach individually and form aggregates) during the 1 hour incubation after collagen coating of microcapsules, and stay in partial aggregate form for 48 hours of culture, until microcapsules are fused for implantation (fig 6.5a, b) . SEM analysis of microcapsules confirmed that accessory cells were attached to microcapsules as aggregates (fig 6.5c, d): there was no difference in the attachment of MSCs or EPs to collagen coated microcapsules. Once the microcapsules are fused, these exterior cells will be localized to the pore space of the fused construct.

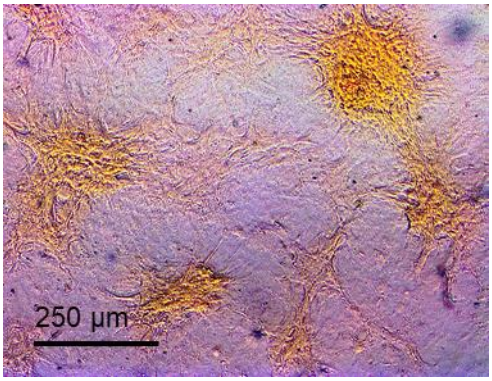

Fig. 6.4 Staining of mineral-containing nodules in OPs prior to encapsulation. MSCs were osteoinduced for 3 weeks, then stained with Alizarin Red S to identify mineral (red/orange regions) and confirm osteoinduction.

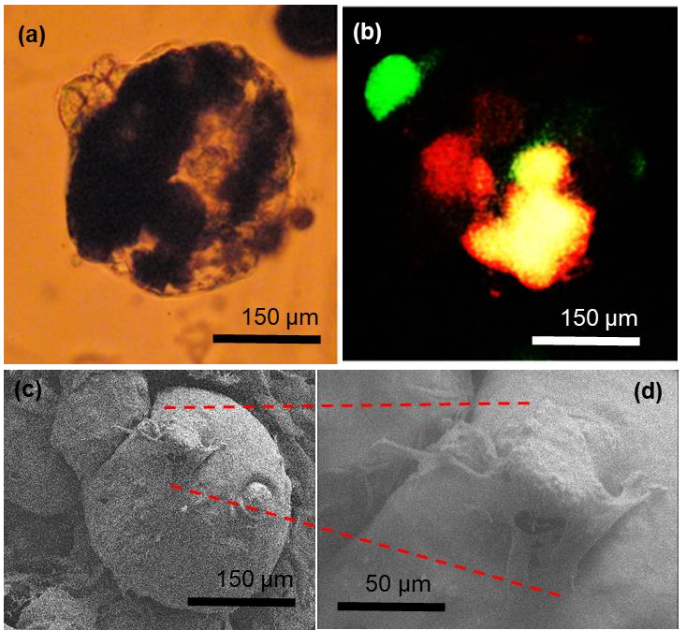

Fig. 6.5: Accessory cell attachment to microcapsule exterior. (a) Phase contrast image of EPs attached to microcapsule exterior. (b) fluorescent image of (a), showing labelled encapsulated OPs (red) and EPs (green). Yellow fluorescence occurs form the overlap of the red and green. (c) SEM image of microcapsule with cell aggregate attached and partially spread on exterior. (d) higher magnification of (c).

6.5.3 Ultrasound Analysis of Fused Construct Vascularization

Blood flow in and around implanted fused constructs was assessed by Doppler US at 1, 2 and 4 weeks post-surgery. US images show after 1 week post-surgery, the constructs have lost their disk-shape, and were likely partially flattened from rat grooming, rat bedding, and possibly from application of the US probe, but further distortion of implant size and shape did not appear to occur over the four weeks post-surgery (fig 6.7). Moreover, US images showed the presence of blood vessels 1 week post-surgery primarily around the periphery (between the implant and skin) of the implants, and the vessels appear to be travelling along the surface of the implants in parallel with the skin/muscle surface (fig. 6.7a, d, g, and j). In the case of the OP+EP and OP+MSC implants, vessels were observed running under the implant surface, closer to the implant center (fig 6.7g and j, respectively). Few vessels were detected with the US probe around or within the implants of any condition after 2 weeks post-surgery, and only some small diameter vessels were observed near the implant surface in the OP+EP and OP+MSC conditions (fig 6.7h and k, respectively). By week 4 post-surgery, acellular implants still showed very little vascularization (fig 6.7c); however, all implants containing cells (OP, OP+EP, OP+MSC) showed blood vessels at the implant border and near the implant center (fig 6.7f, i, l). Specifically, in the case of OP+EP and OP+MSC implants, more vessels appear to have penetrated the interior of the implants, again running parallel with the skin and muscle. US results indicate that after 4 weeks post-surgery, implants with accessory cells attached to the microcapsule exterior have enhanced vascularization, particularly within the construct, and not just at the implant border.

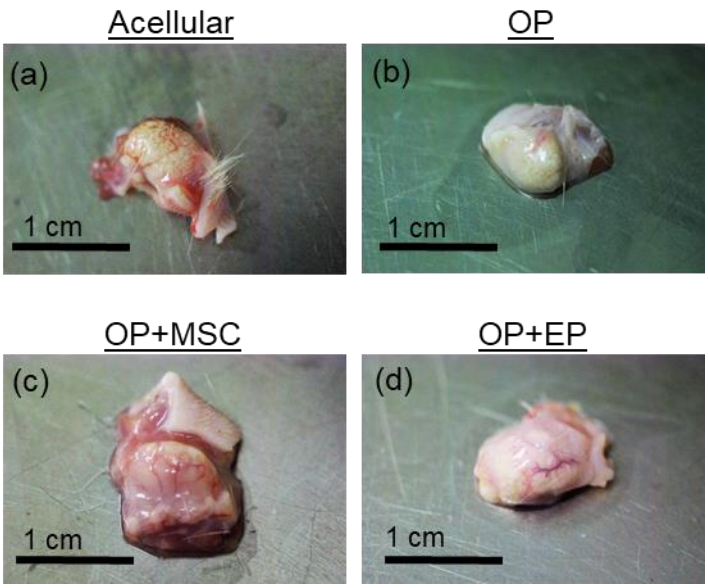

Fig. 6.6: Macroscopic images of implants excised at 4 weeks post-surgery. (a) Acellular, (b) OP, (c) OP+MSC, (d) OP+MSC. All excised implants showed some evidence of larger vessels along the surface of the impalnts. Implants were excised with skin (under implant) attached.

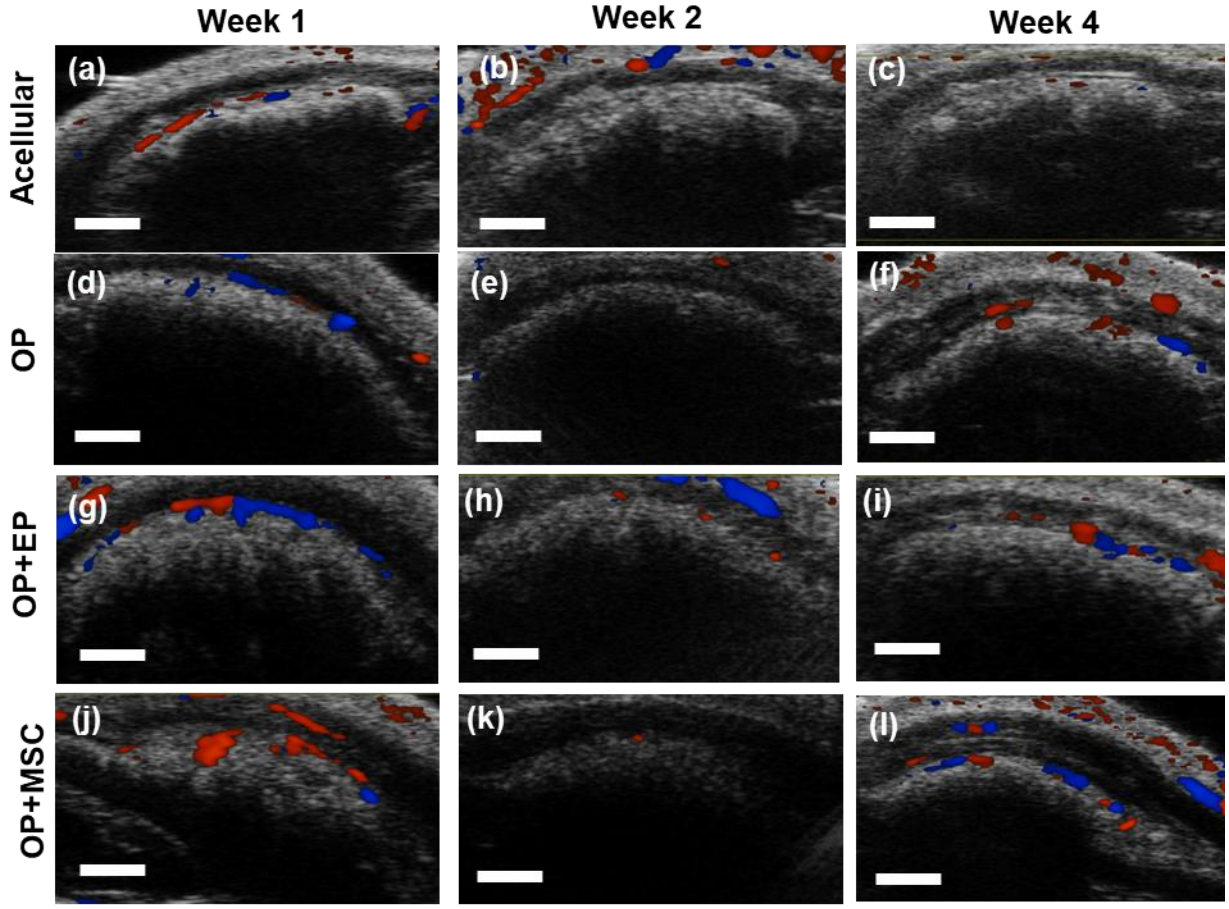

Fig. 6.7: Representative Ultrasound (US) images for weeks 1, 2 and 4 post-surgery. (a-c) Acellular, (d-f) OP, (g-i) OP+EP, and (j-l) OP+MSC fused constructs. Red and blue denote blood flow, scaffold and nearby rat tissue appear gray-white.

A quantitative analysis of the US data shows the temporal change in vascularization for each implant (fig. 6.8). At 1 week post-surgery, all of the implant conditions have similar average VAFs from 0.034 to 0.043 of total implant area. Interestingly, the average VAF appears to decrease for all conditions after 2 weeks post-surgery; additionally, there was no statistical difference between the conditions during week 2. The quantitative analysis shows possible evidence of vascular regression between weeks 1 and 2, at least concerning vessels larger than the lower resolution (30 μm) of the Visual Sonics 2100. After 4 weeks post-surgery, the average VAF for

the OP+EP implants increased significantly above week 2 values for all conditions, showing enhanced vascularization of implanted constructs between weeks 2 and 4. Specifically, the fused constructs with EP had a significantly higher average VAF (0.087 $\pm$ 0.0511) than either OP (0.019 $\pm$ 0.014) and acellular (0.020 $\pm$ 0.019) constructs at 4 weeks post-surgery. The addition of accessory cells (EPs and MSCs) to the exterior of microcapsules in fused constructs appears to stabilize (prevent from regressing) the blood vessel network after 4 weeks post-surgery: the average VAF at week 4 for the OP+MSC implants was not statistically different than week 1, and was not lower. Interestingly, there was no statistical difference in average VAF between OP+EP and OP+MSC implants at week 4. The average VAF of the acellular fused constructs at week 4 were also not statistically lower than week 1. The US data suggests that the addition of EPs and MSCs to the exterior of microcapsules stabilizes the *in vivo* vascularization of fused microcapsule constructs, and may even enhance the vascularization after 4 weeks in the case of implants with EPs. Results from previous studies suggest that improving vascularization of implants leads to faster bone regeneration *in vivo*.

There are some differences when comparing our results to similar studies utilizing US in the literature. A β-Tricalcium phosphate scaffold (β-TCP) seeded with collagen and HUVECs implanted in immunodeficient mice showed increasing VAF between weeks 1 and 2 (the study ended at week 2), instead of the decrease between weeks 1 and 2 observed here [112]. Differences in the scaffold system could explain the differences in vascularization: the β-TCP scaffolds were donut shaped cylinders (8 mm x 5 mm diameter x height) that contained a 3 mm diameter central pore. This large pore would rapidly fill with infiltrating cells, including endothelial cells that could establish a vascular network within the β-TCP scaffold early after implantation. Additionally, the study used a defined endothelial line (HUVECs), instead of the EPs used for the modular fused

constructs. EPs were chosen for this study due to their practical translatability to the clinic: MSCs are easily harvested in the clinic, and the differentiation materials are relatively inexpensive. Moreover, the β-TCP donut scaffold is likely suitable for regenerating large bone segments such as long bones, but the geometry is less suitable for regenerating bone in defects of complex geometry, or where minimally invasive surgical techniques are sought. The modular system designed here is meant to apply in different bone regeneration scenarios requiring bone regeneration of complex geometry, varying size, and possibly utilizing minimally invasive surgical techniques for implantation.

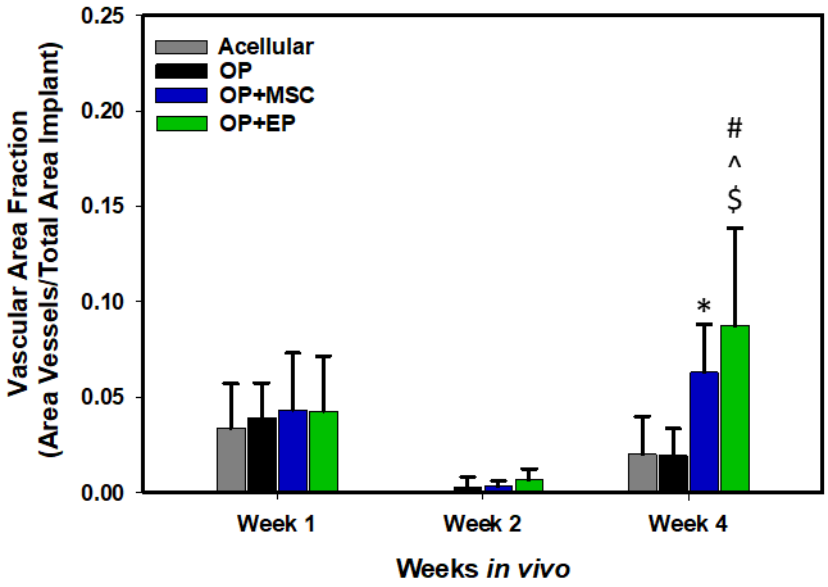

Fig. 6.8: Quantification of Vascular Area Fraction from US data for weeks 1, 2 and 4 post-surgery. P<0.05 (N=4) Relative to Acellular at week 2, # P<0.05 (N=4) Relative to OP at week 4, ^ P<0.05 (N=4) Relative to all conditions week 2, $ P<0.05 (N=4) Relative to Acellular at week 4, @ P<0.05 (N=4) No statistical difference between groups.

It is somewhat surprising that there was no statistical difference in vascularization between the OP+EP and OP+MSC fused construct implants at 4 weeks post-surgery, but reports in the literature have demonstrated that undifferentiated MSCs enhance scaffold vascularization *in vivo*,

without the addition of other exogenous factors [120, 121]. Several possible mechanisms for this have been proposed, including 1) MSC secretion of MMPs that enhance native endothelial cell migration through an implant [120], 2) paracrine signaling via extracellular vesicles containing proangiogenic growth factors (VEGF, TGFB1, IL-8) [122], and 3) supporting blood vessel maturation in a pericyte-like function [121, 123]. The inherent porosity of the fused constructs makes it unlikely that MMP secretion would increase native endothelial cell migration through the implant, so the accessory cells likely promote vascularization via mechanisms 2 and 3. Unfortunately, it is impossible with the current data to determine *specifically* how the accessory cells have enhanced fused construct vascularization in the OP+EP and OP+MSC fused constructs. For instance, the cells were not labelled prior to implant, and it is not possible to distinguish implanted EPs from native endothelial cells (or implanted MSCs from native pericytes) in the implant vasculature.

6.5.4 Histological Evaluation of Fused Constructs

Implants were excised after 1 and 4 weeks post-surgery, and decalcified to aid routine H&E processing. Empty, round voids observed in the histology sections are voids from the decalcification of the spherical HAP microgranules (fig 6.9). H&E staining and assessment of the implant edges of horizontal sections indicates that fused constructs containing cells were quickly infiltrated with native rat tissue cells. After 1 week post-surgery, sparse connective tissue cells are observed infiltrating between the microcapsules at the edge of the Acellular fused construct, and growing along the exterior membrane of the microcapsules (fig 6.9a). Moreover, hematoxylin-stained nuclei can be seen in the microcapsules near the edge in the Acellular construct, indicating that native cells invaded the microcapsule interior in this fused implant condition. In comparison, all fused constructs containing cells showed dense tracks of cells and native tissue leading into the

center of the implant between the microcapsules at the implant edge after 1 week (fig 6.9b-d). In all conditions at week 1, the infiltrating cells mostly appear elongated with round nuclei, consistent with connective tissue/fibroblast cells. Notably, some cells with perfectly round, larger nuclei are present between the microcapsules at the implant edges in the cell-containing implants, and it's possible these could be plasma cells commonly associated connective tissue (fig 6.9b-d). In all conditions 1 week post-surgery, evidence of the microcapsule membrane (stained dark red from eosin staining chitosan) is clearly present, indicating minimal degradation.

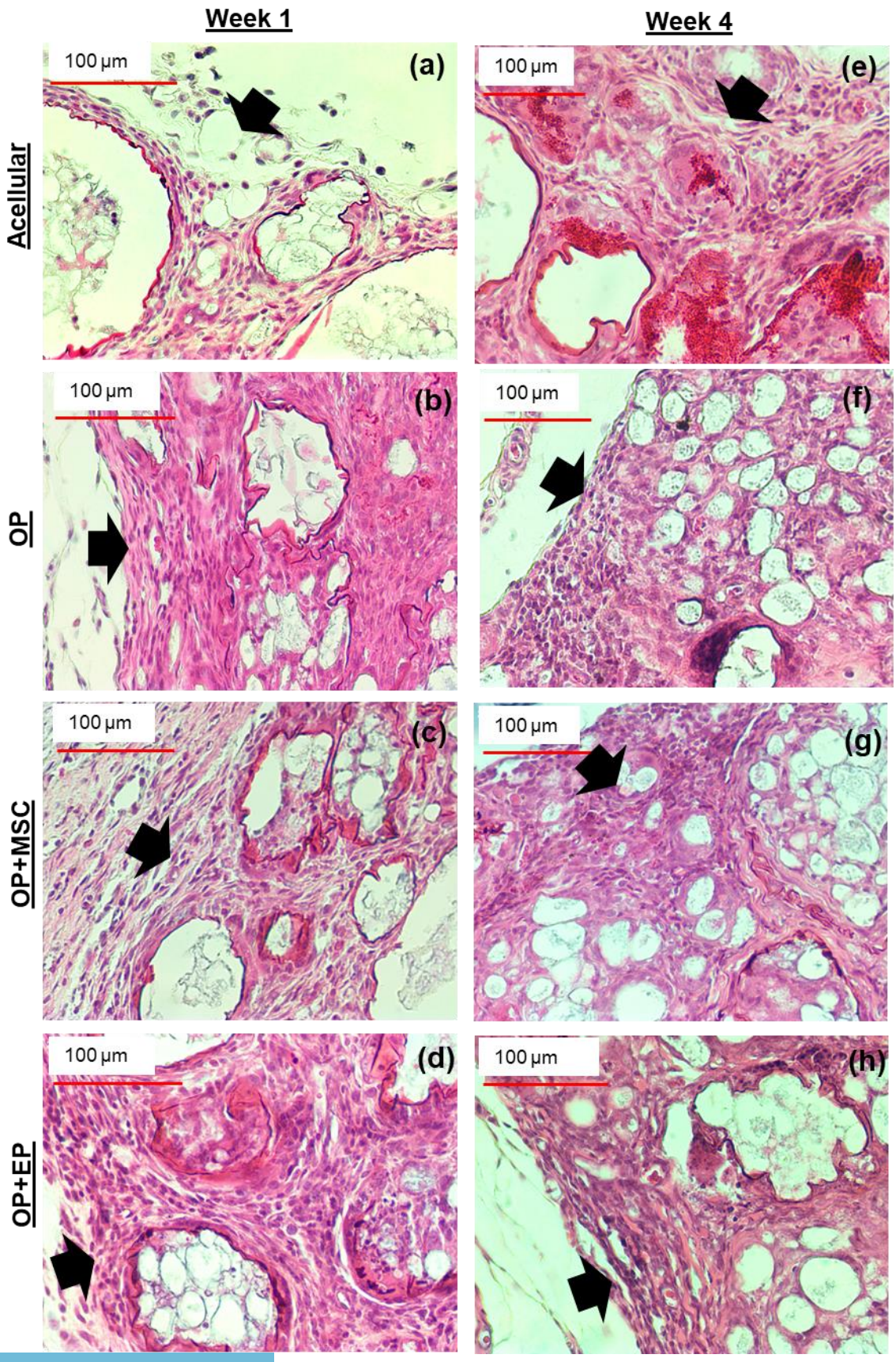

Fig. 6.9: H&E histological assessment of implant edges. (a, e) Acellular implants week 1-4, (b-f) OP implants weeks 1-4, (c-g) OP+MSC implants week 1-4, (d-h) OP+EP implants weeks 1-4. Black arrows point to implant-tissue interface. White spherical voids were filled with HAP microgranules prior to implant decalcification.

After 4 weeks post-surgery, more cells have infiltrated the edges of the Acellular implants, and the connective tissue growing between the microcapsules appears substantially thicker compared with week 1 (fig 6.9a, e). Additionally, the red microcapsule membranes are still clearly evident 4 weeks post-surgery, indicating minimal degradation of the microcapsule material, even after 4 weeks post-surgery and exposure to degrading enzymes (lysozyme, etc…) associated with the *in vivo* environment (fig 6.9e). In contrast, the fused constructs containing cells appeared to have similarly dense connective tissue in the intercapsule space at week 4, compared with week 1 (fig 6.9f-h). Interestingly, very little evidence of the microcapsule membrane was found in the OP, OP+MSC or OP+EP microcapsules at the edge of the implants at week 4, indicating significant degradation of the membrane occurred between weeks 1-4. Moreover, connective tissue can be observed growing and infiltrating between the HAP microgranules formerly encapsulated by the microcapsule membranes, indicating either native cell infiltration inside the microcapsules, enhanced proliferation of OPs inside the microcapsules, or a mix of both mechanisms. No difference in cell infiltration or density was observed between OP and OP+MSC/OP+EP implants at weeks 1 or 4 post-surgery. Histological assessment of implant edges shows that OP, OP+MSC and OP+EP implants facilitated quick native cell and connective tissue infiltration early after 1 week post-surgery, and that cell density was maintained after 4 weeks post-surgery. Additionally, microcapsules near the edge of the OP, OP+MSC and OP+EP implants contained significantly more cells (either native infiltrating cells or proliferating implanted cells) at week 4. Finally, it appears that the microcapsule membrane degraded significantly between weeks 1-4 post-surgery

in the OP, OP+MSC and OP+EP implants, possibly due to the greater cell infiltration and blood flow (with degrading enzymes) compared with Acellular implants.

H&E assessment of the center of the implants shows a trend similar to the implant edges. At week 1, the Acellular implant had very few cells infiltrated to the center of the implant: only a few sparse nuclei could be observed in the intercapsule space, and most of the intercapsule space was acellular and empty (fig 6.10a). The cells in the center of the Acellular implant have rounded nuclei with minimal cytoplasm and a spherical phenotype. Moreover, very few capsules in the center contained nuclei, indicating minimal invasion into the microcapsules by infiltrating native cells. In contrast, the OP, OP+MSC and OP+EP fused constructs all contained significant infiltrating cells at their centers, early 1 week post-surgery (fig 6.10b-d). Similar to the implant edges, the infiltrating cells in the OP, OP+MSC and OP+EP implants appeared to have an elongated, connective tissue fibroblast phenotype. Additionally, most of the capsules in the center of OP, OP+MSC and OP+EP implants contained cells, though it appears more cells were present in the microcapsules at the implant edges at week 1 post surgery (fig 6.10b-d vs. fig 6.9b-d). The higher diffusion of nutrients near the microcapsules at the edge of the implant, or the greater probability of cell invasion, likely contributed to the higher cell density in the microcapsules near the implant edge. Similar to the trend observed at the edges of the implant, more native connective tissue cells have quickly infiltrated to the centers of the OP, OP+MSC, and OP+EP implants, compared to Acellular implants at 1 week post-surgery.

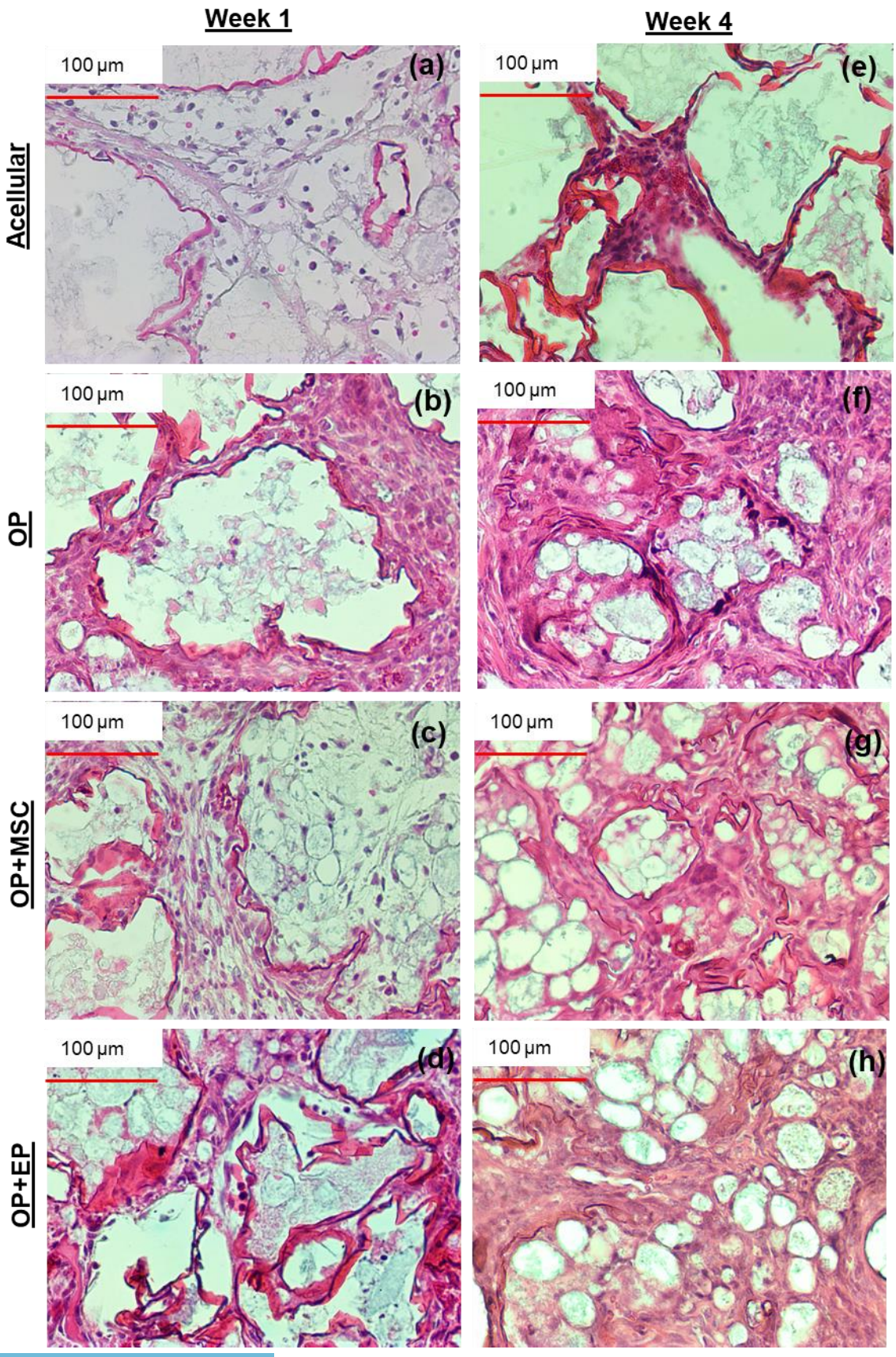

Fig. 6.10: H&E histological assessment of implant center. (a, e) Acellular implants week 1-4, (b-f) OP implants weeks 1-4, (c-g) OP+MSC implants week 1-4, (d-h) OP+EP implants weeks 1-4. White spherical voids were filled with HAP microgranules prior to implant decalcification.

After 4 weeks post-surgery, more connective tissue cells have infiltrated the intercapsule space in the center of the Acellular implant, so minimal empty space is observed compared to week 1 (fig 6.10e). There are still few microcapsules in the center of the Acellular implant that contain nuclei at week 4, indicating minimal cell invasion into the microcapsules. In fact, the microcapsule membranes are clearly intact in the center of the Acellular construct at week 4, showing minimal (if any) degradation. The connective tissue infiltration was significantly more dense in the center of OP, OP+MSC and OP+EP implants than the Acellular condition (fig 6.10f-h). Moreover, microcapsules in the center of the OP, OP+MSC and OP+EP constructs contain significantly more cells at week 4 compared to week 1 (fig 6.10f-h). Interestingly, more evidence of the microcapsule membranes (darker red staining than surrounding cytoplasm) is present in the center of the microcapsule construct than the edges after 4 weeks post-surgery. Results demonstrate that cells quickly proliferated in the center of the fused OP, OP+MSC, and OP+EP constructs, and the cellular density of microcapsules in the center increased between weeks 1 and 4. Moreover, the microcapsule membranes appeared less degraded in the center of the fused constructs than at the edges after 4 weeks post-surgery, likely due to greater exposure to lysozyme in the circulating blood at the implant edges.

It is notable that a significant immune/inflammatory response is not present in the H&E stained sections. The densely-packed neutrophils of an inflammatory response are not obviously present in weeks 1 or 4 *in vivo* when reviewing the H&E stained sections. Additionally, the presence of multi-nucleated foreign body cells or basophils was not obvious either. Previous studies examining the *in vivo* host response to chitosan materials describe an early neutrophil

recruitment, but without neutrophil activation [124, 125]. However, the chitosan used for implanted microcapsules was 95% de-acetylated, which would illicit a significantly reduced inflammatory response [126]. Furthermore, C4S has demonstrated anti-inflammatory properties *in vivo*. It is possible that the OPs, which were of MSC origin, suppressed an inflammatory immune response to the fused constructs. Research indicates that MSCs have a wide array of immunomodulatory properties, including the secretion of the multifunctional tumor necrosis factor-α (TNF-α), stimulated gene/protein 6 (TSG-6), and the IL-1 receptor antagonist [127]. The MSCs may have retained some of these properties during their differentiation to OPs or EP, and actively suppressed an immune response. The combination of microcapsule materials used (deacetylated chitosan and C4S), and MSC-derived cell types, may have suppressed a host immune response to the fused microcapsule implants.

It's clear that fused constructs with exogenous cells significantly enhance cell density of the implanted constructs after 4 weeks *in vivo*. The increased cell density could be the result of a few different mechanisms: 1) exogenous cells in the fused constructs could experience increased proliferation from the nutrients and growth factor milieu available *in vivo*, and/or 2) exogenous OPs, MSCs, and EPs promote homing of native cells to the implant area through paracrine activity. It is possible that some of the transplanted cells proliferated in the implant during weeks 1-4, and several studies have shown that implanted cells contribute to tissue regeneration and anastomosis with host tissue. A specific study that was a partial inspiration for this work (and discussed in-depth in the relevant background, section 2.5) demonstrated that the exogenous EPs implanted in a PCL/HAP scaffold anastomosed with the host vasculature in the defect [50]. Indeed, the encapsulated OPs in the microcapsule system described here are physically constrained by the microcapsule membranes, and will participate in tissue regeneration by depositing matrix and

proliferating within the microcapsule space. It is possible that the membranes of some microcapsules may have become compromised after surgery, but the histological assessment shows that most of the membranes appear in tact at week 1.

Some prior research reports indicate that implanted cells don't participate directly in tissue regeneration in every system, and often migrate away from the implant following hypoxic and chemotactic cues from the surrounding tissue [128]. In fact, a detailed study examining how allogenic MSCs implanted in a ceramic bioscaffold in a mouse model contributed to bone regeneration demonstrated that these MSCs migrated out of the subcutaneous implants into the circulatory flow [129]. Interestingly, the exogenous MSCs did significantly improve recruitment of endogenous cells to the implanted bioscaffold, likely by the release of homing factors as they migrated out of the implant. The paracrine signaling by exosomes containing proangiogenic growth factors released from MSCs has been discussed in the previous section. The MSC-secreted exosomes also contain some chemotactic factors that could induce migration of native cells to the implant area: some chemotactic cues released by MSCs include stromal cell-derived factor 1 (SDF-1) [130], hepatocyte growth factor (HGF) [131], VEGF [132], and interleukin 8 (IL-8) [133]. Of specific interest in this study, MSCs have been shown to induce the migration of fibroblasts via a chemotactic trail [131], and this may explain the increase in connective tissue for OP, OP+MSC and OP+EP implants, compared with Acellular implants. The OPs are derived from MSCs for this study, and studies demonstrate that MSCs continue to secrete GFs and exosomes during osteogenesis [134]. However, the secretome of MSCs undergoing osteogenesis hasn't been completely characterized at the date of this manuscript, so claims of OP exosome-mediated migration are very limited. It's possible that the encapsulated OPs are secreting exosomes with pro-migratory cues, promoting the migration of native cells into the fused constructs. Results

combined with this native cell migration hypothesis demonstrate the utility of adding cells to the fused construct implants to promote rapid cellularization of fused constructs and tissue regeneration.

6.5.5 Blood Vessel Density assessed from Implant Histology

Due to the inability of the ultrasound system to identify blood vessels with diameters less than 30 μm, blood vessels observed in the histological sections were quantified for all implant conditions (fig. 6.11). Representative images showing blood vessels in H&E stained sections are shown in fig. 6.11 (a-d): contrast and brightness are adjusted to better show erythrocytes in vessel lumens. Quantification of the blood vessel density shows a trend slightly different than the VAF determined from the US analysis of larger blood vessels. The vessel density significantly increased for both OP+MSC (1.83±0.07 to 8.06±0.36 vessels/mm^2) and OP+EP implants (1.48±0.07 to 8.53±0.25 vessels/mm^2) between weeks 1-3, respectively (fig. 6.11e). In contrast, the vessel density of Acellular and OP implants stayed relatively the same between weeks 1-3. Interestingly, the vessel density of the OP+MSC and OP+EP implants increased between weeks 1 and 2, contrary to the US data discussed previously. The blood vessel density calculation performed in this section captured the smaller capillaries (D < 30 μm) present in the vessels at week 2 that the US probe missed, due to the resolution limit of the probe. During week 4 of implant period, there was no statistical difference between the OP+MSC and OP+EP implant vessel density, but both were significantly higher than the Acellular and OP implants at week 4. Interestingly, the vessel density of OP+EP implants was lower than OP+MSC and OP implants at week 1 (1.48±0.07 vs. 1.83±0.07 and 2.09±0.11 vessels/mm^2, respectively); however, this could be a feature of the low sample size of tissue sections (n=3) counted for this assessment.

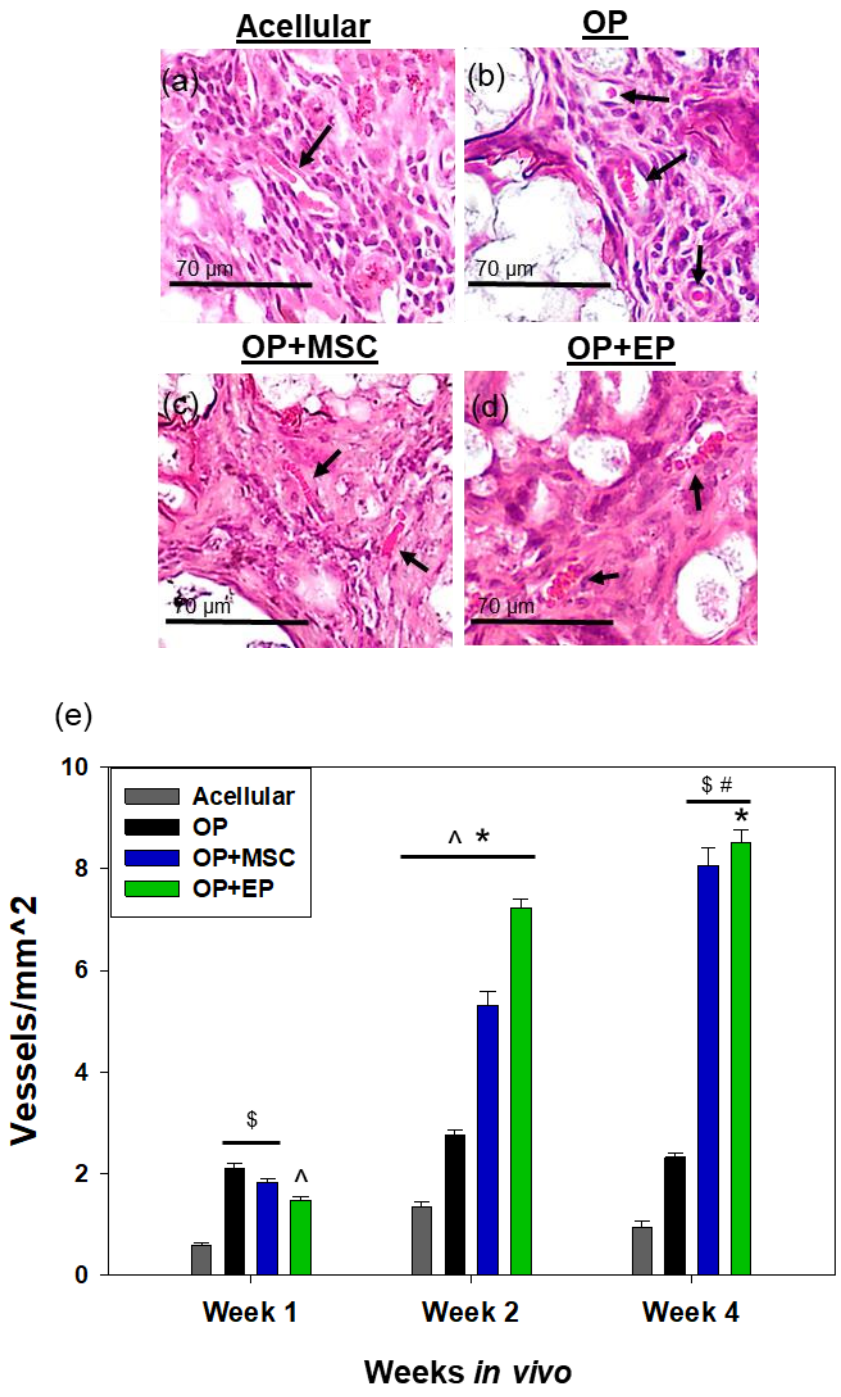

Fig. 6.11: Blood vessel density quantification. Representative histological images showing blood vessels (black arrows) for (a) Acellular, (b) OP, (c) OP+MSC, and (d) OP+EP implants after 4 weeks *in vivo*. (e) Blood vessel density quantification for all implants at 1, 2 and 4 weeks (n=3). * ($P < 0.05$) significant from previous time point.

($P < 0.05$) significant from OP at that time point. $ ($P < 0.05$) significant from Acellular at that timepoint. ^ ($P < 0.05$) significant from all other conditions at that time point.

The blood vessel density quantification exhibits a different trend for the VAF calculations from US assessment. It appears that some larger vessels (present during the first week of *in vivo* implantation) may have remodeled into smaller capillaries via vessel intussusception. Intussusception involves the splitting of an existing vessel in two: the vessel is split along its long axis, to create two vessels with a smaller diameter than the original [135]. It has been demonstrated that vessel intussusception occurs in low-VEGF environments in both chick embryo vascularization models [136] and tumor vasculatures undergoing anti-angiogenic therapy [137]. It's entirely likely that a low VEGF environment was present in the implants during the first couple of weeks after implantation *in vivo*, as the implanted cells would be the only possible source capable of releasing VEGF. The MSCs/EPs contained in the implant may not have sustained VEGF secretion and, even if they initially did secrete VEGF, these cells may have migrated out of the implant during the initial weeks post-surgery. The current data suggests that some large vessels present after week 1 post-surgery are remodeled into smaller capillaries by week 2 in the fused microcapsules constructs, likely via low-VEGF intussusception. A more rigorous study is required to determine the nature of the vascular remodeling, but this study currently demonstrates that including EPs or MSCs in the fused construct implants significantly increases the implant vessel density over the four weeks post-surgery, and this will likely lead to enhanced bone regeneration *in vivo*.

6.5.6 Histological Evaluation of Matrix Deposition in Constructs

Tissue sections analyzed for histology were also analyzed for the presence of ECM (collagen and GAG/protein) in and between microcapsules via Masson's Trichrome staining. Analysis of trichrome staining at the edges of all implants 1 week post-surgery (fig 6.12a-d)

showed that cells infiltrating between the capsules deposited connective tissue collagen (light blue staining from aniline blue dye). Similar to H&E analysis, nuclei were observed in the microcapsules at the edges of the Acellular implants at week 1, indicating cell invasion into the microcapsules (fig 6.12a). The tissue between the microcapsule edges at week 1 appeared to be entirely collagen in Acellular, OP+MSC and OP+EP implants; however, significant red staining was observed in the tissue around the edge microcapsules in the OP implant, indicating the presence of GAGs and non-collagenous proteins (fig 6.12b). Like the H&E analysis, the microcapsule membrane stains red under Masson's Trichrome. Inside the microcapsules, the OP+MSC and OP+EP constructs contained mostly collagen: in contrast, the OP microcapsules contained significant GAGs/non-collagenous proteins. The specific red staining around the HAP microgranules in the OP microcapsules is indicative of osteoid production, a high protein content non-mineralized ECM deposited in the beginning of bone regeneration by osteoinduced MSCs/osteoblasts [138]. Very little has changed in the matrix composition at the edges of the Acellular implants after 4 weeks, and the matrix is still highly collagenous from connective tissue infiltration (fig 6.12e). By week 4, the tissue surrounding OP microcapsules at the edge is composed of collagen and protein/GAGs, indicated by the blue with interspersed red, and was similar in composition to week 1 (fig 6.12f vs. 6.12b). In contrast, the edges of the OP+MSC and OP+EP implants contained significantly more protein/GAG between the microcapsules after 4 weeks compared to week 1, and the tissue at week 4 was a mix of collagen/non-collagenous proteins (fig 6.12g, h vs. fig 6.12c, d). Trichrome staining indicates that initially, loose collagen and connective tissue is deposited between the microcapsules as native connective tissue fibroblasts invade the implant at week 1, and this connective tissue is mostly present at week 4 with additional proteins and GAGs in the OP+MSC and OP+EP implants.

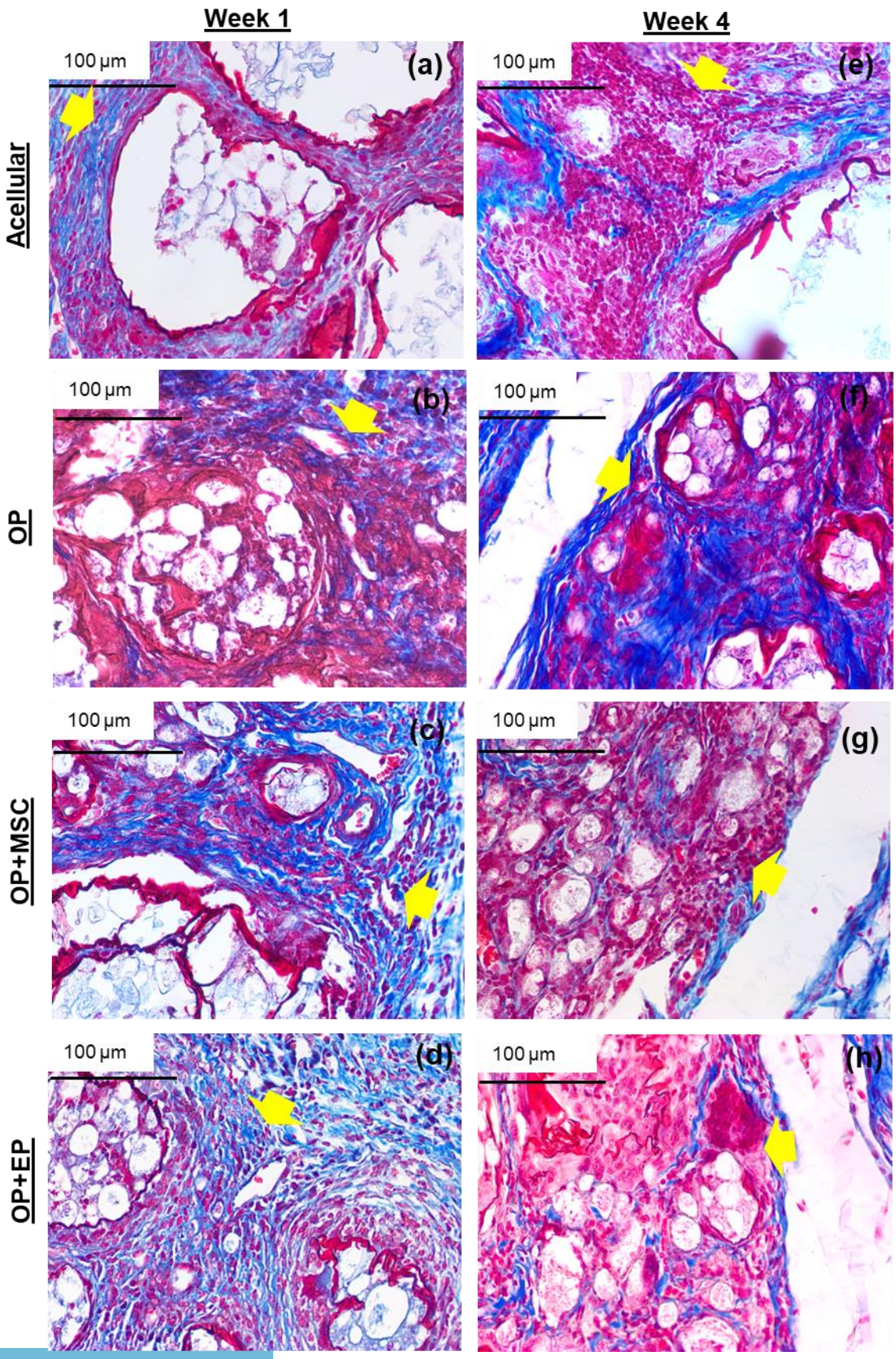

Fig. 6.12: Masson's Trichrome histological assessment of implant edges. (a, e) Acellular implants week 1-4, (b-f) OP implants weeks 1-4, (c-g) OP+MSC implants week 1-4, (d-h) OP+EP implants weeks 1-4. Yellow arrow denotes implant-tissue interface. Nuclei = purple/fuchsia, collagen = blue, osteoid = red/pink, microcapsule membrane = red. White spherical voids were filled with HAP microgranules prior to implant decalcification.

Masson trichrome staining of the center of the implant shows a similar tissue composition to the edges. Minimal tissue was observed in the intercapsule space in the center of Acellular implants at week 1 (fig 6.13a), and no increase was observed by week 4 (fig 6.13e): matrix that was present was faintly blue, indicating very loose collagen. The matrix deposited in the center of OP constructs was mainly red at week 1, indicating non-collagenous protein/GAG containing osteoid, surrounding some acellular islands of blue collagen (fig 6.13b). At 4 weeks post-surgery, the acellular collagen islands in the center of the OP implants were stained significantly darker, indicating more dense collagen deposition characteristic of woven bone regeneration (fig 6.13f) [138]. Similar acellular islands of collagen were observed in the centers of OP+MSC and OP+EP implants, and these also appeared more dense after 4 weeks post-surgery (fig 6.13c, d vs. fig 6.13g, h). Trichrome staining of the central regions of all OP, OP+MSC and OP+EP implants indicates early matrix deposition at week 1 (osteoid-like for OP, collagenous connective tissue for OP+MSC and OP+EP), followed by better organization of deposited collagen to more dense, acellular islands present at week 4. The analysis of deposited matrix shows the deposition of dense collagen, a precursor to unmineralized woven bone, and the potential beginnings of intramembranous ossification within the OP, OP+MSC and OP+EP fused constructs. Results indicate that an optimal bone regeneration fused construct would contain, at a minimum, capsules filled with OPs.

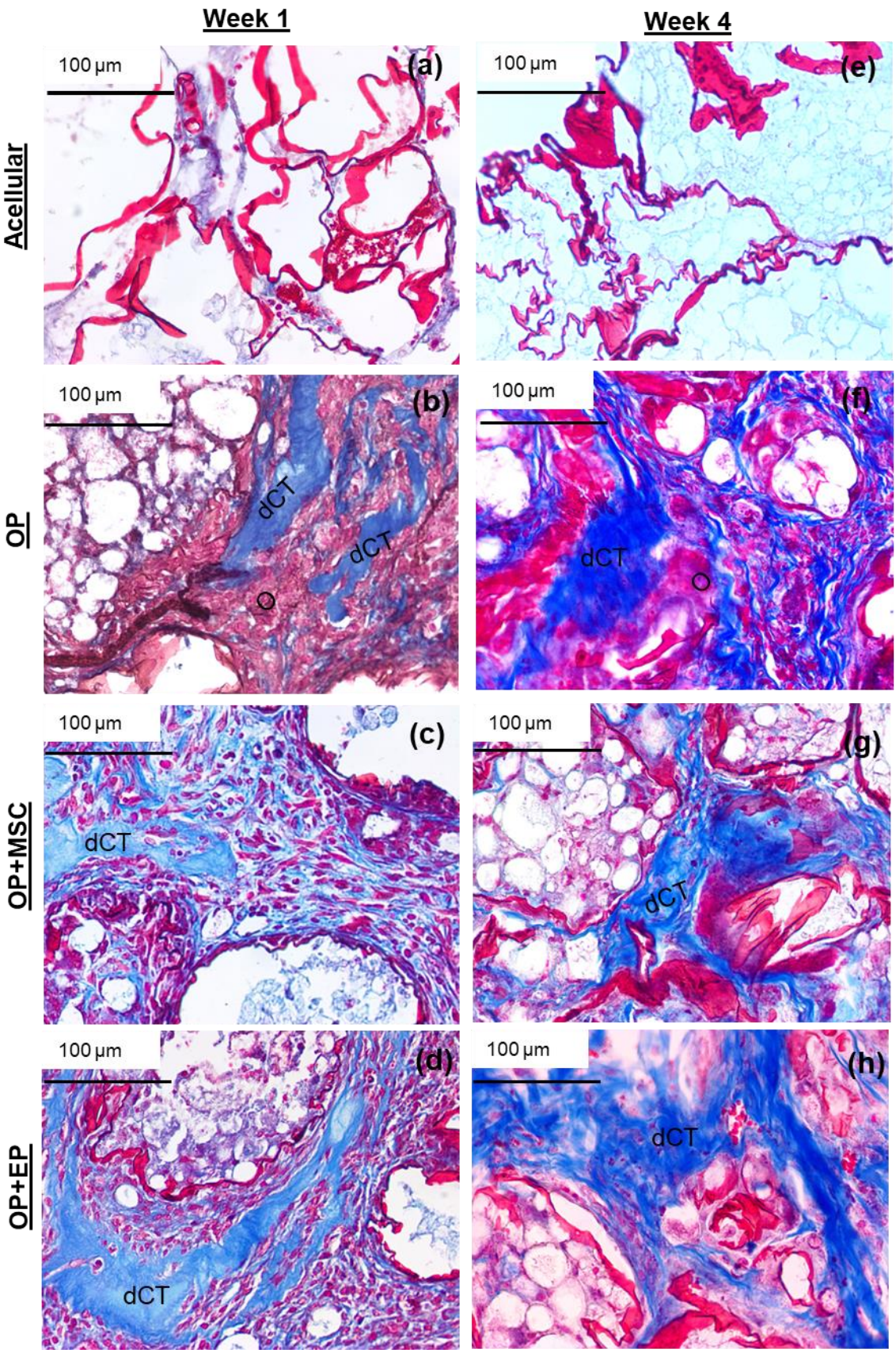

Fig. 6.13: Masson's Trichrome histological assessment of implant center. (a, e) Acellular implants week 1-4, (b-f) OP implants weeks 1-4, (c-g) OP+MSC implants week 1-4, (d-h) OP+EP implants weeks 1-4. Nuclei = purple/fuchsia, collagen = blue, osteoid = red/pink, microcapsule membrane = red. dCT = Dense collagen tissue, O= Osteoid. White spherical voids were filled with HAP microgranules prior to implant decalcification.

6.5.7 Alizarin Red Staining of Undecalcified Implants

Implants that were not decalcified were embedded in MMA blocks and sectioned for mineral staining by Alizarin Red. Mineral deposition was relatively uniform over weeks 1-4 between Acellular, OP+EP and OP+MSC sections (fig. 6.14). The most intense staining appeared in the centers of the HAP microgranules (dark red/black), and less-intense staining occurred at the edges of the HAP microgranules. In the implants containing cells, there could be some cell-deposited mineral around the HAP microgranules: indeed, there appears to be slightly more red staining at week 4 in the OP+EP and OP+MSC sections, than in the Acellular sections at week 4. Currently, more undecalcified implants must be sectioned, stained, and the images analyzed to measure the stained areas and compare between groups. Additionally, the implants must be left *in vivo* for a longer time (possibly 6 weeks or longer) to allow for sufficient mineral deposition to occur from cells implanted with (or migrating into) the fused construct implants. The current results show that the inclusion of OPs and EPs/MSCs may slightly enhance the mineral deposition in the implants over a 4 week period *in vivo*.

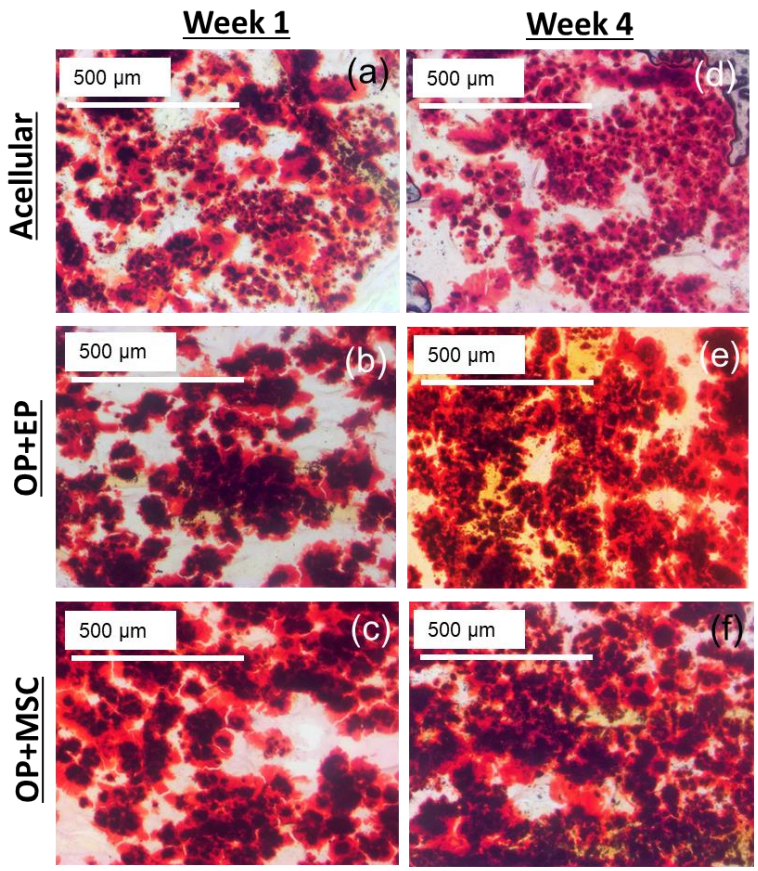

Fig. 6.14: Alizarin Red staining of undecalcified implant sections. (a, d) Acellular implants weeks 1-4, (b, e) OP+EP implants weeks 1-4, (c, f) OP+MSC implants weeks 1-4. Calcium deposits = red. HAP microgranules = dark red/black.

6.6 Summary and Discussion:

We have demonstrated that the addition of accessory cells (MSCs or EPs) to the microcapsule exterior improves the vascularization of fused microcapsule constructs compared with Acellular or OP constructs after a 4 week *in vivo* period. Doppler US data confirms that fused constructs containing accessory cells had similar average VAFs at week 4 compared to week 1, indicating that the accessory cells may have induced more native endothelial cells to migrate to the implant over 4 weeks *in vivo*, preventing the regression of vessels in these implants. Moreover, implants containing allogenic OPs, MSCs and/or EPs experienced significantly higher cell

densities early after the first week of implant, possibly due to allogenic cell proliferation or chemotactic recruitment of native cells. In particular, the OP+EP implants had a significantly higher average VAF than OP and Acellular implants at week 4. Both OP+EP and OP+MSC implants had higher blood vessel density than OP and Acellular implants after 4 weeks. This study demonstrates that a fused construct containing microcapsules with encapsulated OPs and accessory cells (MSC or EP) serves as a viable strategy to promote well-vascularized bone regeneration.

The specific type of tissue infiltrating and regenerating the scaffolds requires more characterization. Currently, it is hypothesized the tissue is mainly composed of connective tissue fibroblasts and mesenchymal cells, based on the cell morphology and that these cells would be the first recruited in a subcutaneous implant model. Future immunohistochemical (IHC) studies should be conducted to probe implants and tissue sections for evidence of connective tissue fibroblasts, MSCs, osteoblasts, etc. Additionally, the tissue sections need to be more closely examined for the presence of an immune response at an earlier time (such as three days post surgery), also via rigorous IHC staining for neutrophils, foreign body giant cells, and plasma cells. Currently, the presence of an inflammatory response appears small (if one is present at all), and the fused constructs show little evidence of significant immune cell recruitment. Moreover, a rigorous quantification of the capillaries present in the implants should be compared to the average VAF data: because the resolution of the US probe only allows detection of vessels greater than 30 μm in diameter, it's possible the US analysis could have missed smaller feeder vessels present throughout the implants. Greater characterization of the immune response earlier *in vivo* may elucidate the mechanism of why vascularization decreases between weeks 1-2, and whether the higher VAFs observed at week 1 were due to inflammation. Overall, the fused construct design contained a high cell density early at 1 week *in vivo* for all constructs containing allogenic cells,

and these cells deposited tissue matrix that could be a precursor to bone, if the implants were harvested later than 4 weeks post-surgery. This study shows that the OP/Accessory cell microcapsule system could serve as a viable platform to promote well-vascularized bone regeneration, and further optimization of the implants with respect to accessory and OP cell density is warranted.

CHAPTER 7: CONCLUSION

The C4S/HAP/Chitosan microcapsules supported the osteogenesis of encapsulated MSCs, and the expected peaks in ALP and BSP expression were observed, consistent with MSC differentiation to an osteoblast phenotype. The differentiating MSCs actively mineralized the microcapsule interior, and deposited mineral around the HAP microgranules and microcapsule membrane. Moreover, the MSCs remained viable in the microcapsule cultures for 28 days, and the presence of mineral did not significantly inhibit viability; however, the mineral buildup may have inhibited nutrient flow through the microcapsule membrane, inhibiting proliferation. It is possible that the mineralization of the microcapsule membrane could inhibit cell proliferation *in vivo*; however, the hypoxic cues that would result, along with other chemotactic cues present *in vivo*, could cause encapsulated cells to migrate and escape the diffusion-limited microcapsule interior. Additionally, lysozymes present *in vivo* could degrade the microcapsule membrane, removing one barrier to nutrient diffusion as the system mineralizes. Results suggests that microcapsules containing MSCs or OPs would rapidly mineralize *in vivo*, in the growth factor and signaling milieu of a bone defect site, and regenerate bone.

Fused microcapsule constructs could be fabricated from mineralized microcapsules, and the presence and architecture of cell-deposited mineral greatly influenced the overall mechanical properties of the constructs. Moreover, it was evident that the organization of the mineral within the microcapsules, and not just the amount of mineral, significantly influenced the mechanical properties of fused constructs. This study suggests that an effective strategy to improve the toughness of fused constructs could involve directly mineralizing the membranes of microcapsules containing HAP microgranules, potentially tethering mineralizing enzymes to the polymer components of the microcapsule.

Accessory cells significantly improved the vascularization of fused constructs *in vivo* 4 weeks post-surgery, compared to acellular constructs, and constructs containing only OPs. There was no statistical difference between the effects of MSCs and EPs on fused construct vascularization in our system, indicating that the extra step of differentiating MSCs to EPs is unnecessary, although a longer *in vivo* implant period should be examined to confirm this. Additionally, all fused constructs with cells exhibited significantly higher tissue growth between the microcapsules, and dense collagen deposition indicating a precursor to bone tissue, compared to the relatively sparse tissue in acellular implants. More work is required to characterize any hard tissue that was deposited in the implants *in vivo*: this requires conducting hard tissue histology on undecalcified implants, and specialized sectioning tools.

Other groups have attempted similar strategies to generate modular bone regeneration systems. An early modular system involved the culture of human amniotic MSCs on porous dextran beads, to generate a 2 x 1 cm (diameter x height) cylinder from the cell laden modules [104]. The amniotic MSCs were cultured on the dextran beads as modular units 700-800 μm in diameter, in a bioreactor system to rapidly proliferate and generate matrix prior to fusion into a construct. The bioreactor-based cell expansion is a useful strategy to increase the cell-density of the modular units, and this strategy could be employed with the microcapsule system described here. Another attempt at modular bone regeneration involved the fabrication of collagen/chitosan hydrogel beads, encapsulating MSCs [103]. These hydrogel beads could be fabricated quickly using an emulsion process that preserved cell viability and osteogenic capability, and could be extruded as a paste to facilitate minimally invasive delivery *in vivo*. Neither of these modular systems had their mechanical properties characterized, however, so it's difficult to determine how they would recapitulate the mechanical properties of native bone *in vivo*.

As the importance of designing vascularization strategies into bone regeneration systems becomes clearer with more data, other research groups are developing modular systems that include a vascular cell component. The field of modular tissue engineering is relatively new, and vascularized bone modular regeneration even more recent, so relatively few studies have been published in this area. Two recent studies of note utilize HUVECs as the vascular cell component, and involve either 1) co-culturing HUVECs and MSCs on gelatin microcarriers [139], or 2) co-culturing HUVECs and MG-63 cells (an immortalized osteoblast cell line) on gelatin microcarriers, and fusing these cell-laden microcarriers into larger constructs [140]. Both of these studies use HUVECs as a model vascular-cell to study the effects co-culturing vascular-osteogenic cells *in vitro*: specifically, both papers pay particular attention to the effects of vascular-cells on MSC or MG-63 osteogenesis (expression of osteogenic markers), and endothelial markers (CD31, VE-Cadherin, vWF) overtime in culture. Both studies show that the HUVECs and osteogenic cells could maintain their expression of tissue-specific markers over a 28-day culture period. These two studies are good models of how both cell types respond in a co-culture with vascular and osteogenic cells on a common biomaterial (gelatin). The study using MG-63 cell line could not be translated to the clinic, unless another non-immortalized cell type was used. Neither study discussed the performance of their vascularized modular system in a non-immunocompromised mammal, which was one of the features of the study detailed in this dissertation. Additionally, the vascular cell-type used in this dissertation can be easily generated in the clinic: MSCs are easily harvested from a patient's bone marrow, and the differentiation medium is relatively inexpensive. The project featured in this dissertation extends the vascularized modular bone regeneration idea to generated tissue in an immunocompetent mammal (rat) using clinically relevant cell sources (OPs and EPs generated from MSCs), helping extend the field beyond model cell types.

The design for a bone regeneration platform presented here shows how modular tissue engineering principles can help engineer tissue with multicellular organization that enhances vascularization *in vivo*, and a unique configuration of cell and ceramic materials that produces mechanically tough tissue. The overall design has shown the ability to rapidly regenerate tissue in a subcutaneous model, and initial results indicate the presence of bone matrix precursor in the subcutaneous implants. The modular bone regeneration platform is a promising system that warrants further development and optimization for future clinical applications involving hard tissue regeneration.

CHAPTER 8: FUTURE WORK

The results of this project indicate that the modular bone regeneration platform shows promise to regenerate vascularized bone; however, more work is required to fully characterize the tissue developed *in vivo* in the microcapsule constructs. The US data showing enhanced vascularization in constructs with EPs/MSCs is impressive, but the limited resolution of the US probe means that microcapillaries (diameter < 30 μm) were not counted in the average VAF data. The tissue explants will be further analyzed for the presence of blood vessels of all sizes via immunohistochemical (IHC) staining of CD31+ cells (endothelial cells) in paraffin sections. Additionally, the presence of an inflammatory response in the tissue sections should be evaluated via IHC staining of Ly-6 proteins (neutrophils), CD38 (plasma B cells), and CD68 (macrophages). Another *in* vivo study should be conducted, this time will all exogenous cells labelled with non-canonical amino acids (distinguishing them from native cells) to determine whether these cells participate directly in tissue regeneration, or if they evacuate the implant but induce native cell infiltration via cell homing [141]. Essentially, implanted cells could be fed a diet of methionine derivatives that cells metabolize into peptides that would normally contain methionine: these "labelled" cells are then implanted in the microcapsule system *in vivo*. The methionine derivatives are easily reacted with fluorophore-conjugated azides, enabling the implanted cells left in the implant to be identified. Ideally, the derivatized methionine labelling is less invasive than other methods, such as transfection for green fluorescent protein (GFP) expression. Finally, undecalcified tissue implants will be sectioned using specialized hard-tissue sectioning equipment, and the presence of mineral deposited *in vivo* in the subcutaneous implants will be evaluated to discern whether the accessory cells enhanced mineralization of the microcapsule system.

Alternative microcapsule fusion strategies need to be developed, to broaden the application of the microcapsules to minimally invasive surgery (arthroscopic injection into bone defect), and 3D printing of tissue constructs, among other applications. The GAG/chitosan complex microcapsule fusion protocol utilized to fuse microcapsules in this study requires a mold and perfusion to fuse microcapsules, inhibiting the use to the microcapsules for arthroscopic injection cases. A better microcapsule fusion system would involve the deposition of either a photoactive polymer layer (such as methacrylated chitosan [142], methacrylated hyaluronan [143] or methacrylated collagen [144]), or crosslinking enzyme layer (tyramine/horseradish peroxidase [145]) on the exterior of the microcapsules. The photoactive/enzyme layers would be engineered in such a way that microcapsules could be injected along with a catalyst (photoinitiator/enzyme cofactor, respectively) that would cause capsules to adhere to one-another after extrusion. A microcapsule fusion strategy that does not require a mold and polymer perfusion will significantly enhance the applications of the microcapsules to regenerate tissue of complex shapes *in situ*, or via 3D printing equipment.

The increase in mechanical properties of the fused microcapsule constructs due to mineralization was impressive, but the mechanics still fall short of native bone. The relatively low mechanical properties stem from 1) the weak microcapsule membrane, and 2) the significant void space in the microcapsule interior, even when the microcapsules are partially filled with HAP. The targeted mineralization of the microcapsule membranes by tethering ALP to one of the polymers involved in microcapsule fabrication was discussed in the Chapter 7. Another strategy to improve fused construct mechanical properties involves decreasing the non-mineral void space in the microcapsule interior. A microcapsule formulation utilizing hyaluronan (HA), C4S and chitosan to form the microcapsules can contract when the microcapsules contain an internal collagen gel

and MSCs (fig 8.1). Essentially, the collagen gel becomes incorporated into the microcapsule membrane, and MSCs are able to contract the gel to collapse the membrane [146]. It's likely fused constructs created form these collapsed capsules would have significantly better mechanical properties than the C4S/chitosan microcapsules presented in this study.

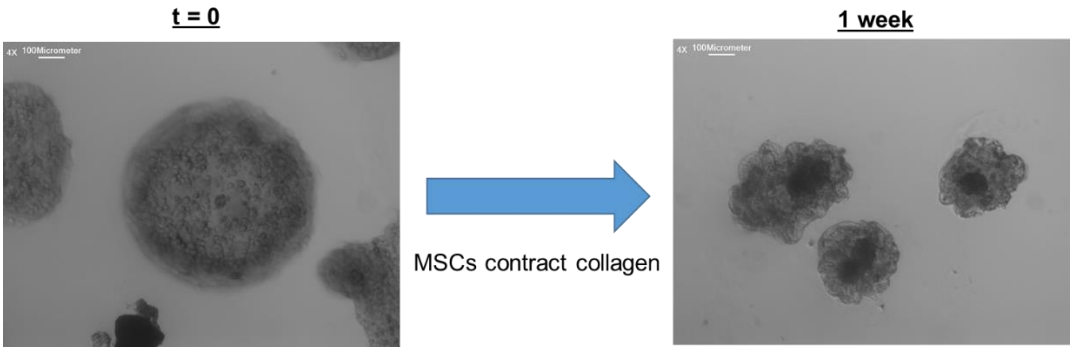

Fig 8.1: Microcapsules with internal collagen gel and hyaluronan in microcapsule membrane can be contracted with encapsulated MSCs in culture. Credit: Patrick Michael Erickson, Undergraduate in Tissue Engineering Lab.

The microcapsule design is inherently tunable, and the microcapsule properties can be augmented by using different polymers for the polyelectrolyte membrane, incorporating different ECM gels/microcarriers in the microcapsule interior, and adjusting the types and density of cells in and attached to the microcapsules. The ability to substantially customize the GAG/chitosan microcapsules for various applications makes these a useful tool that tissue engineers can use to generate tissue with complexity that better mimics physiological tissue. These microcapsules were used to generate bone, but another tissue engineer may use a similar design to generate tissue of greater complexity, and eventually a world without implantable organ shortages.

REFERENCES

1. Joshi, A. and G.C. Kostakis, *An investigation of post-operative morbidity following iliac crest graft harvesting.* British Dental Journal, 2004. **196**(3): p. 167-171.
2. Damien, C.J. and J.R. Parsons, *Bone-Graft and Bone-Graft Substitutes - a Review of Current Technology and Applications.* Journal of Applied Biomaterials, 1991. **2**(3): p. 187-208.
3. Meijer, G.J., et al., *Cell-based bone tissue engineering.* Plos Medicine, 2007. **4**(2): p. 260-264.
4. Arrington, E.D., et al., *Complications of iliac crest bone graft harvesting.* Clinical Orthopaedics and Related Research, 1996(329): p. 300-309.
5. Sieminski, A.L. and K.J. Gooch, *Biomaterial-microvasculature interactions.* Biomaterials, 2000. **21**(22): p. 2233-2241.
6. Koike, N., et al., *Tissue engineering: creation of long-lasting blood vessels.* Nature, 2004. **428**(6979): p. 138-9.
7. Tiruvannamalai-Annamalai, R., D.R. Armant, and H.W. Matthew, *A glycosaminoglycan based, modular tissue scaffold system for rapid assembly of perfusable, high cell density, engineered tissues.* PLoS One, 2014. **9**(1): p. e84287.
8. Carmeliet, P. and R.K. Jain, *Angiogenesis in cancer and other diseases.* Nature, 2000. **407**(6801): p. 249-257.
9. Dean, D.M., et al., *Rods, tori, and honeycombs: the directed self-assembly of microtissues with prescribed microscale geometries.* Faseb Journal, 2007. **21**(14): p. 4005-4012.

10. Yeh, J., et al., *Micromolding of shape-controlled, harvestable cell-laden hydrogels.* Biomaterials, 2006. **27**(31): p. 5391-5398.

11. L'Heureux, N., et al., *A completely biological tissue-engineered human blood vessel.* Faseb Journal, 1998. **12**(1): p. 47-56.

12. Mironov, V., et al., *Organ printing: computer-aided jet-based 3D tissue engineering.* Trends in Biotechnology, 2003. **21**(4): p. 157-161.

13. Yamada, Y., et al., *Injectable Bone Tissue Engineering Using Expanded Mesenchymal Stem Cells.* Stem Cells, 2013. **31**(3): p. 572-580.

14. Turkyilmaz, I., A.M. Company, and E.A. McGlumphy, *Should edentulous patients be constrained to removable complete dentures? The use of dental implants to improve the quality of life for edentulous patients.* Gerodontology, 2010. **27**(1): p. 3-10.

15. Meijer, G.J., et al., *Cell based bone tissue engineering in jaw defects.* Biomaterials, 2008. **29**(21): p. 3053-3061.

16. Weiner, S. and H.D. Wagner, *The material bone: Structure mechanical function relations.* Annual Review of Materials Science, 1998. **28**: p. 271-298.

17. Frohlich, M., et al., *Tissue engineered bone grafts: biological requirements, tissue culture and clinical relevance.* Curr Stem Cell Res Ther, 2008. **3**(4): p. 254-64.

18. Hoang, Q.Q., et al., *Bone recognition mechanism of porcine osteocalcin from crystal structure.* Nature, 2003. **425**(6961): p. 977-80.

19. Denhardt, D.T. and M. Noda, *Osteopontin expression and function: Role in bone remodeling.* Journal of Cellular Biochemistry, 1998: p. 92-+.

20. Termine, J.D., et al., *Osteonectin, a Mineral and Collagen Binding-Protein of Fetal Calf Bone.* Calcified Tissue International, 1981. **33**(3): p. 302-302.

21. Vejlens, L., *Glycosaminoglycans of human bone tissue. I. Pattern of compact bone in relation to age.* Calcif Tissue Res, 1971. **7**(2): p. 175-90.

22. Schneiders, W., et al., *Effect of chondroitin sulphate on material properties and bone remodelling around hydroxyapatite/collagen composites.* Journal of Biomedical Materials Research Part A, 2008. **85A**(3): p. 638-645.

23. Stevens, M.M., *Biomaterials for bone tissue engineering.* Materials Today, 2008. **11**(5): p. 18-25.

24. Franz-Odendaal, T.A., B.K. Hall, and P.E. Witten, *Buried alive: how osteoblasts become osteocytes.* Dev Dyn, 2006. **235**(1): p. 176-90.

25. Manolagas, S.C., *Birth and death of bone cells: basic regulatory mechanisms and implications for the pathogenesis and treatment of osteoporosis.* Endocr Rev, 2000. **21**(2): p. 115-37.

26. Fernandez-Tresguerres-Hernandez-Gil, I., et al., *Physiological bases of bone regeneration II. The remodeling process.* Med Oral Patol Oral Cir Bucal, 2006. **11**(2): p. E151-7.

27. Nombela-Arrieta, C., J. Ritz, and L.E. Silberstein, *The elusive nature and function of mesenchymal stem cells.* Nature Reviews Molecular Cell Biology, 2011. **12**(2): p. 126-131.

28. Chen, X.D., et al., *Extracellular matrix made by bone marrow cells facilitates expansion of marrow-derived mesenchymal progenitor cells and prevents their differentiation into osteoblasts.* Journal of Bone and Mineral Research, 2007. **22**(12): p. 1943-1956.

29. Guan, M., et al., *Directing mesenchymal stem cells to bone to augment bone formation and increase bone mass.* Nature Medicine, 2012. **18**(3): p. 456-U159.

30. Hoemann, C.D., H. El-Gabalawy, and M.D. McKee, *In vitro osteogenesis assays: influence of the primary cell source on alkaline phosphatase activity and mineralization.* Pathol Biol (Paris), 2009. **57**(4): p. 318-23.

31. Huang, Z., et al., *The sequential expression profiles of growth factors from osteoprogenitors [correction of osteroprogenitors] to osteoblasts in vitro.* Tissue Eng, 2007. **13**(9): p. 2311-20.

32. Pazzaglia, U.E., et al., *A model of the intracortical vascular system of long bones and of its organization: an experimental study in rabbit femur and tibia.* J Anat, 2008. **213**(2): p. 183-93.

33. Pazzaglia, U.E., et al., *Morphometry and patterns of lamellar bone in human Haversian systems.* Anat Rec (Hoboken), 2012. **295**(9): p. 1421-9.

34. Muschler, G.F., C. Nakamoto, and L.G. Griffith, *Engineering principles of clinical cell-based tissue engineering.* J Bone Joint Surg Am, 2004. **86-A**(7): p. 1541-58.

35. Bergers, G. and S. Song, *The role of pericytes in blood-vessel formation and maintenance.* Neuro Oncol, 2005. **7**(4): p. 452-64.

36. Wanjare, M., S. Kusuma, and S. Gerecht, *Perivascular cells in blood vessel regeneration.* Biotechnol J, 2013. **8**(4): p. 434-47.

37. Gerhardt, H. and C. Betsholtz, *Endothelial-pericyte interactions in angiogenesis.* Cell Tissue Res, 2003. **314**(1): p. 15-23.

38. Carano, R.A. and E.H. Filvaroff, *Angiogenesis and bone repair.* Drug Discov Today, 2003. **8**(21): p. 980-9.

39. Einhorn, T.A., *The cell and molecular biology of fracture healing.* Clin Orthop Relat Res, 1998(355 Suppl): p. S7-21.

40. Trueta, J., *The Role of the Vessels in Osteogenesis.* Journal of Bone and Joint Surgery-British Volume, 1963. **45**(2): p. 402-418.

41. Street, J., et al., *Vascular endothelial growth factor stimulates bone repair by promoting angiogenesis and bone turnover.* Proc Natl Acad Sci U S A, 2002. **99**(15): p. 9656-61.

42. Villa, M.M., et al., *Bone tissue engineering with a collagen-hydroxyapatite scaffold and culture expanded bone marrow stromal cells.* J Biomed Mater Res B Appl Biomater, 2015. **103**(2): p. 243-53.

43. Renth, A.N. and M.S. Detamore, *Leveraging "Raw Materials" as Building Blocks and Bioactive Signals in Regenerative Medicine.* Tissue Engineering Part B-Reviews, 2012. **18**(5): p. 341-362.

44. Asada, M., et al., *Glycosaminoglycan affinity of the complete fibroblast growth factor family.* Biochim Biophys Acta, 2009. **1790**(1): p. 40-8.

45. Venkatesan, J., et al., *Chitosan-amylopectin/hydroxyapatite and chitosan-chondroitin sulphate/hydroxyapatite composite scaffolds for bone tissue engineering.* International Journal of Biological Macromolecules, 2012. **51**(5): p. 1033-1042.

46. Di Martino, A., M. Sittinger, and M.V. Risbud, *Chitosan: a versatile biopolymer for orthopaedic tissue-engineering.* Biomaterials, 2005. **26**(30): p. 5983-90.

47. Levengood, S.L. and M. Zhang, *Chitosan-based scaffolds for bone tissue engineering.* J Mater Chem B Mater Biol Med, 2014. **2**(21): p. 3161-3184.

48. Kang, Y., et al., *Osteogenic and angiogenic potentials of monocultured and co-cultured human-bone-marrow-derived mesenchymal stem cells and human-umbilical-vein endothelial cells on three-dimensional porous beta-tricalcium phosphate scaffold.* Acta Biomater, 2013. **9**(1): p. 4906-15.

49. Pedersen, T.O., et al., *Endothelial microvascular networks affect gene-expression profiles and osteogenic potential of tissue-engineered constructs.* Stem Cell Res Ther, 2013. **4**(3): p. 52.

50. Yu, H., et al., *Improved tissue-engineered bone regeneration by endothelial cell mediated vascularization.* Biomaterials, 2009. **30**(4): p. 508-17.

51. Karaoz, E., et al., *Characterization of mesenchymal stem cells from rat bone marrow: ultrastructural properties, differentiation potential and immunophenotypic markers.* Histochem Cell Biol, 2009. **132**(5): p. 533-46.

52. Matthew, H.W., et al., *Complex Coacervate Microcapsules for Mammalian-Cell Culture and Artificial Organ Development.* Biotechnology Progress, 1993. **9**(5): p. 510-519.

53. Liu, T.M., et al., *Identification of common pathways mediating differentiation of bone marrow- and adipose tissue-derived human mesenchymal stem cells into three mesenchymal lineages.* Stem Cells, 2007. **25**(3): p. 750-760.

54. Labarca, C. and K. Paigen, *A simple, rapid, and sensitive DNA assay procedure.* Anal Biochem, 1980. **102**(2): p. 344-52.

55. Van Heek, N.T., et al., *Gene expression profiling identifies markers of ampullary adenocarcinoma.* Cancer Biol Ther, 2004. **3**(7): p. 651-6.

56. ter Brugge, P.J., J.G. Wolke, and J.A. Jansen, *Effect of calcium phosphate coating crystallinity and implant surface roughness on differentiation of rat bone marrow cells.* J Biomed Mater Res, 2002. **60**(1): p. 70-8.

57. Hofman, K., et al., *High-throughput quantification of hydroxyproline for determination of collagen.* Anal Biochem, 2011. **417**(2): p. 289-91.

58. Pautke, C., et al., *Characterization of eight different tetracyclines: advances in fluorescence bone labeling.* J Anat, 2010. **217**(1): p. 76-82.

59. Shih, Y.R., et al., *Calcium phosphate-bearing matrices induce osteogenic differentiation of stem cells through adenosine signaling.* Proc Natl Acad Sci U S A, 2014. **111**(3): p. 990-5.

60. Chai, Y.C., et al., *Probing the osteoinductive effect of calcium phosphate by using an in vitro biomimetic model.* Tissue Eng Part A, 2011. **17**(7-8): p. 1083-97.

61. Beck, G.R., Jr. and N. Knecht, *Osteopontin regulation by inorganic phosphate is ERK1/2-, protein kinase C-, and proteasome-dependent.* J Biol Chem, 2003. **278**(43): p. 41921-9.

62. Eapen, A., et al., *Calcium-mediated stress kinase activation by DMP1 promotes osteoblast differentiation.* J Biol Chem, 2010. **285**(47): p. 36339-51.

63. Muller, P., et al., *Calcium phosphate surfaces promote osteogenic differentiation of mesenchymal stem cells.* J Cell Mol Med, 2008. **12**(1): p. 281-91.

64. Kourkoumelis, N. and M. Tzaphlidou, *Spectroscopic assessment of normal cortical bone: differences in relation to bone site and sex.* ScientificWorldJournal, 2010. **10**: p. 402-12.

65. Tzaphlidou, M., *Bone architecture: collagen structure and calcium/phosphorus maps.* J Biol Phys, 2008. **34**(1-2): p. 39-49.

66. Olszta, M.J., et al., *Bone structure and formation: A new perspective.* Materials Science & Engineering R-Reports, 2007. **58**(3-5): p. 77-116.

67. Meyer, J.L., et al., *A scanning electron microscopic study of the growth of hydroxyapatite crystals.* Calcif Tissue Res, 1972. **10**(2): p. 91-102.

68. Bagambisa, F.B., U. Joos, and W. Schilli, *A Scanning Electron-Microscope Study of the Ultrastructural Organization of Bone-Mineral.* Cells and Materials, 1993. **3**(1): p. 93-102.

69. Gafni, G., D. Septier, and M. Goldberg, *Effect of chondroitin sulfate and biglycan on the crystallization of hydroxyapatite under physiological conditions.* Journal of Crystal Growth, 1999. **205**(4): p. 618-623.

70. Jiang, H., et al., *Kinetics and template nucleation of self-assembled hydroxyapatite nanocrystallites by chondroitin sulfate.* J Biol Chem, 2005. **280**(51): p. 42061-6.

71. Yang, D., et al., *In situ mineralization of hydroxyapatite on electrospun chitosan-based nanofibrous scaffolds.* Macromol Biosci, 2008. **8**(3): p. 239-46.

72. Mackie, I.G., et al., *Human bone microstructure studied by collagenase etching.* J Bone Joint Surg Br, 1989. **71**(3): p. 509-13.

73. Boyde, A. and J. Sela, *Scanning Electron-Microscope Study of Separated Calcospherites from Matrices of Different Mineralizing Systems.* Calcified Tissue Research, 1978. **26**(1): p. 47-49.

74. Elsharkawy, S., et al., *Preferential nucleation and crystal growth on microfabricated topography Systems for biomedical and industrial applications.* Materials Today, 2016. **19**(8): p. 478-480.

75. Holbrough, J.L., et al., *Topographical Control of Crystal Nucleation.* Crystal Growth & Design, 2012. **12**(2): p. 750-755.

76. Butler, W.T., A.L. Ridall, and M.D. Mckee, *Osteopontin*. Principles of bone biology. 1996, San Diego: Academic Press.

77. Somerman, M.J., et al., *Cell attachment activity of the 44 kilodalton bone phosphoprotein is not restricted to bone cells.* Matrix, 1989. **9**(1): p. 49-54.

78. Choi, J.H., et al., *Hypoxia Inducible Factor-1alpha Regulates the Migration of Bone Marrow Mesenchymal Stem Cells via Integrin alpha 4.* Stem Cells Int, 2016. **2016**: p. 7932185.

79. Ferretti, A., et al., *Angiogenesis and nerve regeneration in a model of human skin equivalent transplant.* Life Sci, 2003. **73**(15): p. 1985-94.

80. Black, A.F., et al., *A novel approach for studying angiogenesis: a human skin equivalent with a capillary-like network.* Cell Biol Toxicol, 1999. **15**(2): p. 81-90.

81. Mathieu, C., et al., *Stereological analysis of subchondral angiogenesis induced by chitosan and coagulation factors in microdrilled articular cartilage defects.* Osteoarthritis Cartilage, 2013. **21**(6): p. 849-59.

82. Simkin, A. and G. Robin, *Mechanical Testing of Bone in Bending.* Journal of Biomechanics, 1973. **6**(1): p. 31-&.

83. Kraaij, G., et al., *Mechanical properties of human bone-implant interface tissue in aseptically loose hip implants.* J Mech Behav Biomed Mater, 2014. **38**: p. 59-68.

84. Reilly, D.T. and A.H. Burstein, *Elastic and Ultimate Properties of Compact Bone Tissue.* Journal of Biomechanics, 1975. **8**(6): p. 393-&.

85. Bissinger, O., et al., *Micro-CT vs. Whole Body Multirow Detector CT for Analysing Bone Regeneration in an Animal Model.* PLoS One, 2016. **11**(11): p. e0166540.

86. Bauer, J.S., et al., *Structural analysis of trabecular bone of the proximal femur using multislice computed tomography: a comparison with dual X-ray absorptiometry for predicting biomechanical strength in vitro.* Calcif Tissue Int, 2006. **78**(2): p. 78-89.

87. Palacio-Mancheno, P.E., et al., *3D assessment of cortical bone porosity and tissue mineral density using high-resolution microCT: effects of resolution and threshold method.* J Bone Miner Res, 2014. **29**(1): p. 142-50.

88. Lehtinen, J.T., et al., *Total, trabecular, and cortical bone mineral density in different regions of the glenoid.* J Shoulder Elbow Surg, 2004. **13**(3): p. 344-8.

89. Amano, K. and E. Ito, *The action of lysozyme on partially deacetylated chitin.* Eur J Biochem, 1978. **85**(1): p. 97-104.

90. Boonrungsiman, S., et al., *The role of intracellular calcium phosphate in osteoblast-mediated bone apatite formation.* Proc Natl Acad Sci U S A, 2012. **109**(35): p. 14170-5.

91. Dean, D.D., et al., *Matrix vesicles produced by osteoblast-like cells in culture become significantly enriched in proteoglycan-degrading metalloproteinases after addition of beta-glycerophosphate and ascorbic acid.* Calcif Tissue Int, 1994. **54**(5): p. 399-408.

92. Yang, D.Z., et al., *In situ mineralization of hydroxyapatite on electrospun chitosan-based nanofibrous scaffolds.* Macromolecular Bioscience, 2008. **8**(3): p. 239-246.

93. Nudelman, F., et al., *The role of the amorphous phase on the biomimetic mineralization of collagen.* Faraday Discussions, 2012. **159**: p. 357-370.

94. Nudelman, F., et al., *The role of collagen in bone apatite formation in the presence of hydroxyapatite nucleation inhibitors.* Nature Materials, 2010. **9**(12): p. 1004-1009.

95. Engler, A.J., et al., *Matrix elasticity directs stem cell lineage specification.* Cell, 2006. **126**(4): p. 677-689.

96. Pek, Y.S., A.C.A. Wan, and J.Y. Ying, *The effect of matrix stiffness on mesenchymal stem cell differentiation in a 3D thixotropic gel.* Biomaterials, 2010. **31**(3): p. 385-391.

97. Klein, E.A., et al., *Cell-Cycle Control by Physiological Matrix Elasticity and In Vivo Tissue Stiffening.* Current Biology, 2009. **19**(18): p. 1511-1518.

98. Carter, D.R. and W.C. Hayes, *Bone Compressive Strength - Influence of Density and Strain Rate.* Science, 1976. **194**(4270): p. 1174-1176.

99. Cowan, C.M., et al., *Evolving Concepts in Bone Tissue Engineering.* Current Topics in Developmental Biology, 2005. **66**: p. 239-285.

100. Zhao, L., M.D. Weir, and H.H. Xu, *An injectable calcium phosphate-alginate hydrogel-umbilical cord mesenchymal stem cell paste for bone tissue engineering.* Biomaterials, 2010. **31**(25): p. 6502-10.

101. Causa, F., et al., *Poly-epsilon-caprolactone/hydroxyapatite composites for bone regeneration: in vitro characterization and human osteoblast response.* J Biomed Mater Res A, 2006. **76**(1): p. 151-62.

102. Dormer, N.H., et al., *Osteogenic differentiation of human bone marrow stromal cells in hydroxyapatite-loaded microsphere-based scaffolds.* Tissue Eng Part A, 2012. **18**(7-8): p. 757-67.

103. Wang, L., R.R. Rao, and J.P. Stegemann, *Delivery of mesenchymal stem cells in chitosan/collagen microbeads for orthopedic tissue repair.* Cells Tissues Organs, 2013. **197**(5): p. 333-43.

104. Chen, M.Q., et al., *A modular approach to the engineering of a centimeter-sized bone tissue construct with human amniotic mesenchymal stem cells-laden microcarriers.* Biomaterials, 2011. **32**(30): p. 7532-7542.

105. Goldstein, S.A., R. Goulet, and D. McCubbrey, *Measurement and significance of three-dimensional architecture to the mechanical integrity of trabecular bone.* Calcif Tissue Int, 1993. **53 Suppl 1**: p. S127-32; discussion S132-3.

106. Goulet, R.W., et al., *The relationship between the structural and orthogonal compressive properties of trabecular bone.* J Biomech, 1994. **27**(4): p. 375-89.

107. Judex, S., et al., *Combining high-resolution micro-computed tomography with material composition to define the quality of bone tissue.* Curr Osteoporos Rep, 2003. **1**(1): p. 11-9.

108. Kreider, J.M. and S.A. Goldstein, *Trabecular bone mechanical properties in patients with fragility fractures.* Clin Orthop Relat Res, 2009. **467**(8): p. 1955-63.

109. Barnes, G.L., et al., *Growth factor regulation of fracture repair.* J Bone Miner Res, 1999. **14**(11): p. 1805-15.

110. Chen, M.Y., et al., *Endothelial differentiation of Wharton's jelly-derived mesenchymal stem cells in comparison with bone marrow-derived mesenchymal stem cells.* Exp Hematol, 2009. **37**(5): p. 629-40.

111. Oswald, J., et al., *Mesenchymal stem cells can be differentiated into endothelial cells in vitro.* Stem Cells, 2004. **22**(3): p. 377-84.

112. Kang, Y., et al., *Engineering a vascularized collagen-beta-tricalcium phosphate graft using an electrochemical approach.* Acta Biomater, 2015. **11**: p. 449-58.

113. Chen, J.J., et al., *A preclinical study to explore vasculature differences between primary and recurrent tumors using ultrasound Doppler imaging.* Ultrasound Med Biol, 2013. **39**(5): p. 860-9.

114. Castania, V.A., et al., *Advantages of a combined method of decalcification compared to EDTA.* Microsc Res Tech, 2015. **78**(2): p. 111-8.

115. Madri, J.A., B.M. Pratt, and A.M. Tucker, *Phenotypic modulation of endothelial cells by transforming growth factor-beta depends upon the composition and organization of the extracellular matrix.* J Cell Biol, 1988. **106**(4): p. 1375-84.

116. DeLisser, H.M., et al., *Involvement of endothelial PECAM-1/CD31 in angiogenesis.* Am J Pathol, 1997. **151**(3): p. 671-7.

117. Ruggeri, Z.M., *Von Willebrand factor, platelets and endothelial cell interactions.* J Thromb Haemost, 2003. **1**(7): p. 1335-42.

118. Janeczek Portalska, K., et al., *Endothelial differentiation of mesenchymal stromal cells.* PLoS One, 2012. **7**(10): p. e46842.

119. Yu, H.Y., et al., *Improved tissue-engineered bone regeneration by endothelial cell mediated vascularization.* Biomaterials, 2009. **30**(4): p. 508-517.

120. Ghajar, C.M., et al., *Mesenchymal stem cells enhance angiogenesis in mechanically viable prevascularized tissues via early matrix metalloproteinase upregulation.* Tissue Eng, 2006. **12**(10): p. 2875-88.

121. Carrion, B., et al., *Bone marrow-derived mesenchymal stem cells enhance angiogenesis via their alpha6beta1 integrin receptor.* Exp Cell Res, 2013. **319**(19): p. 2964-76.

122. Gallina, C., V. Turinetto, and C. Giachino, *A New Paradigm in Cardiac Regeneration: The Mesenchymal Stem Cell Secretome.* Stem Cells Int, 2015. **2015**: p. 765846.

123. Hirschi, K.K., et al., *Gap junction communication mediates transforming growth factor-beta activation and endothelial-induced mural cell differentiation.* Circ Res, 2003. **93**(5): p. 429-37.

124. VandeVord, P.J., et al., *Evaluation of the biocompatibility of a chitosan scaffold in mice.* J Biomed Mater Res, 2002. **59**(3): p. 585-90.

125. Kosaka, T., et al., *Effect of chitosan implantation on activation of canine macrophages and polymorphonuclear cells after surgical stress.* J Vet Med Sci, 1996. **58**(10): p. 963-7.

126. Barbosa, J.N., et al., *Evaluation of the effect of the degree of acetylation on the inflammatory response to 3D porous chitosan scaffolds.* Journal of Biomedical Materials Research Part A, 2010. **93a**(1): p. 20-28.

127. Prockop, D.J. and J.Y. Oh, *Mesenchymal stem/stromal cells (MSCs): role as guardians of inflammation.* Mol Ther, 2012. **20**(1): p. 14-20.

128. Gamblin, A.L., et al., *Bone tissue formation with human mesenchymal stem cells and biphasic calcium phosphate ceramics: the local implication of osteoclasts and macrophages.* Biomaterials, 2014. **35**(36): p. 9660-7.

129. Tasso, R., et al., *Recruitment of a host's osteoprogenitor cells using exogenous mesenchymal stem cells seeded on porous ceramic.* Tissue Eng Part A, 2009. **15**(8): p. 2203-12.

130. Zhang, M., et al., *SDF-1 expression by mesenchymal stem cells results in trophic support of cardiac myocytes after myocardial infarction.* FASEB J, 2007. **21**(12): p. 3197-207.

131. Shabbir, A., et al., *Mesenchymal Stem Cell Exosomes Induce Proliferation and Migration of Normal and Chronic Wound Fibroblasts, and Enhance Angiogenesis In Vitro.* Stem Cells Dev, 2015. **24**(14): p. 1635-47.

132. Sassoli, C., et al., *Bone marrow mesenchymal stromal cells stimulate skeletal myoblast proliferation through the paracrine release of VEGF.* PLoS One, 2012. **7**(7): p. e37512.

133. Park, C.W., et al., *Cytokine secretion profiling of human mesenchymal stem cells by antibody array.* Int J Stem Cells, 2009. **2**(1): p. 59-68.

134. Kristensen, L.P., et al., *Temporal profiling and pulsed SILAC labeling identify novel secreted proteins during ex vivo osteoblast differentiation of human stromal stem cells.* Mol Cell Proteomics, 2012. **11**(10): p. 989-1007.

135. Kurz, H., P.H. Burri, and V.G. Djonov, *Angiogenesis and vascular remodeling by intussusception: from form to function.* News Physiol Sci, 2003. **18**: p. 65-70.

136. Hlushchuk, R., et al., *Decrease in VEGF expression induces intussusceptive vascular pruning.* Arterioscler Thromb Vasc Biol, 2011. **31**(12): p. 2836-44.

137. Hlushchuk, R., et al., *Tumor recovery by angiogenic switch from sprouting to intussusceptive angiogenesis after treatment with PTK787/ZK222584 or ionizing radiation.* Am J Pathol, 2008. **173**(4): p. 1173-85.

138. Parfitt, A.M., et al., *Bone histomorphometry: standardization of nomenclature, symbols, and units. Report of the ASBMR Histomorphometry Nomenclature Committee.* J Bone Miner Res, 1987. **2**(6): p. 595-610.

139. Zhang, S., et al., *Fabrication of viable and functional pre-vascularized modular bone tissues by coculturing MSCs and HUVECs on microcarriers in spinner flasks.* Biotechnol J, 2017.

140. Zhong, M., et al., *Vascularization in Engineered Tissue Construct by Assembly of Cellular Patterned Micromodules and Degradable Microspheres.* ACS Appl Mater Interfaces, 2017. **9**(4): p. 3524-3534.

141. Calve, S., et al., *Incorporation of non-canonical amino acids into the developing murine proteome.* Sci Rep, 2016. **6**: p. 32377.

142. Flores-Ramirez, N., et al., *Characterization and degradation of functionalized chitosan with glycidyl methacrylate.* J Biomater Sci Polym Ed, 2005. **16**(4): p. 473-88.

143. Fenn, S.L. and R.A. Oldinski, *Visible light crosslinking of methacrylated hyaluronan hydrogels for injectable tissue repair.* J Biomed Mater Res B Appl Biomater, 2016. **104**(6): p. 1229-36.

144. Gaudet, I.D. and D.I. Shreiber, *Characterization of methacrylated type-I collagen as a dynamic, photoactive hydrogel.* Biointerphases, 2012. **7**(1-4): p. 25.

145. Chen, F., et al., *An Injectable Enzymatically Crosslinked Carboxymethylated Pullulan/Chondroitin Sulfate Hydrogel for Cartilage Tissue Engineering.* Sci Rep, 2016. **6**: p. 20014.

146. Young, R.G., et al., *Use of mesenchymal stem cells in a collagen matrix for Achilles tendon repair.* J Orthop Res, 1998. **16**(4): p. 406-13.

ABSTRACT

DESIGN OF A MODULAR ENDOTHELIALIZED PLATFORM FOR VASCULARIZED BONE REGENERATION

by:

KEVIN BARRETT MILES

August 2017

Advisor: Dr. Howard W. T. Matthew

Major: Chemical Engineering

Degree: Doctor of Philosophy

The gold standard for bone regeneration requires harvesting a piece of healthy bone from the patient through a painful procedure, but this piece of autologous bone graft contains the bone and endothelial cells required to rapidly regenerate bone in a defect. We have developed a modular bone regeneration platform, composed of mesenchymal stem cells (MSCs) and hydroxyapatite (HAP) microgranules encapsulated in microcapsules, to replace autologous graft harvesting. The microcapsules are composed of a polyelectrolyte membrane formed by the ionic-complex reaction between chondroitin 4-sulfate (C4S) and chitosan. The specific aims of this thesis were to 1) examine the ability of C4S/HAP/chitosan microcapsules to support osteogenesis of encapsulated MSCs, 2) characterize how microcapsule mineralization influences mechanical properties of fused microcapsule constructs, and 3) analyze how endothelial progenitors (EPs) attached to the microcapsule exterior influence the vascularization of fused constructs *in vivo*.

The microcapsules supported the osteogenesis of encapsulated MSCs, and an *in vitro* analysis showed enhanced alkaline phosphatase (ALP), osteocalcin and osteopontin expression. Furthermore, biochemical assays and Scanning Electron Microscopy (SEM) confirmed that

osteoinduced MSCs deposited a calcium and collagen rich mineralized extracellular matrix (ECM) in the microcapsule interior after 4 weeks osteoinduction *in vitro*. Hydrated, compressive mechanical testing demonstrated that fused constructs composed of mineralized microcapsules exhibited significant resistance to compression, up to a yield strength of 10.4 + 4.4 MPa. Analysis of the yield strength and elastic moduli demonstrated that the compressive mechanical properties depend primarily on active mineralization of the microcapsules by differentiating MSCs, and to a lesser extent on HAP microgranules. Micro computed tomography (MicroCT) and SEM analysis of fused constructs showed that the organization and architecture of the mineral within the microcapsules determined the overall mechanical properties of fused constructs. EPs or MSCs were cultured on the microcapsule exterior, and fused constructs were fabricated with these microcapsules, so that the EPs/MSCs were localized to the intercapsule pore space. Fused constructs containing EPs or MSCs in the pore space were evaluated for their vascularization and tissue regeneration in a rat subcutaneous model. Doppler Ultrasound (US) analysis of blood flow through implanted constructs revealed that microcapsules with EPs or MSCs in the construct pore space had enhanced vascularization 4 weeks post-surgery, compared to fused constructs with only encapsulated osteoprogenitors and acellular constructs. Results indicate that the C4S/HAP/Chitosan microcapsules can function as the basis of a bone regeneration platform, and that culture of either EPs or undifferentiated MSCs can enhance the vascularization of fused microcapsule constructs *in vivo*. Our studies warrant further development and optimization of the C4S/HAP/Chitosan microcapsules as a replacement for painful autologous bone graft harvesting.

AUTOBIOGRAPHICAL STATEMENT

Academic Background:

- **Bachelor of Science in Chemical Engineering**, 2007 –12, Wayne State University, Detroit, MI (Honors)

Teaching Background:

- **Graduate Student Assistant**, 2013 – 2016, Office for Teaching and Learning, Wayne State University, Detroit, MI

Industry Background:

- **Reservoir Services Engineer,** 2011-2012**,** TransCanada Pipelines, Ltd., Troy, MI

Honors/Awards:

- **Predoctoral Fellowship**, Detroit Cardiovascular Training Program, 2016-2017, Wayne State University, Detroit, MI

Publications in Peer Reviewed Journals:

Miles, K. B., Ball, R. L., & Matthew, H. W. T. (2016). Chitosan films with improved tensile strength and toughness from N-acetyl-cysteine mediated disulfide bonds. *Carbohydrate Polymers*, *139*, 1-9. DOI: 10.1016/j.carbpol.2015.11.052

Selected Conference Presentations:

Miles, K. B., Maerz, T., and Matthew, H. W. T. (2015) *A Modular GAG/Chitosan/MSC Approach to Generating Tissue Engineered Bone*. Oral Presentation #426194, American Institute of Chemical Engineers Annual Meeting, Salt Lake City, UT (ISBN: 978-0-8169-1094-6)

Miles, K. B. and Matthew, H. W. T. (2014) *Osteogenesis in Encapsulated Cultures of Mesenchymal Stem Cells: A Modular Platform for Improved Bone Regeneration*. Oral Presentation #306, Annual Meeting, Society for Biomaterials. Denver, CO